INSTITUTO POTOSINO DE INVESTIGACIÓN CIENTÍFICA Y TECNOLÓGICA, A.C.

POSGRADO EN GEOCIENCIAS APLICADAS

Hydrogeological study of the Puebla Valley aquifer: Integration of geophysical, hydrogeochemical and hydrogeological data in a volcano-sedimentary context

Tesis que presenta

Ana Beatriz Rubio Arellano

Para obtener el grado de

DOCTORA EN GEOCIENCIAS APLICADAS

asesorada por

Dr. José Alfredo Ramos Leal

Dra. Claudia Arango Galván

San Luis Potosí, S.L.P., Julio 2025

Constancia de aprobación de la tesis

La tesis **Hydrogeological study of the Puebla Valley aquifer: Integration of geophysical, hydrogeochemical and hydrogeological data in a volcano-sedimentary context** presentada para obtener el Grado de Doctor(a) en Geociencias Aplicadas fue elaborada por **Ana Beatriz Rubio Arellano** y aprobada el **07 de julio de 2024** por los suscritos, designados por el Colegio de Profesores de la División de **Geociencias Aplicadas** del Instituto Potosino de Investigación Científica y Tecnológica, A.C.

Dr. José Alfredo Ramos Leal
(Director de la tesis)

Dra. Claudia Arango Galván
(Codirector de la tesis)

Dra. Janete Morán Ramírez
(Asesor de la tesis)

Dra. Berenice Zapata Norberto
(Asesor de la tesis)

Dr. Oscar Guadalupe Almanza Tovar
(Asesor de la tesis)

Dr. Víctor Manuel Vázquez Báez
(Asesor de la tesis)

IPICYT

Créditos Institucionales

Esta tesis fue elaborada en la División de Geociencias Aplicadas del Instituto Potosino de Investigación Científica y Tecnológica, A.C., bajo la codirección de los doctores José Alfredo Ramos Leal y Claudia Arengo Galván.

Durante la realización del trabajo el autor recibió una beca académica del Consejo Nacional de Ciencia y Tecnología con No. de registro 818486 y del Instituto Potosino de Investigación Científica y Tecnológica, A. C.

(Página en Blanco que se va a utilizar para colocar la copia del acta de examen.)

Dedicatoria

Esta tesis está dedicada a mis padres y hermana, por su amor incondicional. Sin ellos, este sueño no habría sido posible. Gracias por acompañarme en este maravilloso camino que decidí recorrer.

Agradecimientos

Al Dr. José Alfredo Ramos Leal, por su invaluable guía a lo largo de este proceso. Agradezco su generosidad al compartir sus conocimientos y dedicación sin reservas. Su mentoría y amistad fortalecieron mi pasión por la investigación y convirtieron estos años de trabajo en una experiencia enriquecedora.

A la Dra. Claudia Arango Galván, por su invaluable apoyo en esta travesía académica. Sus comentarios y sugerencias enriquecieron sustancialmente este trabajo.

Al Dr. Víctor Manuel Vázquez Báez, por guiarme ininterrumpidamente en mi formación desde los primeros pasos en la licenciatura. Gracias por inspirar en mí una pasión duradera por la ciencia y por cultivar no solo mi mente, sino también una amistad que trasciende lo académico.

A la Dra. Berenice Zapata Norberto, por su invaluable mentoría durante el posgrado. Sus comentarios pertinentes y su apoyo constante crearon el espacio ideal para mi crecimiento académico.

A la Dra. Janete Morán Ramírez, por su invaluable dedicación a mi investigación y su acompañamiento en campo. Agradezco las productivas discusiones académicas que enriquecieron significativamente este proyecto.

Al Dr. Óscar Guadalupe Almanza Tovar, por sus valiosos comentarios y las preguntas críticas que enriquecieron sustancialmente mi investigación. Agradezco profundamente su disponibilidad constante para atender cada una de mis consultas.

Al M.C. David Ernesto Torres Gaytán, por su apoyo y disposición durante esta investigación. Su experiencia fue clave para la obtención e interpretación de los datos geofísicos, así como en el uso de software especializado. Agradezco su profesionalismo a lo largo del proceso.

A Bere, mi compañera de travesía doctoral, por contagiarme su entusiasmo inquebrantable, por ser ese oído siempre disponible en los momentos clave y por acompañarme en todo momento. Atesoro especialmente cómo enriqueció mi investigación con su mirada crítica y apoyo incondicional.

A mis amigos del instituto: Bere, Alexa, Karla, Fabián y Sebastian, porque esta trayectoria no habría sido igual sin sus risas, charlas y aventuras. A Carlos, que llegó como luz en el momento más arduo de mi formación. Gracias por tu cariño y paciencia, por escucharme y por ser el refugio donde siempre encontré oreja y corazón.

A mi Clau, mi mejor amiga. Gracias por cobijarme, cuidarme y hacer de mi estancia en SLP una experiencia inolvidable. Gracias por las charlas, por ser mi cómplice, por escucharme y animarme a alcanzar cada meta. Tu amistad ha sido uno de los regalos más valiosos en este camino.

A Luis Alberto, por estar siempre presente y cuidar de mi familia; por todas las porras y ánimos a lo largo de mi trayectoria académica, y por ser tan optimista y contagiarme con esa energía.

Al IPICYT, por las herramientas para mi formación como investigadora. El instituto moldeó mi perfil académico pero también me permitió encontar personas que enriquecieron mi trayectoria.

Contents

Abstract

In central Mexico, volcanic rocks and materials significantly influence the formation of aquifers in intermontane valleys. Consequently, many strategic aquifers for water supply develop in volcano-sedimentary contexts, where geological heterogeneity poses major challenges for their characterization and management. Such is the case of the Valle de Puebla aquifer, a complex system with intercalations of fractured volcanic materials and unconsolidated sedimentary deposits that directly influence groundwater recharge, storage, and quality.

This research addresses the comprehensive study of the VP aquifer through a multidisciplinary methodological strategy combining geophysical, hydrogeochemical, and hydrogeological methods. The central objective was to analyze the system's functioning by identifying both natural and anthropogenic processes - including intensive extraction, diffuse contamination, and land use change - which have transformed its behavior into a hydrosocial cycle where groundwater is profoundly influenced by human activities.

A conceptual aquifer model was developed within the hydrological cycle framework, serving as the basis for a numerical model capable of simulating response scenarios to both natural and anthropogenic pressures.

The results demonstrate that the Valle de Puebla aquifer functions as a multiphase system, where geological heterogeneity determines its storage capacity and flow patterns, while human pressures alter its natural equilibrium. The applied methodological integration not only answered the research question but also provides a replicable technical framework for managing aquifers in volcano-sedimentary environments, where subsurface complexity demands adaptive approaches.

KEYWORDS: Valle de Puebla Aquifer; Numerical Modeling; Conceptual Hydrogeological Model; Volcano-Sedimentary Setting; Hydrosocial Cycle.

Resumen

En la parte central de México, las rocas y material volcánico tienen una gran influencia en la formación de acuíferos en los valles intermontanos. De tal manera que muchos de los acuíferos estratégicos para el abastecimiento de agua se desarrollan en contextos volcano-sedimentarios, donde la heterogeneidad geológica representa un gran desafío para su caracterización y gestión. Tal es el caso del acuífero Valle de Puebla, un sistema complejo con intercalaciones entre materiales volcánicos fracturados y depósitos sedimentarios poco consolidados, que influyen directamente en la recarga, el almacenamiento y la calidad del agua subterránea.

Esta investigación aborda el estudio integral del acuífero VP mediante una estrategia metodológica multidisciplinaria que combina métodos geofísicos, hidrogeoquímicos e hidrogeológicos. El objetivo central fue analizar el funcionamiento del sistema mediante la identificación de procesos naturales y antropogénicos, como la extracción intensiva, la contaminación difusa y el cambio de uso de suelo, que han transformado su comportamiento hacia un ciclo hidrosocial, en el que el agua subterránea está profundamente influenciada por las actividades humanas.

Se construyó un modelo conceptual del acuífero dentro del ciclo hidrológico, el cual fungió como base para el desarrollo de un modelo numérico, capaz de simular escenarios de respuesta frente a presiones tanto naturales como antrópicas.

Los resultados evidencian que el acuífero del Valle de Puebla funciona como un sistema multifásico, donde la heterogeneidad geológica define su capacidad de almacenamiento y flujo, mientras que las presiones humanas alteran su equilibrio natural. La integración metodológica aplicada no solo permitió responder a la pregunta de investigación, sino que también ofrece un marco técnico replicable para la gestión de acuíferos en medios volcano-sedimentarios, donde la complejidad del subsuelo exige enfoques adaptativos.

PALABRAS CLAVE: Acuífero Valle de Puebla; Modelación numérica; Modelo hidrogeológico conceptual; Medio volcano-sedimentario; Ciclo hidrosocial.

Chapter 1

Introduction

Hydrogeology is the science that studies water movement through geological subsurface environments (Smith, 2015). Hydrogeological investigations utilize geological maps and water sample analysis, from both subsurface and surface sources to obtain detailed information about underground flows (Brassington, 2017). Specifically, hydrogeology focuses on aquifer systems and groundwater distribution.

The comprehensive study of groundwater flow employs key equations to quantify flow rates (Xu et al., 2012). These equations are fundamental for formulating mathematical and numerical simulation models, which are now routinely used as predictive tools for aquifer system responses to real-world conditions, such as pumping extractions (Jacob and Verruijt, 1987).

Groundwater constitutes an integral component of the hydrological cycle, a complex system governing planetary water circulation (McFarlane et al., 1993; Loaiciga et al., 1996). This cycle begins when solar energy evaporates ocean water to form cloud masses transported by global wind systems, later precipitating as rain, snow, or hail when atmospheric conditions permit. A portion of this precipitation accumulates on land, forming streams and rivers that ultimately return to the sea, restarting the process (Loaiciga et al., 1996).

Not all rainfall contributes to surface water flow; some returns to the atmosphere through evaporation from lakes/rivers, soil moisture, and plant transpiration. Water that successfully infiltrates the soil may reach the water table, flowing through rock formations before discharging into streams or rivers (Hornberger et al., 2014).

However, in the last decade, the need to recognize the hybrid nature of water and its interaction with society has emerged (Swyngedouw, 2006; Boelens et al., 2016). For this reason, the term hydrosocial cycle (Linton, 2008; Perrin, 2023) has become present, which serves as an important tool to analyze and understand the interconnection between water and society (Linton and Budds, 2014; Villar-Navascués and Arahuetes, 2020). This approach not only considers the physical and chemical characteristics of water, but also how these influence and are influenced by social and political dynamics. This perspective is particularly relevant in the Puebla Valley aquifer, where groundwater is the primary source of drinking water supply.

Over time, various investigations have been carried out to understand the dynamics of the Puebla Valley aquifer (Silva Pérez, 2003; Jiménez, 2005; Morales et al., 2015). Despite significant advances in hydrogeological knowledge, there are still gaps in the understanding of the system, especially regarding the mechanisms that control groundwater flow, the interactions between the physical and chemical properties of groundwater, characteristics of the deeper hydrogeological units, the quantification of recharge, and the effects of land use change. This underscores the need for deeper research and comprehensive analysis.

To address the problem in the current context, the aim is to monitor the Puebla Valley aquifer by integrating different methodologies to achieve a common objective: to carry out efficient hydrogeological evaluation studies that support decision-making related to the proper water management of this system.

To achieve this objective, it is proposed to employ the design of a conceptual hydrogeological model based on the integration of geological, hydrogeological and geophysical data, which reflects the reality of the system. MODFLOW from the USGS is also used as a predictive tool in the evaluation of the hydrodynamic functioning of the Puebla Valley aquifer.

Finally, the research aims to show the hydrogeochemical functioning of the PV aquifer, in order to conduct a comprehensive evaluation of water quality, both for human consumption and for agricultural use, which are the main demands in the study region. This will provide solid foundations to identify the areas of greatest aquifer vulnerability and understand their relationship with the geological environment, thus offering essential information for more effective and sustainable management of water resources in the region.

1.1 Justification

Research on the integration of disciplines for aquifer studies has become essential, particularly in regions where sustainable access to groundwater is crucial for population welfare. In the specific case of the PV aquifer, the lack of comprehensive understanding of its hydrogeological and hydrogeochemical dynamics poses significant challenges for the sustainable management of this vital resource.

This investigation not only addresses this gap but proposes a pioneering integration of geophysical, hydrogeochemical, and hydrogeological methods. Through this disciplinary synergy, we aim to develop a mathematical-numerical model to synthesize the acquired knowledge about this hydraulic system. This approach will enable not only a deeper understanding of the PV aquifer but also the capacity to effectively anticipate and manage changes in its dynamics.

By incorporating the hydrosocial dimension, we analyze how human activities (extraction, contamination, and land use changes) alter the groundwater cycle and, in turn, how these alterations impact communities dependent on the aquifer. Our model will evaluate management scenarios that consider both the aquifer's natural capacities and population demand requirements.

The multidisciplinary nature of our research allows us to unravel the complexity of the PV aquifer from a comprehensive perspective. We seek to understand sources/sinks, flows, and chemical signatures to project water stress scenarios and link these findings with potential solutions for more efficient water management.

Ultimately, this investigation aspires not only to fill knowledge gaps but to provide practical tools that significantly contribute to sustainable water resource management. By integrating quantitative models with adaptive solutions, our work represents a milestone in the comprehensive understanding of aquifers and their implications for populations, benefiting both the resource and the communities that depend on it.

1.2 Research Question

What natural or anthropogenic factors explain the sources, sinks, and chemical signature of groundwater in the Puebla Valley aquifer?

1.3 Hypothesis

Changes in water quality and quantity in the Puebla Valley aquifer result from the interaction between water-rock processes in the natural hydrological cycle and anthropogenic activities; where land use changes, irrigation return flows, and increased extraction rates have altered the natural hydrological balance, leading to contamination issues and declining groundwater levels.

1.4 Objectives

1.4.1 General Objective

Analyze the hydrological cycle functioning of the Valle de Puebla aquifer in terms of water quality and quantity, comparing natural hydrological cycle conditions with the hydrosocial cycle, and identifying changes induced by anthropogenic activities.

1.4.2 Specific Objectives and Goals

- Develop a conceptual model of the PV aquifer based on a regional hydrogeological framework, integrating the delineation of hydrogeological units through the Transient Electromagnetic Method.
- Quantify the influence of natural and anthropogenic factors on groundwater availability and quality in the Puebla valley.
- Assess the intrinsic vulnerability of the aquifer by adapting the DRASTIC methodology to a volcano-sedimentary environment and validating it with water quality indices for human use and consumption.
- Identify the hydrogeochemical processes occurring in the aquifer system to understand interactions with the geological environment and anthropogenic activities.
- Develop a regional hydrogeological model of the PV aquifer to simulate changes in groundwater levels and evaluate the hydrological response of the system to natural and anthropogenic stresses.

Chapter 2

Hydrogeochemical characterization and processes: Multivariate analysis

This research article was submitted to the journal *Environmental Science and Pollution Research* under the title *"Integrated assessment of hydrogeochemical processes and sources of contamination in the Puebla Valley aquifer: Multivariate analysis approach"*. The publication aimed to identify the hydrogeochemical processes affecting groundwater quality in the VP aquifer and classify it according to its chemical characteristics.

Seventy-one water extraction points were analyzed using a multivariate approach combining Principal Component Analysis (PCA) and Hierarchical Cluster Analysis (HCA) to simplify the complexity of hydrogeochemical data, reduce the number of variables, and detect hidden patterns.

The results distinguished five groundwater groups. Group 1 is characterized by good quality water with no evidence of anthropogenic contamination; Group 2 is associated with anthropogenic contamination influenced by wastewater from the Atoyac River and agricultural irrigation returns

Integrated assessment of hydrogeochemical processes and sources of contamination in the Puebla Valley aquifer: Multivariate analysis approach

Ana Beatriz Rubio-Arellano [†a], José Alfredo Ramos-Leal [*†a], Janete Morán-Ramírez [†b], Víctor Manuel Vázquez-Báez [†c]

[a] *División de Geociencias Aplicadas, Instituto Potosino de Investigación Científica y Tecnológica (IPICYT), Camino a la Presa de San José 2055, Lomas 4ta Secc., 78216, San Luis Potosí, México.*

[b] *Cátedras Conacyt, Instituto Potosino de Investigación Científica y Tecnológica (IPICYT), Camino a la Presa de San José 2055, Lomas 4ta Secc., 78216, San Luis Potosí, México.*

[c] *Facultad de Ingeniería, Benemérita Universidad Autónoma de Puebla (BUAP), Blvd. Valsequillo y Av. San Claudio s/n, Ciudad Universitaria, Col. Jardines de San Manuel, Puebla, 72570, Puebla, México.*

Abstract

This study aimed to characterize the hydrogeochemical processes affecting groundwater quality in the Puebla Valley aquifer and classify groundwater based on its chemical characteristics. Groundwater samples were analyzed using a multivariate approach that combines Principal Component Analysis (PCA) and Hierarchical Cluster Analysis (HCA) to simplify the complexity of hydrogeochemical data by reducing the number of variables and detecting hidden patterns, thereby facilitating the interpretation of large datasets and identification of contamination sources. The results of the multivariate analysis distinguished five groups in groundwater, each associated with different water qualities. Group 1 is characterized by good quality water without evidence of anthropogenic contamination; Group 2 is linked to anthropogenic contamination, influenced by wastewater from the Atoyac River and agricultural return flows; Group 3 exhibits signatures of industrial and urban waste contamination; Group 4 shows contamination from agricultural fertilizers; and Group 5 represents the highest anthropogenic contamination in the system. Each of the groups identified in the multivariate analysis reveals unique chemical characteristics and varying levels of contamination, prominently reflected in water-rock interaction diagrams and water groupings obtained through Alekin's classification.

Keywords: Multivariate statistical methods, Water-rock interaction, Groundwater quality, Alekin diagram, Hydrogeochemical characteristics

1. Introduction

Sustainable management of groundwater resources is necessary to ensure the supply of drinking water, agriculture, and industry, especially in regions with water stress (Singh et al., 2019; Zhang et al., 2020; Mukherje et al., 2021). Although changes in the quantity and quality of groundwater usually occur slowly, they are difficult to reverse (Zhang et al., 2023; Sadeghi-Lari et al., 2024); therefore, the hydrogeochemical characterization of aquifers is important to understand the natural and anthropogenic processes affecting groundwater quality and availability. The advantage of evaluating groundwater contamination is

* Corresponding author.

Email addresses: ana.rubio@ipicyt.edu.mx (Ana Beatriz Rubio-Arellano †), jalfredo@ipicyt.edu.mx (José Alfredo Ramos-Leal *†), janete.moran@ipicyt.edu.mx (Janete Morán-Ramírez †), manuel.vazquez@correo.buap.mx (Víctor Manuel Vázquez-Báez †)

[1] These authors contributed equally to this work.

that potential contaminant sources and areas at higher risk of contamination can be identified, leading to proper water resource management (Usman et al., 2025; Jimenez et al., 2025).

Various studies conducted in different parts of the world have shown that the deterioration of groundwater quality is attributed to overexploitation, increased use of fertilizers, unsanitary conditions in rural and urban areas, as well as inadequate water planning (Tong et al., 2021; Chaudhari et al., 2024; Zhang et al., 2025). Mexico, like many developing countries, faces increasing pressure on its water resources due to population growth, economic development, water quality degradation, and climate variability (Ortiz-Letechipia et al., 2021; Sheikh and Kolo, 2019; Sarkar et al., 2024).

The Puebla Valley aquifer (PV), located in central Mexico, is a clear example of this situation, where the demand for groundwater has intensified due to increasing surface water scarcity and the overexploitation of water resources (Rubio-Arellano et al., 2024). Considering that the PV aquifer is a vital source of water for the local population and economy, it is essential to understand the hydrogeochemical dynamics of the aquifer to develop effective management and conservation strategies to address the challenges of intensive exploitation and contamination in the system.

Traditional hydrogeological analysis methods, although valuable, often do not capture the complexity of interactions between the various variables that influence groundwater quality. To address this limitation, multivariate techniques such as Principal Component Analysis (PCA) (Chai et al., 2021; Taher et al., 2021; Zhang et al., 2023) and Hierarchical Cluster Analysis (HCA) have been applied.

PCA simplifies the complexity of hydrogeochemical data by reducing the number of variables and detecting hidden patterns, facilitating the interpretation of large datasets and the identification of contamination sources (Ahmad et al., 2024; Hamma et al., 2024; Patnaik et al., 2024). On the other hand, HCA organizes data into a dendrogram, which illustrates the relationships and similarities between samples. In the hydrogeochemical context, HCA allows for the identification of hydrochemically homogeneous zones and the differentiation of areas affected by different contamination processes or water-rock interactions, helping to delineate hydrogeochemical zones and make informed water resource management decisions (Owen et al., 2015; Arumugam et al., 2023; Liu et al., 2023; Khan et al., 2023). This technique is particularly useful for highlighting patterns and trends that are not evident through traditional analysis methods.

Previous studies have demonstrated the utility of PCA and cluster analysis in the characterization of aquifers in various regions of Mexico and around the world (Marín-Celestino et al., 2019; Zhang et al., 2021; Castillo et al., 2021; Krishan et al., 2023; Arıman et al., 2024). However, the application of these techniques in the metropolitan area has been limited (Sánchez et al., 2017). This study aims to fill this knowledge gap by providing a detailed characterization of the PV groundwater using PCA and HCA.

The main objective of this study is to integrate multivariate statistical techniques with hydrogeochemical methods to evaluate the effects of anthropogenic activities on the groundwater quality of the Valle de Puebla aquifer, a volcano-sedimentary system. The results provide a comprehensive assessment of groundwater quality in the PV aquifer and offer valuable insights for water resource management. Identifying distinct water groups and their potential contamination sources supports the development of targeted strategies for groundwater use and protection. Furthermore, the application of Alekin's classification complements the multivariate analysis results, enhancing the understanding of both geological and anthropogenic processes influencing the aquifer.

2. Study Area

2.1. Localization

Geopolitically, the Puebla Valley Aquifer (PV) is located between latitudes 18°54' - 19°01' N and longitudes 98°01'-98°39' W, covering an area of 2025 km^2. This aquifer is crossed by the Atoyac River, which is the main water collector in the study area. It originates in the high mountains of Iztaccíhuatl, on the borders of the states of Mexico and Puebla, and receives contributions from several tributaries, including the Tlahuapan, Turín, Otlati, Atotonilco, and San Jerónimo Rivers (Fig. 1). It adopts the name Atoyac after the confluence with the tributary rivers Tlahuapan and Turín.

The Zahuapan River, a tributary of the Atoyac River, originates in the Tlaxco mountain range, north of the city of Tlaxcala, and flows southward. After receiving contributions from the Jilotepec, San Juan, and Soledad rivers, it joins the Atoyac River. After the union of the Zahuapan and Atoyac rivers, the latter crosses the valley and collects wastewater from Puebla and nearby towns, finally discharging into the Manuel Ávila Camacho dam, where the incoming water is regulated and used for Irrigation District No. 30, Fig. 1.

The southwest-northwest portion (Sierra Nevada) and northeast portion (La Malinche) of the aquifer have a high index of wooded and mountainous areas, these areas are considered the main recharge zones; furthermore, the southeast part is covered by urban areas and the northeast portion by agricultural areas, reflecting the diversity in land use within the study area.

According to Rubio-Arellano et al. (2024), the agricultural areas of the Puebla valley show intensive use of fertilizers and chemical products, which has negatively impacted the quality of groundwater. The areas located south of the city of Puebla, where flows from the Sierra Nevada and La Malinche converge, present the most severe salinization problems. This condition is mainly associated with the return flow of irrigation water through the Atoyac River.

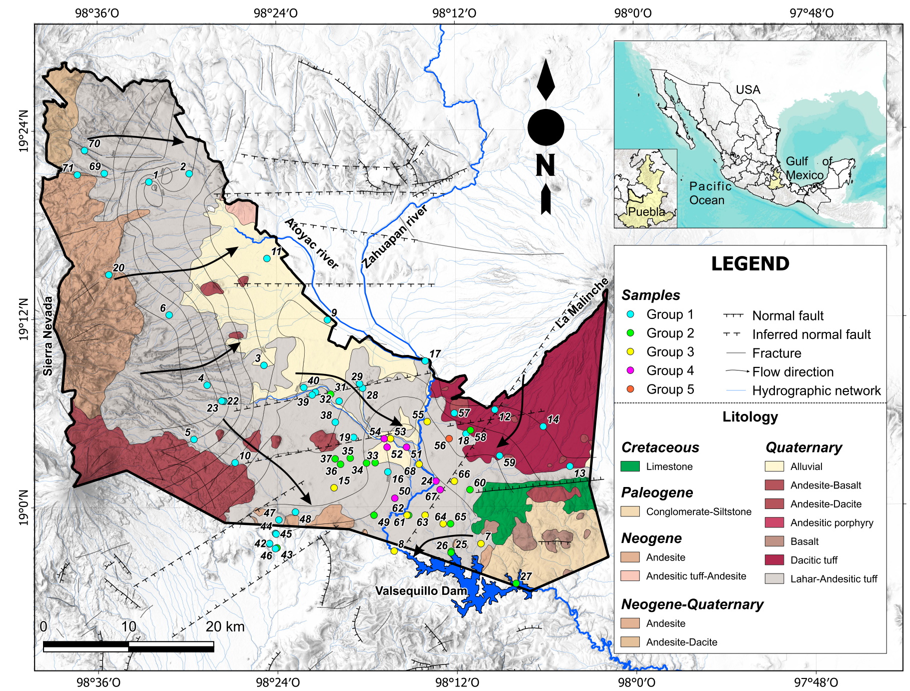

Fig. 1: Map showing the location of the PV aquifer, regional geology, groundwater sampling sites, and groundwater flow directions.

2.2. Hydrogeology

The PV aquifer is a hydrogeological system composed of three main aquifer units, characterized through transient electromagnetic soundings (TEM). Fig. 2a shows a WSW–ENE oriented profile approximately 18 km in length, located within the valley. The delineation of the shallow, intermediate, and deep aquifers was based on the electrical resistivity values identified for each unit. Units U1b, U2a-b, and U3a correspond to the aquifers, while unit U2c represents the confining layers between them. In contrast, unit Ua1 corresponds to the unsaturated surface volcano-sedimentary deposits. The Fig. 2b shows the spatial distribution of this aquifer system:

1. **Granular aquifer**, formed by Quaternary sedimentary and volcanic deposits. Its thickness ranges from a few meters (approximately 3 m) at the edges to up to 150 m in the central part of the valley. Most of the water in this unit corresponds to recent recharge.
2. **Intermediate aquifer**, characterized by the presence of sulfurous waters, is composed of volcanic rocks from the Pliocene to Oligocene (volcanic rocks and tuffs). Beneath the city of Puebla, its thickness ranges from 8 to 40 m, although in other areas it can average up to 200 m. This variation is associated with the presence of tectonic structures such as

faults, grabens, and horsts. Intensive groundwater pumping has led to a loss of pressure in this unit, favoring the gradual ascent of poor-quality water from deeper zones.

3. **Fractured aquifer**, located at greater depths (around 1000 masl), composed of Cretaceous marine formations, mainly limestones with a high degree of tectonic fracturing, which gives it significant secondary permeability. Although its thickness could not be determined using TEM soundings, it is inferred that the geological basement is composed of metamorphic schists.

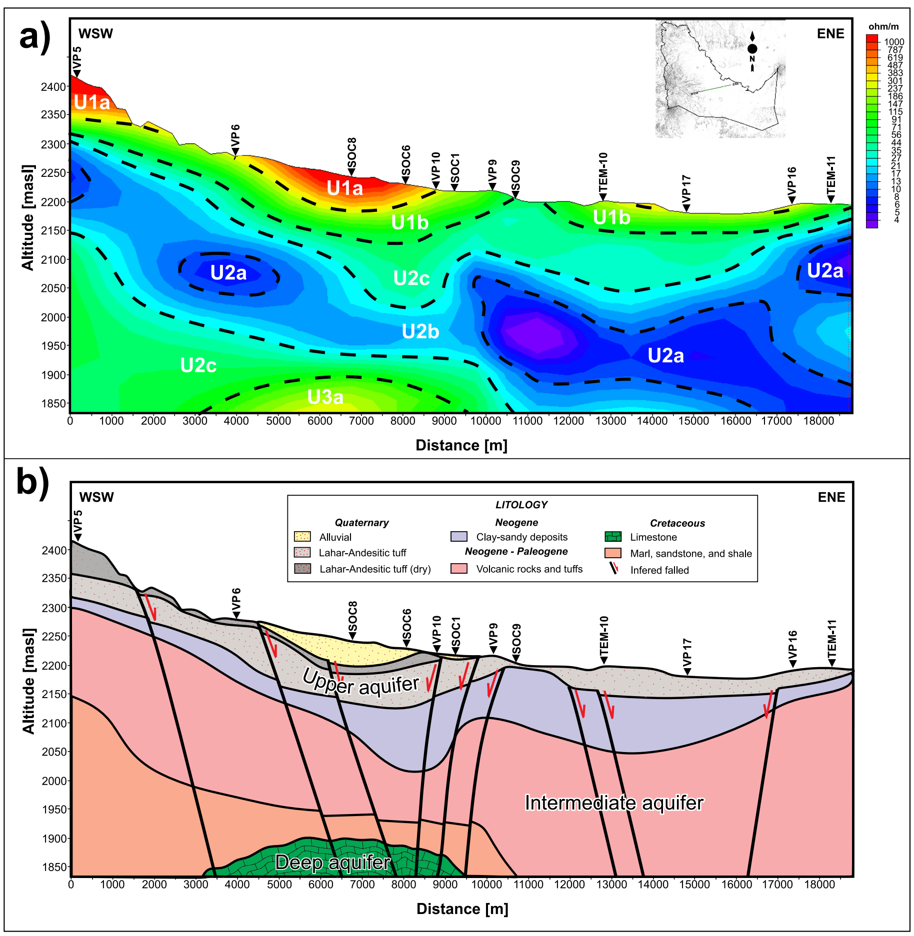

Fig. 2: Hydrogeological characterization of the PV aquifer. a) Geophysical profile obtained through TEM; b) Geological section showing the distribution of aquifer units and their confining layers.

The separation between the shallow and intermediate aquifers is defined by an aquitard composed of lacustrine clay-silt deposits. In contrast, an aquiclude made up of marls, sandstones, and shales separates the intermediate aquifer from the deep one.

3. Materials and methods

3.1. Water Samples

Groundwater samples were collected from 71 locations of wells and springs within the PV aquifer in December 2021, Fig. 1. High-quality sealed polyethylene bottles were used for sample collection, 120 ml for cation analysis, 60 ml for anions, 60 ml for trace elements, and 20 ml for organic matter. The anions and cations were analyzed in the laboratory of CGEO UNAM (National Autonomous University of Mexico).

Some physicochemical parameters were analyzed on-site using the Hanna HI 98194 multiparameter, these were Total Dissolved Solids (TDS), Electrical Conductivity (EC), Hydrogen potential (pH), and sample Temperature (Temp). Likewise, water alkalinity was measured in situ. For each of the collected samples, the Charge Balance Error method was applied (Liu et al., 2021; Dong et al., 2025), ensuring the accuracy of the analyzed samples. The majority of these exhibited CBE concentrations below 10%.

3.2. Hydrogeochemical characterization

The hydrogeochemical characterization of the PV aquifer was conducted using a combination of graphical and spatial analysis of the water's ionic composition through the use of GIS, multivariate statistical analysis, and hydrogeochemical diagrams. This approach allowed for a comprehensive understanding of groundwater quality and the geological and chemical processes influencing it.

Sampling spatially covered recharge, urban, and agricultural areas. Physicochemical parameters were measured in situ, and laboratory analysis determined the concentrations of cations and anions using ICP and colorimetry, respectively. Quality control procedures were also implemented to ensure result accuracy.

Subsequently, multivariate statistical analysis was performed on the data to ensure that each variable had equal weight in the analysis, and techniques such as hierarchical cluster analysis (HCA) and principal component analysis (PCA) were applied.

Finally, various hydrogeochemical diagrams such as Alekin, bivariate diagrams, Gibbs, among others, were used to classify water types and discuss interactions between the main ions in groundwater.

Maps were produced using QGIS software with data obtained from the Mexican Geological Service (SGM) and the National Institute of Statistics and Geography (INEGI). PCA and HCA were conducted using R statistical software, this program provides robust and flexible tools for the exploration and analysis of multivariate data, allowing for a detailed understanding of variable relationships and pattern identification in the data. Specific R packages such as 'stats' for PCA analysis and 'cluster' for HCA were used, following standard procedures for statistical analysis.

4. Results

4.1. General hydrochemistry

The Fig. 3 displays a longitudinal hydrogeochemical profile of the PV aquifer, showing the spatial distribution of pH, EC, TDS, and groundwater temperature. The data reveal significant variability in physicochemical properties, linked to lithological heterogeneity and groundwater flow dynamics. Table 1 presents the descriptive statistics of the physicochemical parameters and major ions of the PV aquifer.

Table 1: Descriptive statistics of the physicochemical parameters and major ions of the groundwater from the PV aquifer

Variable	Unit	Mean	STD	Min	Max
Temp	°C	20.72	3.18	10.40	31.35
pH	-	7.21	0.57	5.14	8.30
TDS	mg/L	478.96	501.48	30.00	2860.00
EC	µS/cm	777.37	688.25	50.00	3340.00
TH	mg/L	282.70	301.70	30.00	1407.00
HCO_3	mg/L	5.68	5.36	0.49	18.93
Cl	mg/L	0.57	0.67	0.00	3.03
SO_4	mg/L	1.59	2.76	0.02	15.82
NO_3	mg/L	0.65	1.82	0.00	8.76
Ca	mg/L	3.49	4.20	0.04	21.52
Mg	mg/L	2.62	2.27	0.27	9.03
Na	mg/L	1.83	1.60	0.22	5.91
K	mg/L	0.23	0.18	0.03	0.77
Fe	mg/L	0.15	0.47	0.00	2.52
Mn	mg/L	0.09	0.25	0.00	1.29

The pH values range from 5.2 to 8.3, with a mean value of 7.2. Groundwater temperatures vary from 10.4 to 31.4°C, with mean and standard deviation values of 20.7 and 3.2°C, respectively. Electrical conductivity ranges from 50 to 3340 mg/L, with a mean value of 777 mg/L and a standard deviation of 688 µS/cm. The total dissolved solids values range between 30 and 2860 mg/L, with a mean and standard deviation of 479 and 501.5 mg/L, respectively. The total hardness of water ranges from 30 to 1407 mg/L. The evolution of groundwater flow and the lithological characteristics of the aquifer modify the physical and chemical composition of the groundwater.

In the PV aquifer, there is no clear evolutionary trend in pH values. It is expected that recharge zones would exhibit acidic pH values; however, in the Sierra Nevada recharge zone, alkaline pH values are observed. This is because the samples collected correspond to upward-flowing vertical springs. The remaining recharge zones do show acidic values. In fractured volcanic rocks, recharge occurs more rapidly, resulting in lower pH values, whereas in sedimentary materials, pH tends to be higher due to low hydraulic conductivity, which enhances the solubility of chemical compounds from the minerals constituting the granular aquifer material. The sampled sites exhibit acidic pH levels, except for the springs, which have alkaline pH because they emerge from deep groundwater sources.

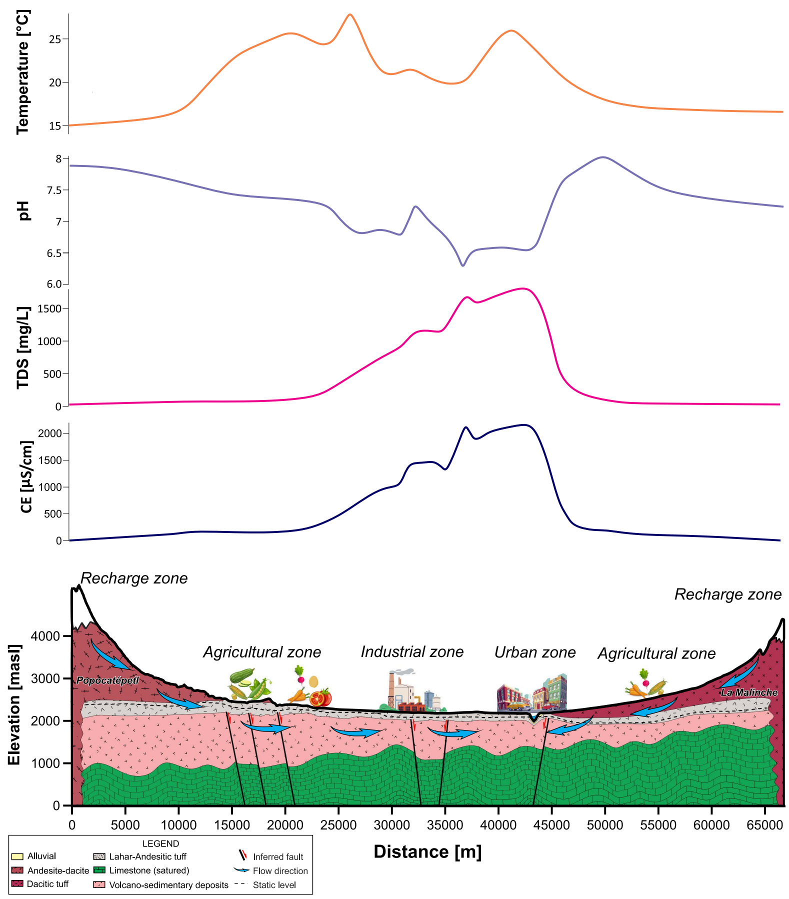

Fig. 3: Distribution of hydrogeochemical parameters in the PV aquifer: pH, EC, TDS, and temperature

The distribution of groundwater temperatures shows a homogeneous pattern, with the lowest values recorded in the recharge zones and higher values in the valley and discharge zones. Overall, the temperature suggests that there is no thermal activity in the shallow aquifer.

EC varies with the depth of the aquifer; shallower parts have lower conductivity compared to deeper parts. For the PV aquifer, a well-defined zone with low electrical conductivity is associated with the recharge areas of the system. In the foothills of the Sierra Nevada, conductivities range from 50 to 250 µS/cm, while on the side of La Malinche they range between 150 and 250 µS/cm. In the valley, where most of the wells are concentrated, conductivities vary from 250 to 500 µS/cm. In the urban area of Puebla city, conductivities range from 750 to 2000 µS/cm, gradually increasing towards the discharge zone; the highest EC values were detected near the Atoyac River. It is also possible to establish a relationship between EC and the flow direction. The Popocatépetl and Iztaccíhuatl volcanoes, as well as La Malinche, contribute a significant portion of the recharge to the aquifer, and the flow is directed towards the Atoyac River, then continues its course south of the city of Puebla.

4.2. Water Families

Based on the Alekin (1948) classification, the "Alekin diagram" was developed to represent and classify the groundwater of the PV aquifer based on its chemical composition. This diagram is useful for visualizing the relationships between different ions and better understanding the chemical nature of the water.

In Fig. 4, the classification of the groundwater from the PV aquifer is shown based on class, group, and type. The 45% of the samples are classified as magnesium bicarbonate waters, followed by 40% calcium bicarbonate waters, and 15% sodium bicarbonate waters.

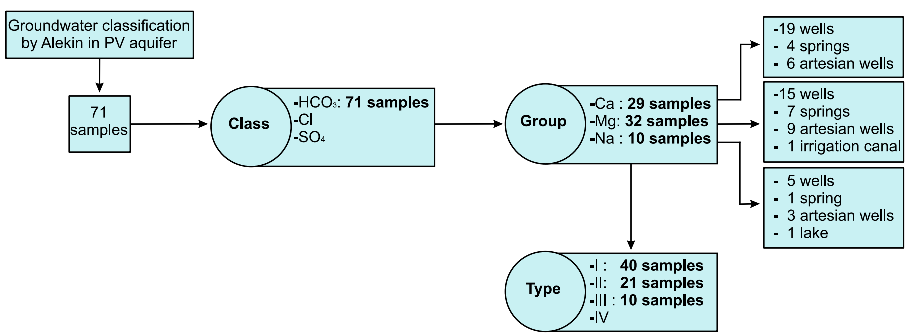

Fig. 4: Classification of water families in the PV aquifer by Alekin (1948).

4.3. Principal components analysis (PCA)

Multivariate statistical analysis using PCA was employed to study the characterization of the hydrogeochemical processes of the groundwater in the PV aquifer, with the aim of producing principal components that explain the different processes controlling the hydrogeochemical properties of the water, its origin, circulation, and distribution.

Thirteen variables were used, producing 13 orthogonal, uncorrelated factors, called principal components (PC). Factor loadings were also calculated to explain the contribution of the original variables, while factor scores show the observations converted into PC. The 13 variables were Temp, pH, TDS, HCO_3, Cl, SO_4, NO_3, Ca, Mg, Na, K, EC, and TH.

4.3.1. Correlation Analysis

From PCA, a Pearson correlation matrix was generated showing the correlation coefficient (r) between all variables. An $r \geq 0.5$ is considered significant, as shown in Table 2.

A strong positive correlation (greater than 80%) was observed between Ca and SO_4, Mg and HCO_3, Na and HCO_3, Ca and HCO_3, Na and Mg, Na and K, Mg and K, and Ca and Cl. The high positive correlation between TDS and other major ions (HCO_3, Cl, SO_4, Ca, Mg, Na, and K) is expected and commonly reported in groundwater studies, as is the case with EC and TH. Conversely, pH exhibits a negative correlation with most major elements, except for Cl, NO_3, Fe, and Mn.

The PCA diagonalizes the correlation matrix, thereby mitigating issues arising from differing units of measurement among the original variables, as all variables are automatically standardized during the process.

A strong positive correlation (greater than 80%) was observed between Ca and SO_4, Mg and HCO_3, Na and HCO_3, Ca and HCO_3, Na and Mg, Na and K, Mg and K, and Ca and Cl. The high positive correlation between TDS and other major ions (HCO_3, Cl, SO_4, Ca, Mg, Na, and K) is expected and commonly reported in groundwater studies, as is the case with EC and TH. Conversely, pH exhibits a negative correlation with most major elements, except for Cl, NO_3, Fe, and Mn.

The PCA diagonalizes the correlation matrix, thereby mitigating issues arising from differing units of measurement among the original variables, as all variables are automatically standardized during the process.

4.3.2. Determination of the number of factors

In PCA, determining the appropriate number of factors to retain is important to identify the underlying structure of hydrogeochemical data. There are different criteria to ensure an informed and robust selection (Jackson, 2005), such as explained variance (Jolliffe, 2002), breakpoint criterion (Cattell and Jaspars, 1967), Elbow Method (Cattell, 1996), Kaiser-Guttman criterion (Kaiser, 1960, 1961), Scree Analysis (Cattell, 1996), among others.

For this study, the Kaiser (1960) criterion was followed, which suggests retaining only those factors whose eigenvalues are greater than 1. In our research, the eigenvalues of the correlation matrix revealed that the first four factors surpassed this threshold, Fig. 5a, indicating that these components explain more variance than a single original variable. The factor loadings associated with these factors highlight the strongest correlations between the original variables and the extracted components.

Table 2: Correlation matrix of 15 physicochemical variables and major ions in the PV aquifer. Bold numbers indicate a significant correlation with $r \geq 0.9$, blue numbers indicate a correlation of $0.8 \leq r < 0.9$, purple numbers correspond to $0.5 \leq r < 0.8$, and red numbers indicate an inverse correlation.

	Temp	**pH**	**TDS**	**EC**	**TH**	**HCO_3**	**Cl**	**SO_4**	**NO_3**	**Ca**	**Mg**	**Na**	**K**	**Fe**	**Mn**
Temp	1														
pH	-0.34	1													
TDS	0.32	-0.62	1												
EC	0.34	-0.64	**0.96**	1											
TH	0.33	-0.61	**0.96**	**0.97**	1										
HCO_3	0.27	-0.59	0.86	**0.91**	**0.91**	1									
Cl	0.24	-0.46	0.84	0.83	0.82	0.71	1								
SO_4	0.35	-0.54	0.87	0.84	0.84	0.64	0.79	1							
NO_3	0.03	-0.04	0.00	0.06	-0.02	-0.10	-0.02	0.06	1						
Ca	0.32	-0.56	**0.94**	**0.93**	**0.94**	0.83	0.81	0.88	0.11	1					
Mg	0.29	-0.60	0.78	0.87	0.85	0.85	0.65	0.63	0.27	0.74	1				
Na	0.22	-0.53	0.72	0.81	0.75	0.84	0.71	0.56	0.03	0.63	0.83	1			
K	0.17	-0.51	0.63	0.70	0.68	0.76	0.55	0.41	0.22	0.58	0.82	0.83	1		
Fe	-0.34	0.21	-0.15	-0.18	-0.14	-0.14	-0.15	-0.08	-0.09	-0.14	-0.17	-0.15	-0.18	1	
Mn	0.00	-0.38	0.46	0.50	0.47	0.56	0.33	0.13	-0.11	0.30	0.56	0.61	0.63	-0.05	1

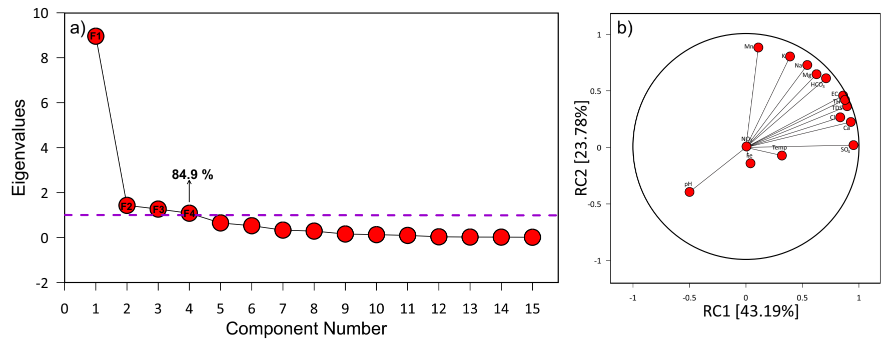

Fig. 5: Scree plot and component loading visualization. a) Scree plot showing the variance explained by the first three principal components; b) Scatter plot of principal component loadings.

4.3.3. Varimax Rotation

In Fig. 5a, four PCs accounting for 84.9% of the total variance are presented, which is sufficient to capture the main hydrogeochemical variations in the PV aquifer. To enhance the interpretability of these components, a Varimax orthogonal rotation was applied.

This technique redistributes the explained variance among the components (Xiao et al., 2019; Deng et al., 2025), maximizing factor loadings so that each variable loads strongly on a single component, thereby facilitating clearer interpretation. The Varimax rotation was carried out using R software, employing the 'psych' package for the analysis. The Varimax-rotated factor loadings for the 15 variables across the four principal components are shown in Table 3, with bold values indicating strong loadings (r$\geq$ 0.7).

The first rotated component (RC1) accounts for 43.19% of the total variance and groups TDS, EC, TH, HCO_3, Cl, SO_4, and Ca on the positive axis (Fig. 5b). The co-occurrence of these variables suggests that their concentrations tend to increase simultaneously. RC1 can be interpreted as representing water–rock interaction and mineral dissolution processes.

RC2 is primarily associated with Na, K, and Mn, and explains 23.78% of the total variance (Fig. 5b). This component likely reflects ion exchange processes and anthropogenic influences, particularly from agricultural activities and the return flow of irrigation water.

RC3 explains 10.12% of the total variance and exhibits a strong positive correlation with temperature and a negative relationship with Fe; that is, as iron concentrations increase, the contribution of RC3 decreases (Fig. 5b).

Finally, RC4 accounts for 7.82% of the variance and is strongly correlated with NO_3 (Table 3), indicating the influence of anthropogenic inputs in the mineralization of groundwater in the study area.

Table 3: Varimax rotated factor loading

	RC1	RC2	RC3	RC4
Temp	0.32	-0.07	**0.75**	-0.02
pH	-0.50	-0.39	-0.34	-0.01
TDS	**0.90**	0.36	0.12	-0.03
EC	**0.86**	0.46	0.15	0.04
TH	**0.88**	0.42	0.11	-0.03
HCO_3	**0.71**	0.61	0.11	-0.10
Cl	**0.83**	0.27	0.07	-0.03
SO_4	**0.95**	0.02	0.10	0.06
NO_3	0.00	0.01	0.04	**0.99**
Ca	**0.93**	0.22	0.11	0.09
Mg	0.62	0.65	0.14	0.27
Na	0.54	**0.73**	0.09	0.04
K	0.39	**0.80**	0.10	0.25
Fe	0.04	-0.14	-0.84	-0.07
Mn	0.11	**0.88**	-0.04	-0.17
Eigenvalue	8.96	1.43	1.26	1.08
Variability [%]	43.19	23.78	10.12	7.82
Cumulative [%]	43.19	66.96	77.08	84.90

4.3.4. Factor scores

Factor scores are numerical values calculated for each observation in the dataset and reflect the position of each case within the multidimensional space defined by the extracted factors (Tabachnick, 2013). These scores provide a means to represent individual samples according to the underlying structure identified through factor analysis (Sunkari et al., 2021; Abu et al., 2024). After applying Varimax rotation to improve factor interpretability, the factor scores were computed using R software. This step enables the projection of each original observation into the rotated factor space, facilitating the identification of spatial patterns and latent relationships among the hydrogeochemical variables.

4.3.5. Clustering in Factor Space

Clusters were computed in the factor space to identify natural groupings of observations in the reduced-dimensionality environment, enabling the detection of underlying hydrogeochemical patterns and structural relationships within the dataset. In this study, clustering was performed in R software using the K-means algorithm, a widely applied non-hierarchical method valued for its computational efficiency and conceptual simplicity (Uzcategui-Salazar and Lillo, 2023; Ghasempour and Kirca, 2025).

As shown in Fig. 6a, five distinct clusters were identified based on the factor scores. These clusters represent groups of groundwater samples with similar hydrogeochemical signatures, facilitating the interpretation of natural and anthropogenic processes influencing groundwater composition.

Fig. 6b presents the spatial distribution of the factor scores and their grouping into clusters, providing a visual means to assess the relationships among observations in the reduced factor space. Cluster 1 comprises 39 samples, including 11 springs and 28 wells. Cluster 2 includes 15 samples mainly located in agricultural zones of the study area. Cluster 3 groups 10 well samples primarily from the discharge zone and near the springs of the Atoyac River. Cluster 4 contains six samples, consisting of one sulfurous spring used for recreational purposes and five wells situated near the Atoyac River and industrial areas. Finally, Cluster 5 consists of a single deep well sample characterized by sulfurous, poor-quality water.

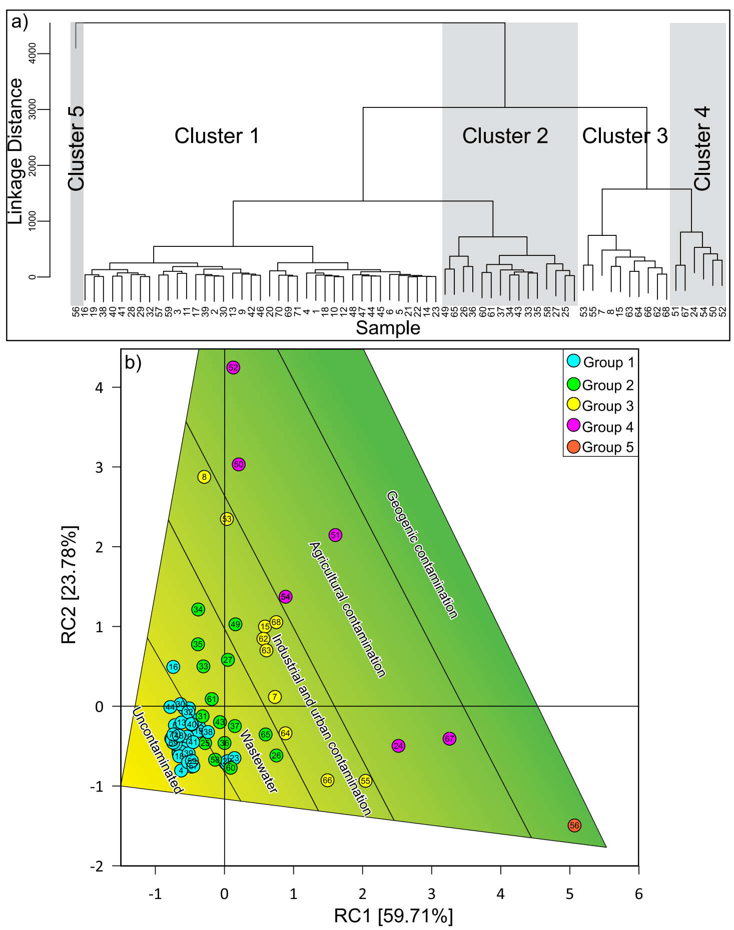

Fig. 6: Principal component analysis for dissolved trace elements in PV aquifer. a) Clusters identified in the factorial space; b) Plot of component rotated loadings in space.

5. Discussion of results

5.1. Water Families

According to Alekin's classification (Alekin, 1948), the waters of the PV aquifer fall into types I, II, and III, as shown in Fig. 7.

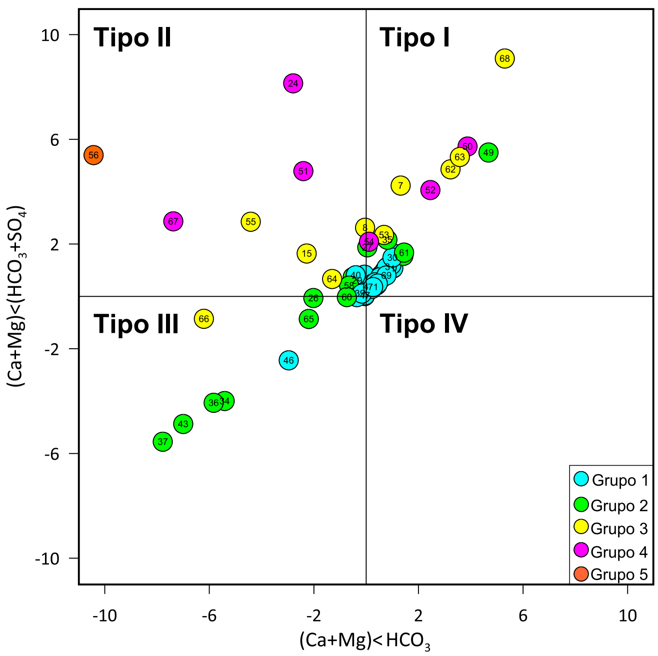

Fig. 7: Alekin diagram, for hydrogeochemical classification of groundwater. Type I: Recently infiltrated waters, belonging to recharge zones, with silicate alteration; Type II: Waters associated with sedimentary rocks or low mineralization; Type III: Highly mineralized waters, isolated waters, marine intrusions, or saline intrusions; Type IV: Waters with the absence of the HCO_3 ion, acidic waters

Type I waters (HCO_3 > Ca+Mg and HCO_3+SO_4 > Ca+Mg): Samples plotted near the origin (0,0) are associated with recently infiltrated waters and are primarily located in Sierra Nevada and La Malinche. These samples also indicate interaction with volcanic and carbonate rocks that contribute to their high HCO_3 content.

Type II waters (HCO_3 < Ca+Mg and HCO_3+SO_4 > Ca+Mg): These waters are related to contact with the clayey material of sedimentary rocks rich in sodium and magnesium minerals. The combination of high levels of HCO_3 and SO_4 compared to Ca and Mg suggests that the groundwater has significantly interacted with carbonated and sulfated rocks. The dissolution of these minerals has released bicarbonates and sulfates into the water, and possible ion exchange and precipitation processes have kept calcium and magnesium concentrations low.

Type III waters (HCO_3 + SO_4 < Ca+Mg and HCO_3+SO_4 < Ca+Mg): These are associated with highly mineralized waters. The high content of HCO_3 relative to Ca y Mg is lower than the content of HCO_3 and SO_4, suggesting that besides the dissolution of carbonates, there is a significant influence of sulfated minerals in the aquifer. The sulfates come from the dissolution of minerals like gypsum and anhydrite. In summary, the samples categorized as type III result from a greater dissolution of bicarbonates and sulfates, possibly accompanied by ion exchange processes and precipitation of secondary minerals.

5.2. Water-rock interaction processes

In Fig. 8a, the bivariate Na vs. Cl diagram is presented, highlighting the 1:1 relationship indicative of equivalent molar proportions of sodium and chloride. In the PV aquifer, an enrichment of sodium relative to chloride is observed, suggesting an excess of sodium attributable to ion exchange processes, where sodium ions replace calcium and magnesium ions in groundwater. Two distinct trend lines can be distinguished in this diagram, corresponding to different directions of groundwater flow.

Fig. 8b shows the bivariate diagram of Ca + Mg versus HCO_3 + SO_4, where a few samples align with carbonate dissolution, while the majority are associated with silicate weathering.

The first trend line corresponds to carbonate dissolution, indicating the dissolution of calcite and dolomite minerals in groundwater. This process is driven by water acidity generated by dissolved carbon dioxide (CO_2) interacting with carbonate rocks, leading to the release of Ca^{2+}, Mg^{2+}, and HCO_3^- ions into the water.

The second trend line relates to silicate weathering, resulting from the reaction between carbonic acid and silicate minerals, which releases Ca, Mg, Na, K, and SiO_2 into groundwater. Feldspars, abundant in the rhyolites and basalts comprising this volcanosedimentary aquifer, are a primary source of these ions. Deviations from the 1:1 line indicate ion exchange processes where Ca and Mg are exchanged from the water for Na adsorbed in the soil, as also illustrated in Fig. 8a.

Owen and Cox (2015) proposed the CCR index, which, combined with the $Cl/(Cl + HCO_3)$ ratio, enables analysis of the chemical evolution of groundwater (Fig. 8c). Generally, the PV aquifer shows a low $Cl/(Cl + HCO_3)$ ratio and a high CCR index value, indicating elevated concentrations of Ca and Mg relative to Na and K. This is consistent with the composition of the andesitic and basaltic rocks comprising the aquifer. The evolutionary pathway (indicated by the red arrow) illustrates the groundwater flow evolution, where sample 45 exhibits higher Ca and Mg content, representing local flow. This sample is the least evolved, with the shortest circulation time within the aquifer. As groundwater travels through the rock matrix, it evolves towards equilibrium by increasing its chloride content, making sample 46 the most evolved, which corresponds to a regional flow spring.

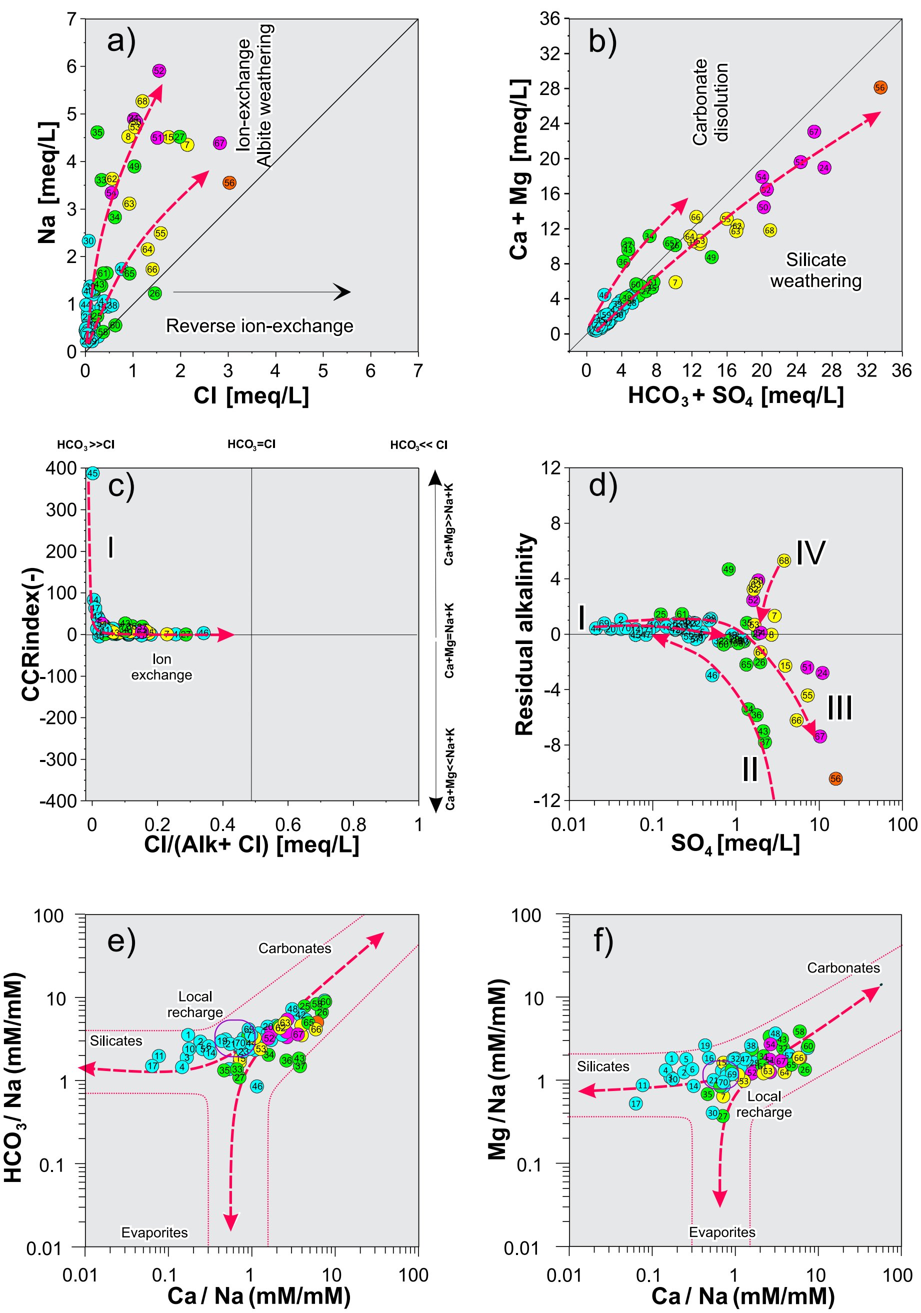

Fig. 8: Bivariate diagrams to identify sources and hydrogeochemical processes in the PV aquifer. a) Na^{+} vs Cl^{-}; b) Ca^{2+}+Mg^{2+} vs HCO_3^{-}+SO_4^{2-}; c) CCR index vs Cl^{-}/(Alk+Cl^{-}); d) Residual alkalinity vs SO_4^{2-}; e) HCO_3^{-}/Na^{+} vs Ca^{2+}/Na^{+}; f) Mg^{2+}/Na^{+} vs Ca^{2+}/Na^{+}

Residual alkalinity is a measure of water's capacity to neutralize acids and maintain stable pH levels (Sawyer et al., 2003; Appelo and Postma, 2005). In groundwater, this capacity is critical for protecting water quality and ensuring suitability for human consumption, agriculture, and industrial uses. Using this index, the relationship between Residual Alkalinity and SO_4 concentration was examined, as shown in Fig. 8d.

Overall, Fig. 8d shows four evolutionary paths. Paths I and III indicate initially low SO_4 content and balanced HCO_3 with Ca and Mg. Evolutionary path II shows areas with high SO_4 and low residual alkalinity, suggesting acidification from sulfide oxidation exceeding neutralization capacity. Path IV indicates high SO_4 with high residual alkalinity, meaning good neutralization despite sulfates. These samples relate to deep, sulfated flows, initially linked to carbonate mineral dissolution contributing bicarbonates and carbonates to the groundwater.

To estimate the sources of major ions in the PV aquifer, bivariate plots of the molar ratios HCO_3/Na vs. Ca/Na and Mg/Na vs. Ca/Na were employed (Gaillardet et al., 1999), as shown in Fig. 8e and Fig. 8f, respectively. These bivariate plots primarily identify silicate weathering and carbonate dissolution as the main processes controlling the groundwater chemistry. The geological formations in the study area mainly consist of basaltic-andesitic and occasionally dacitic materials, which serve as significant sources of silica. Starting from the recharge zone, and depending on the lithology present, groundwater follows at least three pathways (Morán-Ramírez et al., 2022): interaction with carbonates, interaction with silicates, or evaporation processes.

In Fig. 8e, a cluster of samples falls within the carbonate dissolution domain, indicating a high concentration of HCO_3 and Ca relative to Na. This reflects groundwater interaction with carbonate rocks, specifically limestone. Conversely, another group of samples lies in the silicate weathering domain, characterized by elevated HCO_3 and relatively low Ca compared to Na. The local recharge zone is also highlighted within a red oval, corresponding to samples with lower overall ion concentrations.

Additionally, Fig. 8f displays the Mg/Ca vs. Ca/Na relationship, reaffirming that silicate weathering and carbonate dissolution dominate the geochemical processes in the PV aquifer.

5.3. Relationship of Hydrogeochemical Processes with PCA Analysis

The bivariate diagrams used for hydrogeochemical characterization show distinctions among the five groups obtained from the PCA. Thus, it is associated that Group 1 is mostly related to recharge zones, both from Sierra Nevada and La Malinche, and consists of high-quality waters, being the only group that does not present evidence of anthropogenic contamination. Group 2 is classified as waters associated with anthropogenic contamination, resulting from wastewater from the Atoyac River and irrigation return flow. Group 3 is related to contamination from industrial and urban waste. Group 4 considers contamination from fertilizer use, as the samples within this group are spatially located in agricultural areas. Group 5, which includes only one sample, is distinguished by presenting high contamination levels resulting from surface runoff from the Atoyac River and wastewater discharge from industrial parks through geological faults. This water sample stands out from the other groups because it was obtained from a deep well (over 100 meters deep), as documented by Sánchez et al. (2017).

6. Conclusions

In this study, the chemical composition of groundwater and the factors controlling its evolution in recharge, agricultural, and urban areas were analyzed using multivariate statistical analysis and hydrogeochemical methods. Principal Component Analysis (PCA) and Hierarchical Cluster Analysis (HCA) were applied to assess the impact of human activities on groundwater chemistry. These tools enabled the classification of groundwater into five distinct groups, each characterized by specific chemical signatures and varying degrees of contamination, associated with both geogenic and anthropogenic processes.

Silicate weathering and carbonate dissolution were identified as the dominant water-rock interaction processes, influencing the concentrations of key ions such as HCO_3 Ca, Mg, and Na, and thus controlling the overall groundwater chemistry.

Group 1 is associated with recharge zones from Sierra Nevada and La Malinche and is characterized by high-quality water without signs of anthropogenic contamination, highlighting the importance of these areas as critical recharge zones. In contrast, Groups 2, 3, and 4 are affected by different contamination sources: Group 2 by wastewater from the Atoyac River and agricultural return flows, Group 3 by industrial and urban discharges, and Group 4 by fertilizers used in agriculture. Group 5, consisting of a single sample from a deep well, showed the poorest water quality, likely due to the combined effects of surface runoff from the Atoyac River and wastewater discharge from nearby industrial parks.

The classification of hydrochemical facies using the Alekin diagram, along with PCA and cluster analysis, provided comprehensive insights into the hydrogeochemical processes and anthropogenic impacts affecting groundwater. These results are essential for developing informed and sustainable groundwater management strategies in the PV aquifer.

References

Abu M, Zango MS, Kazapoe RW (2024) Controls of groundwater mineralization assessment in a mining catchment in the Upper West Region, Ghana: Insights from hydrochemistry, pollution indices of groundwater, and multivariate statistics. Innov Green Dev 3(1):100099. https://doi.org/10.1016/j.igd.2023.100099.

Ahmad S, Umar R, Ahmad I (2024) Assessment of groundwater quality using Entropy-Weighted Quality Index (EWQI) and multivariate statistical techniques in Central Ganga plain, India. Environ Dev Sustain 26(1):1615-1643. https://doi.org/10.1007/s10668-022-02776-8.

Alekin OA, (1948) General Hydrochemistry (Gidrometeoizdat). Leningrad.

Appelo CAJ, Postma D (2005) Geochemistry, groundwater and pollution. CRC Balkema, Rotterdam. https://doi.org/10.1201/9781439833544.

Arıman S, Soydan-Oksal NG, Beden N, Ahmadzai H (2024) Assessment of Groundwater Quality through Hydrochemistry Using Principal Components Analysis (PCA) and Water Quality Index (WQI) in Kızılırmak Delta, Turkey. Water 16(11):1570. https://doi.org/10.3390/w16111570.

Arumugam T, Kinattinkara S, Kannithottathil S, Velusamy S, Krishna M, Shanmugamoorthy M, Sivakumar V, Boobalakrishnan KV (2023) Comparative assessment of groundwater quality indices of Kannur District, Kerala, India using multivariate statistical approaches and GIS. Environ Monit Assess 195(29). https://doi.org/10.1007/s10661-022-10538-2.

Castillo J, Ramos-Leal JA, Martínez-Cruz DA, Cervantes-Martínez A, Marín-Celestino AE (2021) Identification of the dominant factors in groundwater recharge process, using multivariate statistical approaches in a semi-arid region. Sustainability 13(20):11543. https://doi.org/10.3390/su132011543.

Cattell RB (1996) The scree test for the number of factors. Multivariate Behav Res 1(2):245–276. https://doi.org/10.1207/s15327906mbr0102_10.

Cattell RB, Jaspars JMF (1967) A General Plasmode (no. 30-10-5-2) for Factor Analytic Exercises and Research. (No. 67).

Chai N, Yi X, Xiao J, Liu T, Liu Y, Deng L, Jin Z (2021) Spatiotemporal variations, sources, water quality and health risk assessment of trace elements in the Fen River. Sci Total Environ 757:143882. https://doi.org/10.1016/j.scitotenv.2020.143882.

Chaudhari MP, George A, Sanyal M, Shrivastav PS (2024). Hydrochemistry and groundwater quality assessment of Gujarat, India: A compendious review. Phys Chem Earth (Pt A B,C) 135:103635. https://doi.org/10.1016/j.pce.2024.103635.

Deng Y, Lu Y, Du X, Ye X, Feng J (2025) Identifying spatial patterns and driving factors of anthropogenic impacts on the groundwater environment based on groundwater chemical kinetics. J Clean Prod 486:144436. https://doi.org/10.1016/j.jclepro.2024.144436.

Dong F, Yin H, Yang Z, Zhou W, Cheng W, Liu Y (2025) Delineating the controlling mechanisms of geothermal waters quality and suitability zoning in the Lower Yellow River Basin, China. Environ Technol Innov 38:104126. https://doi.org/10.1016/j.eti.2025.104126.

Gaillardet J, Dupré B, Louvat P, Allegre CJ (1999). Global silicate weathering and CO_2 consumption rates deduced from the chemistry of large rivers. Chem Geol 159(1-4):3–30. https://doi.org/10.1016/S0009-2541(99)00031-5.

Ghasempour R, Kirca VSO (2025) Spatiotemporal assessment of groundwater quality under climate change using multiscale clustering technique. Groundw Sustain Dev 28:101407. https://doi.org/10.1016/j.gsd.2025.101407.

Hamma B, Alodah A, Bouaicha F, Bekkouche MF, Barkat A, Hussein EE (2024) Hydrochemical assessment of groundwater using multivariate statistical methods and water quality indices (WQIs). Appl Water Sci 14:33. https://doi.org/10.1007/s13201-023-02084-0.

Jackson JE (2005). A user's guide to principal components. John Wiley & Sons.

Jimenez JI, Tripathi NK, Pandey A, Chao KC, Shrestha S (2025) Assessment of the spatiotemporal dynamics of river discharge and groundwater recharge to support sustainable water management for irrigated agriculture in the Padsan river watershed. Earth Sci Inform 18(2):1-21. https://doi.org/10.1007/s12145-025-01707-1.

Jolliffe IT (2002) Principal component analysis for special types of data. Springer New York, pp. 338-372.

Kaiser HF (1960) The application of electronic computers to factor analysis. Educ Psychol Meas 20(1):141–151. https://doi.org/10.1177/001316446002000116.

Kaiser HF (1961) A note on Guttman's lower bound for the number of common factors. Br J Stat Psychol. https://doi.org/10.1111/j.2044-8317.1961.tb00061.x.

Khan MYA, ElKashouty M, Khan N, Subyani AM, Tian F (2023) Spatio-temporal evaluation of trace element contamination using multivariate statistical techniques and health risk assessment in groundwater, Khulais, Saudi Arabia. Appl Water Sci 13:123. https://doi.org/10.1007/s13201-023-01928-z.

Krishan G, Bhagwat A, Sejwal P, Yadav BK, Kansal ML, Bradley A, Singh S, Sharma LM, Muste M (2023) Assessment of groundwater salinity using principal component analysis (PCA): a case study from Mewat (Nuh), Haryana, India. Environ Monit Assess 195(37). https://doi.org/10.1007/s10661-022-10555-1.

Liu F, Zhang J, Wang S, Zou J, Zhen P (2023) Multivariate statistical analysis of chemical and stable isotopic data as indicative of groundwater evolution with reduced exploitation. Geosci Front 14(1):101476. https://doi.org/10.1016/j.gsf.2022.101476.

Liu J, Gao Z, Zhang Y, Sun Z, Sun T, Fan H, Wu B, Li M, Qian L (2021) Hydrochemical evaluation of groundwater quality and human health risk assessment of nitrate in the largest peninsula of China based on high-density sampling: A case study of Weifang. J Clean Prod 322:129164. https://doi.org/10.1016/j.jclepro.2021.129164.

Marín-Celestino AE, Ramos-Leal JA, Martínez-Cruz DA, Tuxpan-Vargas J, De-Lara-Bashulto J, Morán-Ramírez J (2019) Identification of the Hydrogeochemical Processes and Assessment of Groundwater Quality, Using Multivariate Statistical Approaches and Water Quality Index in a Wastewater Irrigated Region. Water 11(8):1702. https://doi.org/10.3390/w11081702.

Morán-Ramírez J, Ramos-Leal JA, Fuentes-Rivas RM, Arango-Galvan C, Fonseca-Montes de Oca RMG, Marín-Celestino AE, Sandoval-Montes IC (2022) Hydrogeochemical processes in aquifers of volcano-sedimentary origin using inverse modeling. J. S Am Earth Sci 117:103888. https://doi.org/10.1016/j.jsames.2022.103888.

Mukherjee A, Scanlon BR, Aureli A, Langan S, Guo H, McKenzie A (2021). Global groundwater: from scarcity to security through sustainability and solutions. In: Mukherjee, A., Scanlon, B.R., Aureli, A., Langan, S., Guo, H., McKenzie, A.A. (Eds.), Glob. Groundwater. Elsevier, pp. 3-20. https://doi.org/10.1016/B978-0-12-818172-0.00001-3.

Ortiz-Letechipia J, González-Trinidad J, Júdez-Ferreira HE, Bautista-Capetillo C, Dávila-Hernández S (2021) Evaluation of groundwater quality for human consumption and irrigation in relation to arsenic concentration in flow systems in a semi-arid Mexican region. Int J Environ Res Public Health 18(15):8045. https://doi.org/10.3390/ijerph18158045.

Owen DD, Cox ME (2015) Hydrochemical evolution within a large alluvial groundwater resource overlying a shallow coal seam gas reservoir. Sci Total Environ 523:233–252. https://doi.org/10.1016/j.scitotenv.2015.03.115.

Owen DD, Raiber M, Cox ME (2015) Relationships between major ions in coal seam gas groundwaters: Examples from the Surat and Clarence-Moreton basins. Int J Coal Geol 137:77-91. https://doi.org/10.1016/j.coal.2014.11.004.

Patnaik M, Tudu C, Bagal DK (2024). Monitoring groundwater quality using principal component analysis. Appl Geomat 16:281–291. https://doi.org/10.1007/s12518-024-00552-z.

Rubio-Arellano AB, Ramos-Leal JA, Morán-Ramírez J, Vázquez-Báez VM (2024). Geogenic and anthropogenic factors influencing groundwater quality for irrigation purposes from a volcano-sedimentary aquifer in the Puebla State, Mexico. Environ Sci Pollut Res 31:61576–61591. https://doi.org/10.1007/s11356-024-35346-8.

Sadeghi-Lari A, Bahrami M, Dastandaz T (2024) Temporal and spatial variations of groundwater quantity and quality for drinking and irrigation purposes in the arid and hot weather of Southern Iran. Phys Chem Earth (Pt A B,C). 134:103582. https://doi.org/10.1016/j.pce.2024.103582.

Sánchez ERS, Hoyos SEG, Esteller MV, Morales MM, Astudillo AO (2017) Hydrogeochemistry and water-rock interactions in the urban area of Puebla Valley aquifer (Mexico). J Geochem Explor 181:219-235. https://doi.org/10.1016/j.gexplo.2017.07.016.

Sarkar SK, Alshehri F, Shahfahad, Rahman A, Pradhan B, Shahab M (2024) Mapping groundwater potentiality by using hybrid machine learning models under the scenario of climate variability: a national level study of Bangladesh. Environ Dev Sustain 1-29. https://doi.org/10.1007/s10668-024-04687-2.

Sawyer CN, McCarty PL, Parkin GF (2003) Chemistry for environmental engineering and science. McGraw-Hill.

Sheikh MS, Kolo K (2024) Environmental impacts of a sprawling rural city on drinking water supply and quality in view of population growth prognostics and climate changes: a case study. Sustain Water Resour Manag 10(1):40. https://doi.org/10.1007/s40899-023-01002-1.

Singh A, Saha D, Tyagi AC (2019) Emerging Issues in Water Resources Management: Challenges and Prospects. In: Singh, A., Saha, D., Tyagi, A.C. (Eds.), Water Governance: Challenges and Prospects. Springer Water. Springer Singapore, Singapore, pp. 1-23. https://doi.org/10.1007/978-981-13-2700-1_1.

Sunkari ED, Abu M, Zango MS (2021) Geochemical evolution and tracing of groundwater salinization using different ionic ratios, multivariate statistical and geochemical modeling approaches in a typical semi-arid basin. J Contam Hydrol 236:103742. https://doi.org/10.1016/j.jconhyd.2020.103742.

Taher MES, Ghoneium AM, Hopcroft RR, ElTohamy WS (2021) Temporal and spatial variations of surface water quality in the Nile River of Damietta Region, Egypt. Environ Monit Assess 193(3). https://doi.org/10.1007/s10661-021-08919-0.

Tong S, Li H, Tudi M, Yuan X, Yang L (2021) Comparison of characteristics, water quality and health risk assessment of trace elements in surface water and groundwater in China. Ecotoxicol Environ Saf 219:112283. https://doi.org/10.1016/j.ecoenv.2021.112283.

Usman AG, Jibrin AM, Mati S, Abba SI (2025) Evidential-bio-inspired algorithms for modeling groundwater total hardness: A pioneering implementation of evidential neural network for feature selection in water resources management. J Environ Chem Ecotoxicol 7:494–505. https://doi.org/https://doi.org/10.1016/j.enceco.2025.02.012.

Uzcategui-Salazar M, Lillo J (2023) Assessment of social vulnerability to groundwater pollution using K-means cluster analysis. Environ Sci Pollut Res 30(6):14975–14992. https://doi.org/10.1007/s11356-022-22810-6.

Xiao J, Wang L, Deng L, Jin Z (2019) Characteristics, sources, water quality and health risk assessment of trace elements in river water and well water in the Chinese Loess Plateau. Sci Total Environ 650:2004–2012. https://doi.org/10.1016/j.scitotenv.2018.09.322.

Zhang B, Hu X, Yang Y, Deng X, Li B, Gong X, Xiang X, Cai X, Liu T (2025) Comprehensive evaluation of groundwater quality in population-dense and extensive agricultural regions and study on its relationship with agricultural production and human activities. Environ Geochem Health 47(3);1-23. https://doi.org/10.1007/s10653-025-02364-5.

Zhang D, Sial MS, Ahmad N, Filipe AJ, Thu PA, Zia-Ud-Din M, Caleiro AB (2020) Water Scarcity and Sustainability in an Emerging Economy: A Management Perspective for Future. Sustainability 13(1):144. https://doi.org/10.3390/su13010144.

Zhang J, Chen L, Li J, Chen Y, Ren X, Shi X (2021) Analysis of mining effects on the geochemical evolution of groundwater, Huaibei coalfield, China. Environ Earth Sci 80:(98). https://doi.org/10.1007/s12665-021-09399-8.

Zhang J, Zhou J, Chen Y, Wei X, Zeng Y, Sun Y (2023) Identifying the factors controlling surface water and groundwater chemical characteristics and irrigation suitability in the Yarkant River Basin, northwest China. Environ Res 223:115452. https://doi.org/10.1016/j.envres.2023.115452.

Chapter 3

Groundwater quality for agricultural use

This research article was published in the journal *Environmental Science and Pollution Research* under the title *"Geogenic and anthropogenic factors influencing groundwater quality for irrigation purposes from a volcano-sedimentary aquifer in Puebla State, Mexico"*.

The publication aimed to investigate the hydrogeochemical characteristics and water quality of the VP aquifer, a volcano-sedimentary system predominantly influenced by water-rock interactions and ion exchange processes.

The research evaluates the suitability of groundwater for agricultural irrigation by applying various water quality indices, including salinity and sodicity indices, as well as Wilcox and USSL diagrams. For this purpose, 71 water extraction points were analyzed, measuring physicochemical parameters and ionic concentrations of the water, which allowed identification of the main hydrogeochemical facies: HCO_3-Mg and HCO_3-Ca.

The results indicate an increased risk of salinization, particularly in agricultural and urban areas, highlighting the need for continuous monitoring. Natural processes, such as water-rock interaction and ion exchange, are the main factors influencing groundwater quality. However, anthropogenic activities, particularly fertilizer use and irrigation return flows from the Atoyac River, contribute significantly to water quality degradation. This study emphasizes the need for sustainable water resource management to ensure long-term aquifer viability.

Environmental Science and Pollution Research (2024) 31:61576–61591
https://doi.org/10.1007/s11356-024-35346-8

RESEARCH ARTICLE

Geogenic and anthropogenic factors influencing groundwater quality for irrigation purposes from a volcano-sedimentary aquifer in the Puebla State, Mexico

Ana Beatriz Rubio-Arellano[1] · José Alfredo Ramos-Leal[2] · Janete Morán-Ramírez[3] · Víctor Manuel Vázquez-Báez[4]

Received: 25 April 2024 / Accepted: 14 October 2024 / Published online: 21 October 2024

Abstract
This study investigates the hydrogeochemical characteristics and water quality of the Puebla Valley aquifer, a volcano-sedimentary system predominantly influenced by water-rock interactions and ion exchange processes. The research assesses the suitability of groundwater for agricultural irrigation by applying various water quality indices, including salinity and sodicity indices and Wilcox diagrams and USSL. Seventy-one water samples were analyzed to determine key physicochemical parameters and dominant ion concentrations, revealing that the primary hydrogeochemical facies are HCO_3-Mg and HCO_3-Ca. The results indicate a heightened risk of salinization, particularly in agricultural and urban areas, underscoring the need for ongoing monitoring. Natural processes such as water-rock interaction and ion exchange are the main factors influencing groundwater quality. However, anthropogenic activities, particularly the use of fertilizers and irrigation return flows from the Atoyac River, exacerbate groundwater quality degradation. This study emphasizes the necessity of sustainable water resource management to ensure the long-term viability of the aquifer.

Keywords Water Quality Index · Irrigation water · Salinity · Volcano-sedimentary aquifer · Hydrogeochemical facies · Chloro-alkaline index · Anthropogenic contamination

Introduction

Groundwater quality, encompassing physical, chemical, and biological attributes, is crucial for sustaining ecosystems and supporting human activities (Votruba and Corman 2020; Bozorg-Haddad et al. 2021). As the global population grows and urban areas expand, the importance of managing water quality becomes increasingly evident (Zhao et al. 2013; Gao et al. 2020). Water, being a potent solvent, has a unique capacity to dissolve various chemicals, which is particularly significant in groundwater as it flows through soil and rocks (Ossai et al. 2020; Subba Rao et al. 2024).

Numerous studies have shown that water quality is influenced by both natural and anthropogenic factors, such as weathering of bedrock, atmospheric deposition, evapotranspiration, and the decomposition of organic matter (Zemunac et al. 2021; Shi 2023; Yang et al. 2023; Gao et al. 2024; Vranešević et al. 2024). Furthermore, point and non-point sources of contamination, including wastewater discharges, industrial activities, and agricultural practices, pose significant challenges for the management and conservation of water resources (Ayub et al. 2019; Motevalli et al. 2019; Mosthaf et al. 2024).

Agriculture is a major water consumer, using about 70% of the world's extracted water. In OECD countries, over 40% of water is allocated to agriculture, while in Mexico, 75.7% of water resources go to this sector, with 62.9% from surface water and 37.1% from groundwater (CONAGUA 2023). Mexico faces challenges in balancing water demands for drinking, agriculture, and industry, especially in arid regions, leading to over-exploitation of groundwater, declining water levels, and deteriorating quality. The Puebla Valley (PV)

Responsible editor: Xianliang Yi

Ana Beatriz Rubio-Arellano, José Alfredo Ramos-Leal, Janete Morán-Ramírez, and Víctor Manuel Vázquez-Báez contributed equally to this work

Extended author information available on the last page of the article

aquifer, a vital source for various activities, is especially crucial given the scarcity of surface water in the semi-arid region, and urban expansion in the area further pressures its water resources.

In accordance with the Registry of Water Rights of the year 2018, the increasing demand for water resources is evident in the distribution of registered wells, with 21% allocated for human consumption, 42.2% for agricultural use, and 16.5% for industrial purposes. Water quality indices serve as valuable tools for detecting potential threats to a water system's quality, contributing to more effective water resource management. Notably, the Water Quality Index (WQI) is a widely recognized method used to comprehensively evaluate the overall water quality in a given area (RamyaPriya and Elango 2018; Marín Celestino et al. 2019; Kothari et al. 2021).

The assessment of irrigation water quality is an intricate undertaking due to its dependence on a multitude of factors. These factors encompass the chemical composition of the water, the distinctive characteristics of the soil and subsoil, the prevailing regional climate, the diversity of cultivated crops, and the various drainage management systems in place (Ayenew et al. 2013; Dinka 2016). This complexity is particularly pertinent in the PV aquifer, where agriculture stands as a primary economic activity.

In the PV aquifer, assessing water quality for agricultural purposes is essential due to the region's reliance on agriculture as a key economic activity. A thorough evaluation of groundwater quality has been carried out, focusing on various water quality indices, including salinity, sodium levels, and potentially harmful ions like NO_3 and SO_4.

This article aims to assess water quality for agricultural use, employing salinity and sodicity indices, and to identify the factors responsible for groundwater quality evolution in the PV aquifer. By achieving these objectives, decision-makers will be provided with valuable information so that the regional water resource can be managed efficiently and used in a sustainable manner. The novelty of this research lies in its ability to identify and differentiate the main natural and anthropogenic processes that modify water quality in the PV aquifer.

Materials and methods

Study area

The PV aquifer is situated in the extreme western region of the state of Puebla, sharing borders with the states of Mexico and Tlaxcala (Fig. 1). Encompassing an area of approximately 2025 km^2, the aquifer lies within the Trans-Mexican Neovolcanic Axis physiographic province, specifically the "Lagos y Volcanes de Anáhuac" sub-province. This region boasts a diverse geological landscape, featuring volcanic formations like Popocatépetl and Iztaccíhuatl, alongside alluvial and lacustrine plains.

The PV aquifer is of the volcano-sedimentary type; therefore, it presents heterogeneity and anisotropy. According to CONAGUA (2020), it is classified as an unconfined aquifer but also presents local semiconfined conditions due to the presence of lacustrine deposits. The valley area is located at 2000 ms above sea level (masl), with the Sierra Nevada to the west reaching altitudes of 5500 masl, and La Malinche to the northeast with an altitude of 4467 masl.

Hydrologically, the PV aquifer is part of Hydrological Region No. 18, within the Balsas River Basin, specifically in the Atoyac River Basin. The Atoyac River is the primary drainage system of the area, originating in Sierra Nevada, around 4000 ms above sea level (Fig. 1). Along its course, the river receives tributaries such as the Tlahuapan and Turín rivers. After merging with the Zahuapan River, the Atoyac enters the city of Puebla, where it receives additional inflows, including wastewater. The river ultimately flows into the Manuel Ávila Camacho Dam, where its water is regulated for irrigation in Irrigation District No. 30.

Hydrogeological framework

The geological column of the study area includes extrusive sedimentary and igneous rocks ranging from the Cretaceous to Recent periods, distributed within the metavolcanic-sedimentary sequence of the Guerrero Terrain. The geological map shows various surface units, including Oligocene volcanic formations, Miocene volcanic complexes, Lower Pliocene volcanic units, Middle Pliocene lacustrine deposits, Upper Pliocene volcanic units referred to as "Sierras Menores," and Plio-Pleistocene vulcanites with extensive pyroclastic fans (Fig. 1). Pleistocene volcanic units and vulcanites from the Chichinautzin group, extending eastward to the Puebla basin, act as natural barriers, preventing the flow of alluvial and lacustrine deposits into the Puebla basin.

Recharge zones for both surface and groundwater components of the PV aquifer are primarily influenced by the Iztaccíhuatl, La Malinche, and Popocatépetl volcanoes (Fig. 1). The upper section of the aquifer consists of unconsolidated alluvial materials, gravel, and sand, with an average thickness of 130 ms and medium to high permeability. The lower section comprises fractured extrusive igneous rocks, such as basalts and andesites, extending over several hundred meters, underlain by calcareous rocks considered the hydrogeological basement of the basin.

Static water levels exceed 150 ms in the mountainous areas of Sierra Nevada and La Malinche. In contrast, in the central valley, water levels are only a few meters below the land surface (30 ms), leading to significant water loss through evapotranspiration.

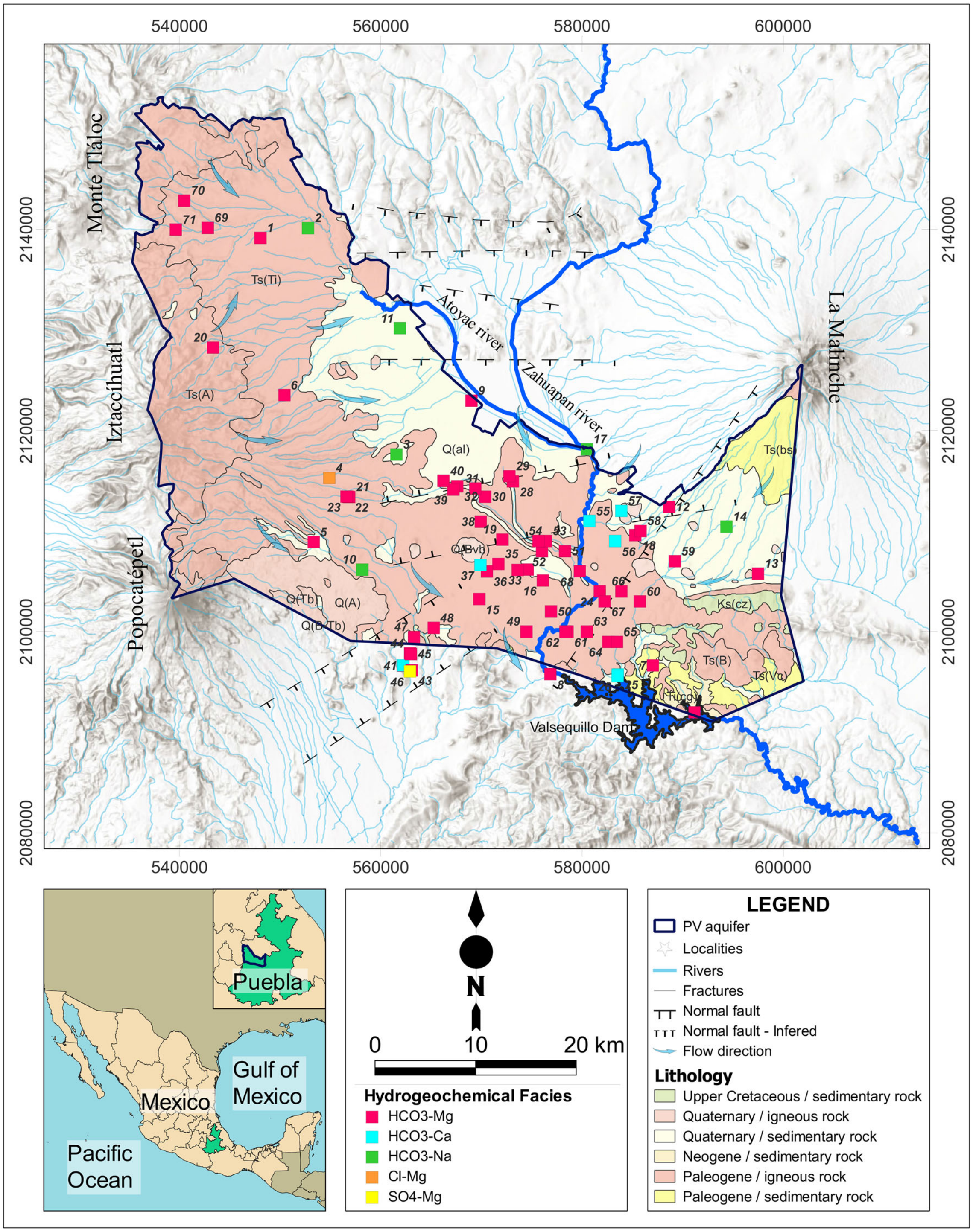

Fig. 1 Sample location, hydrogeochemical facies, groundwater flow directions, and geology of the PV aquifer

Soils

PV aquifer is covered by a variety of soil types, with Regosol being the most common, followed by Cambisol, Litosol, Feozem, Fluvisol, Vertisol, Andasol, and others (INEGI 2014). Regosols, forming from sediment deposits, are young and sediment-laden, featuring a compact "ochric" layer that impedes water infiltration and makes them less suitable for agriculture (Krasilnikov et al. 2013; Semarnat 2019). Cambisols evolve into Feozems over time, which are fertile and ideal for agriculture but are prone to erosion (Semarnat 2019). Lithosols, characterized by their stoniness and low fertility, are associated with rhyolitic rocks and are not well-suited for farming. Vertisols, formed from weathered or sedimented igneous and sedimentary rocks, have a high clay content that causes significant expansion and contraction, leading to deep cracks in dry seasons (Torres Guerrero et al. 2016).

Overall, while Regosols are less suitable for agriculture due to their low moisture and fertility, Vertisols, Feozems, and Cambisols are more favorable for agricultural use. The soils in the study area generally have fine textures and natural fertility but may compact under cultivation, affecting productivity. Adequate organic matter is essential for maintaining soil fertility and productivity.

Field sampling

In December 2021, a total of 71 groundwater samples were collected from the Valle de Puebla aquifer. The sample locations are depicted in Fig. 1. At each sampling point, we utilized the Hanna HI 98194 multiparameter instrument to measure various physicochemical parameters, including temperature, pH, electrical conductivity (EC), and dissolved oxygen (DO). Additionally, alkalinity was assessed in the field through acid titration using phenolphthalein and bromophenol blue at a pH of 4.5.

The collected samples were placed in polyethylene bottles. For the analysis of anions, we collected 120 mL of each sample, whereas for cations, 60 mL samples were acidified on-site to reach a pH of 2. It is noteworthy that bottles designated for anions were meticulously washed and rinsed seven times with deionized water. For cations, a cleansing process involving 10% HCl was followed, and the bottles were subsequently rinsed seven times with deionized water. All collected samples were stored at a temperature below 4 °C until they underwent laboratory analysis.

Laboratory methods

For the analysis of cations, Ca^{2+}, K^{+}, Mg^{2+}, and Na^{+}, the ICP-OES (Inductively Coupled Plasma Optical Emission Spectroscopy) method was employed. For the analysis of anions such as Cl^{-}, SO_4^{2-} and NO_3^{-}, the colorimetry method was utilized. Additionally, an ion balance error was calculated to assess the accuracy of the results, all of which fell within the range of ±10%. The chemical composition of the water samples was determined at the CGEO UNAM (National Autonomous University of Mexico) laboratory.

Evaluation of water quality for irrigation

The productivity of plants and agricultural soils predominantly hinges on the chemical composition of the water used for irrigation and its mineral content. Consequently, the assessment of water quality for irrigation in the valley of Puebla holds great significance for the region's thriving agricultural production.

The quality of irrigation water was assessed through various indices reported in scientific studies and widely accepted in the literature (El-Kholy et al. 2022; Pashahkha et al. 2022; Lal et al. 2023; Baye et al. 2024). For this case study, the agricultural indices listed in Table 1 were used.

The choice of these agricultural indices is due to their proven ability to accurately and specifically evaluate the risks associated with irrigation water quality in terms of sodicity, salinity, and their effects on soil structure and plant health. For this case study, the SAR and ESP indices were used to predict soil particle dispersion due to high sodium levels, while RSC and PS were employed to identify imbalances that could lead to the precipitation of harmful salts. SSP, Na%, KR, and PI were used for the integrated evaluation of sodicity and its impact on soil permeability. MAR, OP, and ES allowed for the quantification of effective salinity and its osmotic stress on plants to avoid soil degradation and ensure agricultural productivity. Chloralkaline indices are used to differentiate the ion exchange processes that occur between groundwater and the geological formations through which they circulate within the subsoil.

In this research, various diagrams were also used to identify problems in the groundwater and soils of the Puebla Valley. Among them, the Wilcox (1955) diagram was used to make decisions regarding the management of irrigation water; the extended Durov diagram (Durov 1948; Chadha 1999) diagram was used to identify processes such as water mixing, mineral dissolution, precipitation, and ionic exchanges. The USSL (US Salinity Laboratory) diagram (Richards 1954) was employed to assess the risk of soil salinization and sodification. Additionally, the Gibbs (1970) diagrams were used to understand the groundwater chemistry and the processes controlling it.

Results

Hydrogeochemical analysis

The physicochemical properties of the groundwater samples were subjected to statistical analysis. The minimum, maximum, average, and standard deviation values for each parameter can be found in Table 2. The pH values of the groundwater samples ranged from 5.1 to 8.3, with a mean of 7.2. The recharge area of Sierra Nevada exhibits a slightly alkaline pH (8-—8.3); this is due to the sampled water sources being associated with a high retention of water within the rocky medium. However, to the northeast of the aquifer, it is possible to find sources with acidic pH (5.1–5,5), suggesting recently infiltrated water. The valley area shows neutral waters (7-—7.5).

Table 1 Indices for evaluating groundwater quality in agriculture

Description	Index	Equation	Reference
Sodium absorption rate	SAR	$\frac{Na^{+}}{\sqrt{\frac{Ca^{2+}+Mg^{2+}}{2}}}$	Richards (1954)
Residual sodium carbonate	RSC	$\left(CO_3^{2-}+HCO_3^{-}\right)-\left(Ca^{2+}+Mg^{2+}\right)$	Eaton (1950)
Soluble sodium percent	SSP	$\left(\frac{Na^{+}}{Ca^{2+}+Mg^{2+}+Na^{+}}\right)\times 100$	Todd and Mays (2004)
Percentage of sodium	Na%	$\left(\frac{Na^{+}+K^{+}}{Ca^{2+}+Mg^{2+}+Na^{+}+K^{+}}\right)\times 100$	Wilcox (1955)
Kelly ratio	KR	$\frac{Na^{+}}{Ca^{2+}+Mg^{2+}}$	Kelley (1940)
Permeability index	PI	$\left(\frac{Na^{+}+\sqrt{HCO_3^{-}}}{Ca^{2+}+Mg^{2+}+Na^{+}}\right)\times 100$	Doneen (1964)
Magnesium adsorption ratio	MAR	$\left(\frac{Mg^{2+}}{Ca^{2+}+Mg^{2+}}\right)\times 100$	Raghunath (1987)
Osmotic pressure	OP	OP (atm) $\approx$ EC (mS/cm) $\times$ 0.36	Wilcox (1955)
Exchangeable sodium percentage	ESP	$-\frac{100\times(-0.0126+0.01475\times SAR)}{1+(-0.0126+0.01475\times SAR)}$	Richards (1954)
Potential salinity	PS	$Cl^{-}+\frac{1}{2}\left(SO_4^{2-}\right)$	Palacios and Aceves (1970)
Effective salinity	ES	If $Ca^{2+}>(CO_3^{2-}+HCO_3^{-}+SO_4^{2-})$, then $ES=\sum cations-(CO_3^{2-}+HCO_3^{-})$; If $Ca^{2+}<(CO_3^{2-}+HCO_3^{-}+SO_4^{2-})$, but $Ca^{2+}>(CO_3^{2-}+HCO_3^{-})$, then $ES=\sum cations-Ca^{2+}$; If $Ca^{2+}<(CO_3^{2-}+HCO_3^{-})$, but $(Ca^{2+}+Mg^{2+})>(CO_3^{2-}+HCO_3^{-})$, then $ES=\sum cations-(CO_3^{2-}+HCO_3^{-})$; If $(Ca^{2+}+Mg^{2+})<(CO_3^{2-}+HCO_3^{-})$, then $ES=\sum cations-(Ca^{2+}+Mg^{2+})$	Palacios and Aceves (1970)
Chloro-alkaline index	CAI$_1$	$\frac{Cl^{-}-(Na^{+}+K^{+})}{Cl^{-}}$	Schoeller (1977)
Chloro-alkaline index	CAI$_2$	$\frac{Cl^{-}-(Na^{+}+K^{+})}{SO_4^{2-}+HCO_3^{-}+CO_3^{2-}+NO_3^{-}}$	Schoeller (1977)

Total dissolved solids (TDS) include inorganic salts and a minimal number of organic compounds. The TDS values for the sampled water sources indicate a wide range from 30 to 2860.0 mg/L, with an average of 479 mg/L. Electrical conductivity (EC) serves as an effective indicator for assessing water quality. EC values varied from 50 to 3340 mS/cm, with an average of 777.4 mS/cm. Higher concentrations of TDS and EC are associated with more pronounced water-rock interactions, including mineral dissolution and evaporative concentration processes.

Table 2 Physicochemical groundwater characteristics

Parameters	Min	Max	Average	Median	STD
pH	5.1	8.3	7.2	7.3	0.6
TDS (mg/L)	30.0	2860.0	479.0	263.0	501.5
EC (mS/cm)	50.0	3340.0	777.4	512.0	688.3
Ca^{2+} (mg/L)	0.8	431.2	69.9	32.9	84.1
Mg^{2+} (mg/L)	3.2	109.7	31.9	23.5	27.6
Na^{+} (mg/L)	5.1	135.8	42.1	29.2	36.9
K^{+} (mg/L)	1.4	30.1	8.9	6.6	7.1
Cl^{-} (mg/L)	0.1	107.4	20.2	8.9	23.8
HCO_3^{-} (mg/L)	30.0	1155.0	346.7	195.0	327.3
SO_4^{2-} (mg/L)	1.0	760.0	76.5	25.0	132.4
NO_3^{-} (mg/L)	0.0	543.0	40.4	5.0	112.6

Among cations, Ca^{2+} exhibited the highest average concentration (mean = 70 mg/L), followed by Na^{+} (mean = 42 mg/L) and Mg^{2+} (mean = 32 mg/L). The cation order was $Ca^{2+} > Na^{+} > Mg^{2+} > K^{+}$, with respective average values of 70 mg/L, 40 mg/L, 32 mg/L, and 9 mg/L. Regarding anions, HCO_3^{-} dominated in all samples, followed by SO_4^{2-}, NO_3^{-}, and Cl^{-} in terms of abundance. HCO_3^{-} concentrations ranged from 30 to 1155 mg/L, with a mean of 347 mg/L; SO_4^{2-} concentrations varied from 1 to 760 mg/L and NO_3^{-} concentrations varied from 0 to 543 mg/L.

In Fig. 2, the main process identified is ionic exchange, and the dominant hydrogeochemical facies in the study area is the magnesium bicarbonate, present in 56 of the 71 analyzed

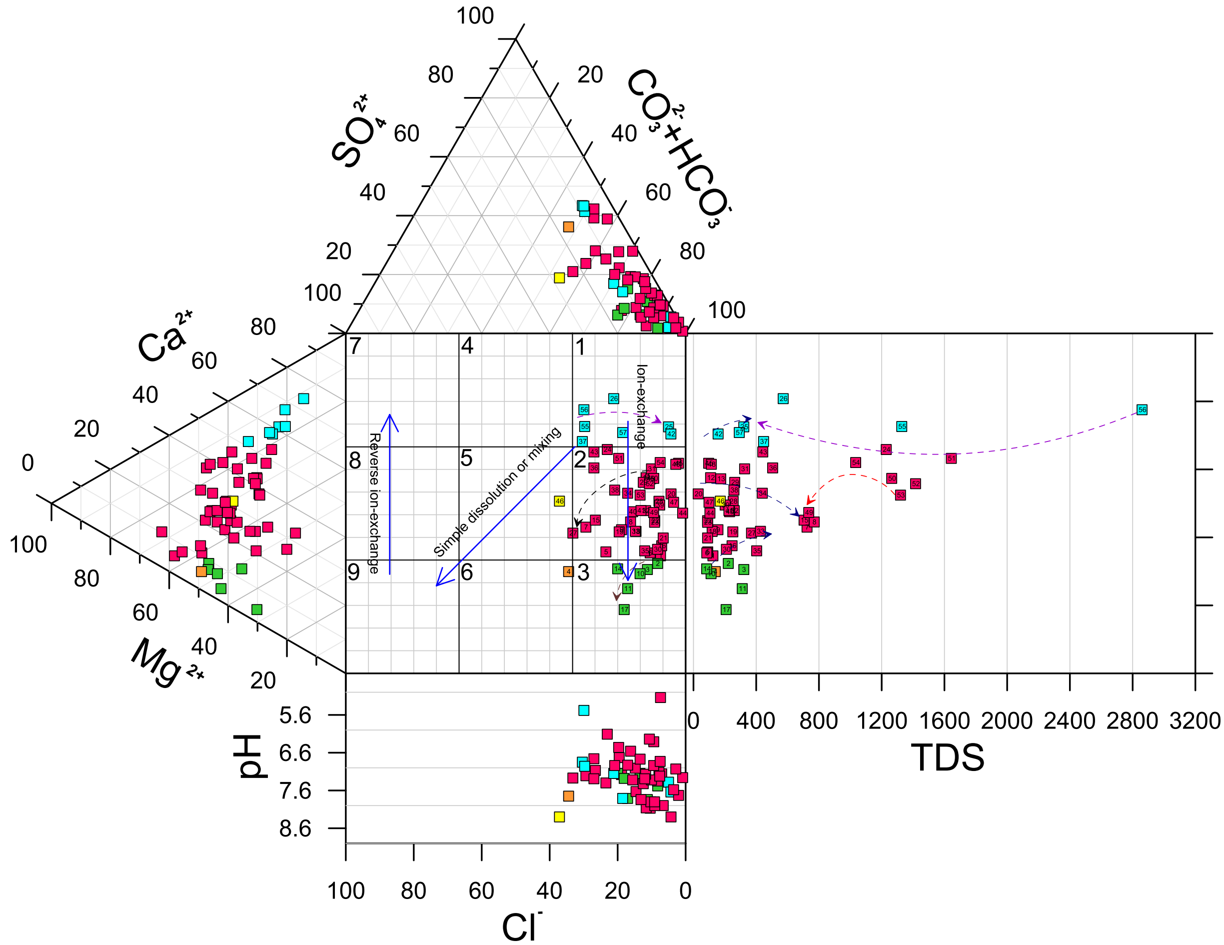

Fig. 2 Durov diagram for groundwater samples. (1) Infiltration waters of HCO_3-Ca type. (2) Cation exchange reactions. (3) Cation exchange waters of HCO_3-Na type. (4) Calcite and gypsum dissolution. (5) Mixing reactions from various origins. (6) Mixing and cation exchange waters. (7) Mixing and reverse cation exchange waters of Cl-Ca type. (8) Mixing and reverse cation exchange reactions. (9) Mixing with seawater

samples. Seven samples are classified as calcium bicarbonate, six samples as sodium bicarbonate, and one sample is categorized as magnesium sulfate.

Numerous researchers have applied CAI as a method to gauge the extent of ion exchange in groundwater across various geographic areas (Sharma et al. 2021; Fentahun et al. 2023; Obiri-Nyarko et al. 2023; Abugu et al. 2024; Kumar et al. 2024). A positive CAI value indicates an exchange of Na^+ and K^+ from water with Mg^{2+} and Ca^{2+} from rocks, while a negative CAI suggests exchange of Mg^{2+} and Ca^{2+} from water with Na^+ and K^+ from rocks.

From Table 3, it can be put forth that the CAI_1 values range from −187.49 to 0.05 and CAI_2 values vary from −0.65 to 0.01. From these values, it can be interpreted that most of the samples in the study area have negative values, and only one sample shows reverse ion exchange. The high base exchange reaction in which alkaline earth elements are exchanged for Na^+ ions can be called base exchange softened water (Jeevanandam et al. 2012; Krishna Kumar et al. 2014). In this study, most of the samples are hard water with base exchange due to the precipitation process.

The chloro-alkaline indices, such as CAI_1 and CAI_2, provide information about ionic exchange in groundwater along its trajectory (Fig. 3). These indices are used to comprehend changes in the chemical composition of groundwater and its interaction with the geological environment. Generally, groundwater flows in the PV aquifer tend to evolve towards equilibrium as they move along their path.

Considering that the PV aquifer is located in a volcanic environment, where basalt and andesite predominate, the Ca^{2+} and Mg^{2+} in the water are derived from these rocks. On the other hand, as the flow progresses and comes into contact with clays, the ionic exchange stabilizes. The springs of Popocatépetl are highly negative in CAI_1, as the Ca^{2+} and Mg^{2+} in the water exchange with the Na^+ and K^+ of the rock. However, samples from the valley show negative values of CAI_2, indicating an ionic exchange between chlorides and ions of bicarbonates, sulfates, and nitrates.

Table 3 Chloro-alkaline indices computed in the PV aquifer

Sample	CAI_1	CAI_2	Sample	CAI_1	CAI_2
1	−3.51	−0.25	37	−3.13	−0.12
2	−4.01	−0.32	38	−0.97	−0.11
3	−7.04	−0.43	39	−14.22	−0.39
4	−1.45	−0.28	40	−19.33	−0.31
5	−1.92	−0.23	41	−1.94	−0.21
6	−4.52	−0.32	42	−10.19	−0.14
7	−1.14	−0.24	43	−5.01	−0.11
8	−4.76	−0.33	44	−81.31	−0.41
9	−1.35	−0.24	45	−187.49	−0.31
10	−2.93	−0.33	46	−1.51	−0.16
11	−3.47	−0.36	47	−43.42	−0.35
12	−1.33	−0.15	48	−7.39	−0.14
13	−3.30	−0.23	49	−3.11	−0.22
14	−1.64	−0.32	50	−4.00	−0.21
15	−1.73	−0.25	51	−2.40	−0.15
16	−9.07	−0.38	52	−3.30	−0.25
17	−3.31	−0.52	53	−3.99	−0.32
18	−2.63	−0.29	54	−5.71	−0.16
19	−2.13	−0.19	55	−0.71	−0.07
20	−8.99	−0.25	56	−0.28	−0.02
21	−17.12	−0.34	57	−0.51	−0.06
22	−10.47	−0.26	58	−0.39	−0.03
23	−14.82	−0.40	59	−0.87	−0.05
24	−4.10	−0.15	60	−0.03	0.00
25	−2.39	−0.10	61	−4.15	−0.20
26	0.05	0.01	62	−6.24	−0.20
27	−1.48	−0.43	63	−2.94	−0.16
28	−7.61	−0.24	64	−0.84	−0.09
29	−8.24	−0.25	65	−1.05	−0.10
30	−34.75	−0.65	66	−0.43	−0.05
31	−6.82	−0.20	67	−0.74	−0.08
32	−8.31	−0.31	68	−3.82	−0.21
33	−10.58	−0.51	69	−17.53	−0.27
34	−4.80	−0.19	70	−17.08	−0.38
35	−19.01	−0.59	71	−7.32	−0.28
36	−3.68	−0.12			

Natural processes controlling groundwater chemistry

In this research, the Gibbs (1970) diagram is used to evaluate the influence of processes controlling groundwater chemistry, facilitating the identification of areas susceptible to contamination and the implementation of appropriate strategies for water resource management.

Figure 4 presents a modification to the Gibbs diagram, and in order to analyze the origin of sulfates in the study area, the groundwater samples of the PV aquifer were projected in the rock dominance zone, which suggests that rock weathering and leaching are major processes affecting groundwater chemistry. However, the distribution of these groundwater samples showed a slightly increasing trend with the evaporation dominance zone (Fig 4a). The main factors governing groundwater chemistry in this area are rock weathering and evaporation, because these samples are located a few meters from the Atoyac river. The arrows in Fig. 4 show the evolution of the different flow paths in the basin.

The arrows in Fig. 4 indicate the direction in which the water moves through the rock medium; the purple arrows correspond to the flow path from recharge areas to the valley; the pink arrows are associated with water movement in the valley area, and the brown arrows indicate that as the groundwater flows evolve. There is an increase in sulfates in Fig. 4a and calcium in Fig. 4b.

We also associate the movement trend of groundwater sampling points from the rock domain towards the evaporation domain due to salinity in groundwater, where the semi-arid climate intensifies Na^+ and $C1^-$ ion concentrations with a subsequent increase in TDS. Similarly, the influence of anthropogenic activities (agricultural, industrial, and urban) also causes the higher Na^+ and $C1^-$ contents with a subsequent increase of TDS with the evolution of water (Fig. 4b).

Groundwater quality for irrigation in terms of salinity and sodicity

The quality of water in the agricultural sector is of great importance in the PV aquifer because this activity is primary for the inhabitants of the region. Therefore, the quality of the groundwater in this aquifer was evaluated using various indices (SAR, MAR, PI, %Na, SSP, RCS, KR, PS, OP, ESP, and ES). Table 4 displays these essential chemical parameters for irrigation, and in the Supplementary Information, the spatial distribution of these indices can be consulted.

Sodium absorption rate

The maximum and minimum SAR values in the study area are 2.9 (sample 27) and 0 (sample 71), respectively. This indicates that the groundwater is excellent and suitable for irrigation purposes, with no danger of sodicity in the water extracted from the PV aquifer (see Fig. 5a).

Residual sodium carbonate

The RSC index reveals that 87% of the samples have values greater than 1.25 meq/L, while the remaining samples have values below this threshold and are considered safe for agricultural irrigation (13%) (see Fig. 5b). The maximum and

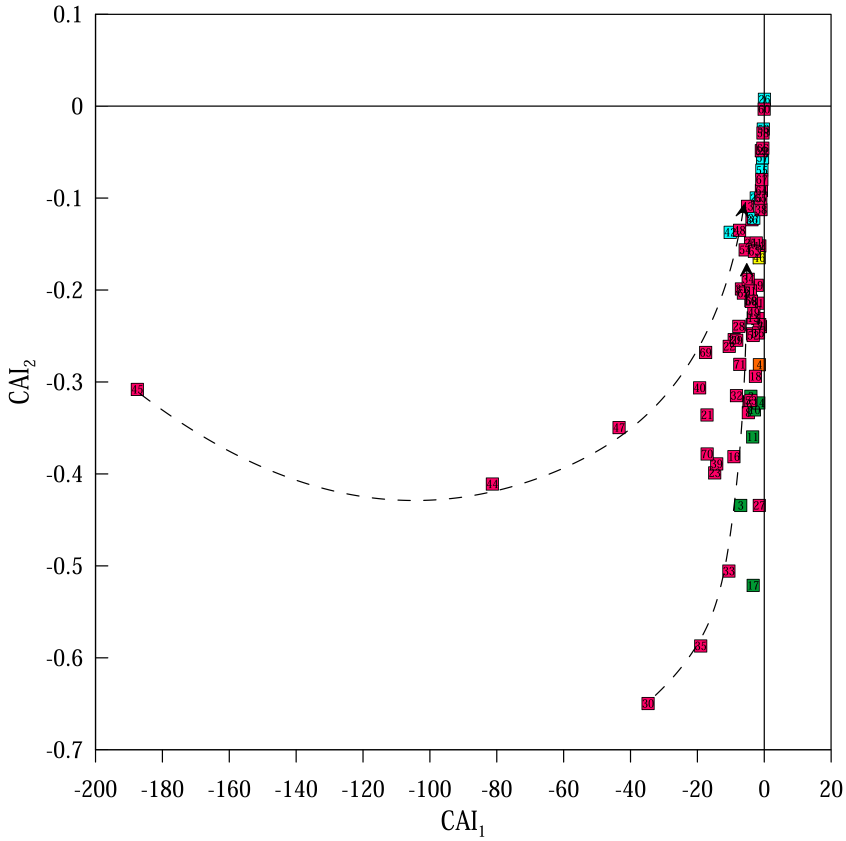

Fig. 3 Relationship of the chloro-alkaline indices with the flow directions in the PV aquifer

minimum RSC values are 5.3 meq/L (sample 68) and −10.4 meq/L (sample 56), respectively (see Table 2).

Soluble sodium percent

As depicted in Table 2, the maximum value recorded in the SSP index was 63% in sample 17, while the minimum was 9% in sample 60. Only three samples exceed the allowable limit, which can be attributed to the hardness and permeability of the soil (Fig. 5c).

Percentage of sodium

In the study area, the %Na of groundwater varies between 10.3 and 53.5%. Specifically, 26% of the samples are categorized as excellent quality water, 49% fall under the classification of good quality, and the remaining 25% are considered admissible water, as illustrated in Fig. 5d.

Kelly ratio

In this study, the KR index shows only three samples exhibit a value exceeding 1. This behavior has been associated with

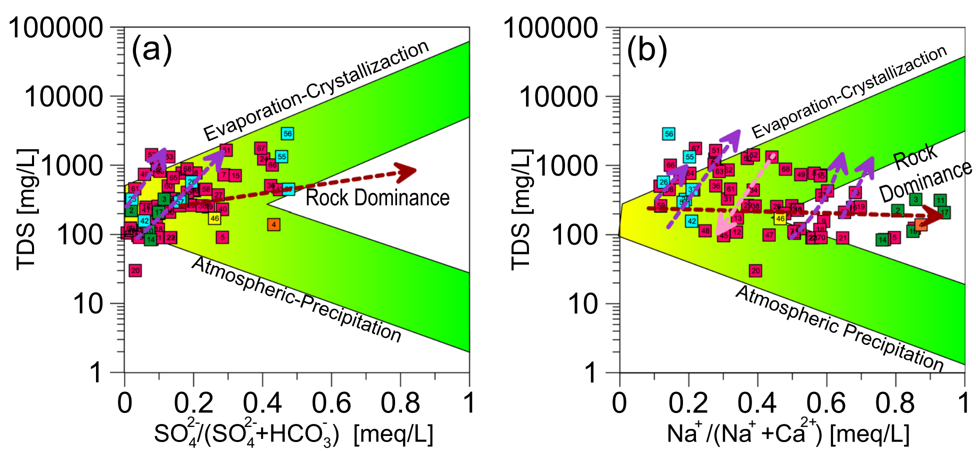

Fig. 4 Gibbs diagrams indicating the groundwater natural evolution mechanisms. **a** TDS vs. SO_4^{2-}/(SO_4^{2-}+HCO_3^-). **b** TDS vs. Na^+/(Na^++Ca^{2+})

Table 4 Maximum, minimum, and average values of salinity and sodicity indices

Parameters	Unit	Min	Max	Average
SAR	–	0.00	2.90	1.06
MAR	–	16.27	91.91	52.93
PI	%	24.50	159.55	73.75
%Na	%	10.28	66.14	29.87
SSP	%	8.96	62.99	27.24
RCS	meq/L	−10.43	5.30	−0.43
KR	–	0.10	1.70	0.42
PS	meq/L	0.02	10.94	1.37
OP	mS/cm	0.02	1.20	0.28
ESP	–	−2.92	0.96	−0.31
ES	meq/L	0.29	12.29	2.92

the organic matter content in the Feozem soils. In conclusion, the water from the PV aquifer can be considered suitable for irrigation, as depicted in Fig. 5e.

Permeability index

The PI values in the study area range from 24.5 to 159.5%. Considering this index and the permissible limits, the results indicate that 38% of the samples are suitable quality water, while 62% are classified as water acceptable quality, as shown in Fig. 5f.

Magnesium adsorption ratio

In this study, the maximum and minimum values found were 92% (sample 11) and 16% (sample 26), respectively. Among the samples, 45% are classified as of excellent quality, while 55% are considered inadequate for irrigation, indicating that not all the water is suitable for this purpose, as illustrated in Fig. 5g.

Osmotic pressure

The results obtained concluded that groundwater in the PV aquifer has a maximum OP value of 1.2 atm and a minimum

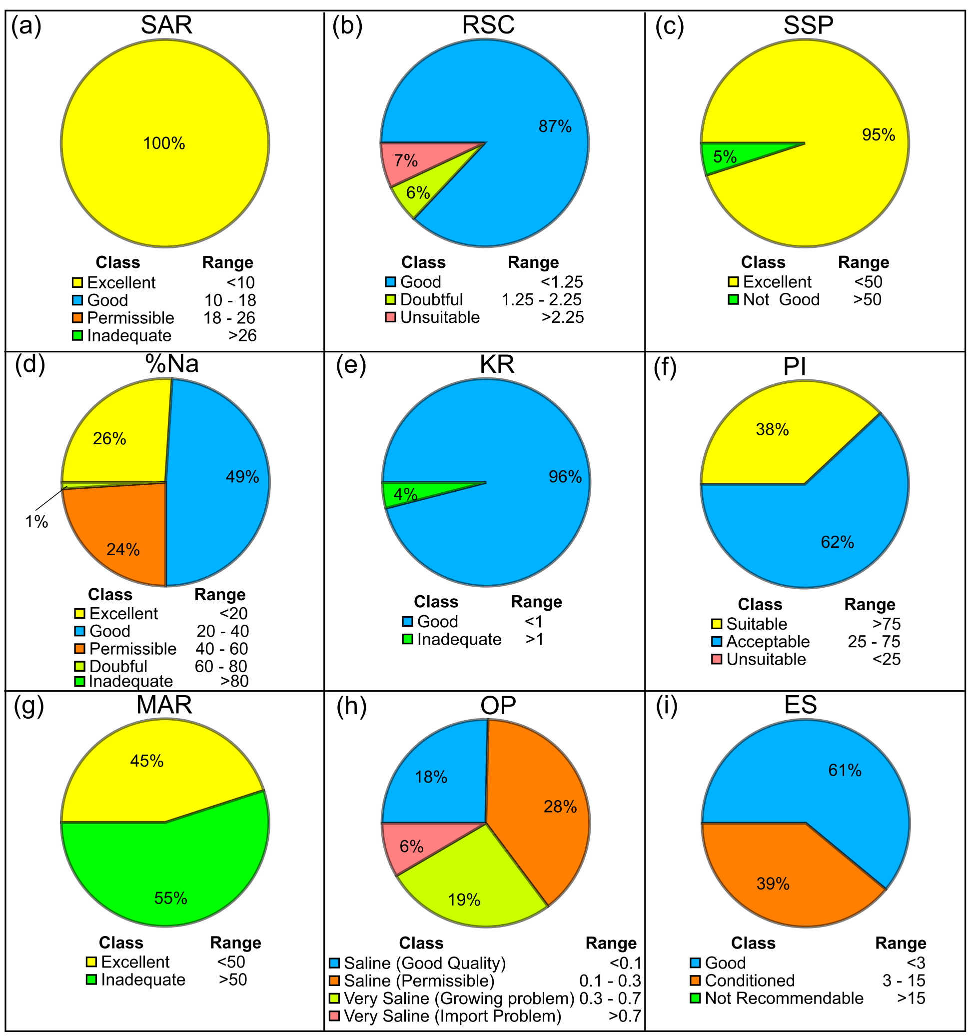

Fig. 5 Percentage of water quality of samples in terms of irrigation index

of 0 atm. In this case study, 18% of the samples demonstrate good quality, and 28% fall within the permissible range, while the remaining 25% are considered waters with significant salinity problems, as illustrated in Fig. 5h.

Effective salinity

For this study, water quality with regard to salinity, as assessed by the ES index (Fig. 5i), classifies 61% of the samples as good quality water, while the remaining 39% are categorized as conditioned water. The maximum and minimum values were 12.3 meq/L (sample 67) and 0.3 meq/L (sample 20), respectively.

Discussion

Water-rock interaction processes

Through the Durov diagram (Fig. 2) and the Gibbs diagrams (Fig. 4), the processes of water-rock interaction were identified. Both graphs show the complexity of the study area, where most of the process occurs in the different flow paths. In the Durov diagram (Fig. 2), ion exchange (black arrow) and mixing (purple arrow) are observed. The occurrence of ion exchange is consistent with the soil types in the region, given the predominance of clay material and organic matter. The mixing process is a result of rainwater infiltrating the subsoil and the circulation of groundwater through the rocky material of the aquifer, but mixing also occurs in agricultural areas due to irrigation return flows, and in urban areas due to wastewater carried by the Atoyac River.

Figures 5 a, d, and e support the conclusion that there are no sodicity problems in the PV aquifer, but some cases of salinity have been identified that may intensify over time, as discussed in previous studies (Gárfias et al. 2010). While CONAGUA (2020) highlights the suitability of groundwater for agricultural irrigation, the study by Gárfias et al. (2010) points out the presence of sulfides and anaerobic conditions in deep waters. This difference in results suggests variability in the chemical composition of groundwater depending on the depth and location of each water sample within the aquifer.

Although there is no documented evidence of salinization problems in the VP aquifer in the literature, it can be found that some volcano-sedimentary-type aquifers present such problems due to natural and anthropogenic sources (Aboubaker et al. 2013, Cruz-Fuentes et al. 2014, Ahmed et al. 2017, Okan and Güven 2019).

Water quality classification

In this case study, the Wilcox diagram shows 45 out of the 71 collected samples classified as good to excellent, 20 as permissible to good, 5 as doubtful to unsuitable, and one sample falls into the unsuitable category, which is associated with sulfurous water from a deep well (greater than 100 ms), as shown in Fig. 6a. It is important to note that there are no previous studies on water quality that can serve as a reference. In terms of the spatial distribution of the samples, the inadequate quality waters are located in the urban areas of Puebla,

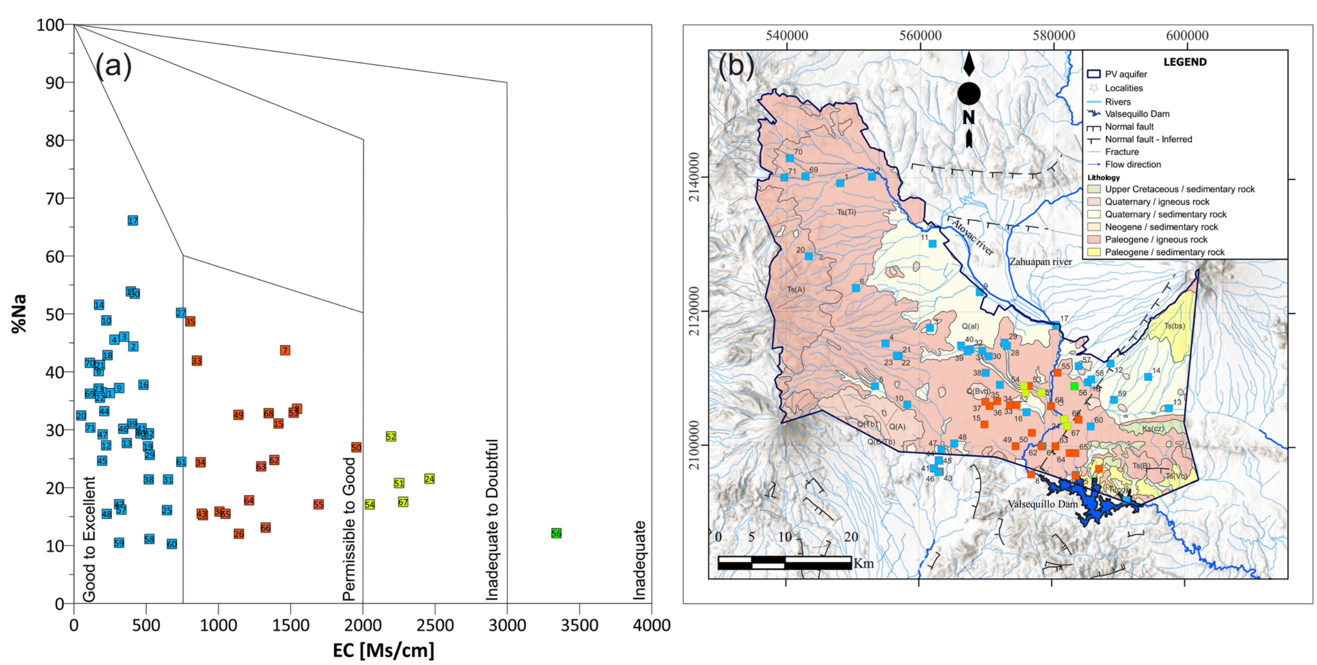

Fig. 6 Wilcox diagram for groundwater in aquifer PV

Cuautlancingo, and Cholula, as well as close to the Atoyac River. Conversely, samples of excellent quality correspond to all the sampled springs, as well as wells located far from urban areas, as depicted in Fig. 6b.

From the above, it can be inferred that the high sodium content in the groundwater of the PV aquifer is the result of water-rock interaction leading to ion exchange. Additionally, agricultural activities in the region, including the use of fertilizers and agrochemicals, contribute to the increased sodium content. It is crucial to address soil salinization promptly since the PV aquifer is shallow, and groundwater contamination occurs rapidly due to agricultural practices.

In Fig. 7a, we can see the results of the USSL diagram. Of the 71 samples, collected 18 are classified as C1S1 water,indicating a low risk of salinity and sodium; 27 samples are categorized as C2S1, representing the medium risk of salinity and low risk of sodification due to salinity; 25 samples fall into the C3S1 classification, signifying high risk of salinity and low risk of sodification; and one sample is classified as C4S1, suggesting the need for its use in soils with good water permeability (El-Kholy et al. 2022). However, it should be noted that this sample corresponds to a deep well (100 m) with sulfurous water.

In general, the use of water from the PV aquifer is limited by salinity rather than sodification. Consequently, all samples fall into the category of medium-low sodium salinity water that can be used for irrigation across various soil types with minimal risk of harmful exchangeable sodium levels. In terms of distribution, once again, samples with the highest salt content are found in the urban areas of Puebla and close to the Atoyac River, while samples of excellent quality are associated with the Sierra Nevada springs (Fig. 7b).

The scatter plot in Fig. 8a reveals a direct correlation between the ES and PS indices in most of the samples. When ES increases, PS also increases, indicating that as water evolves towards the valley area, it tends to shift from good quality water to conditioned water. The combined information from these indices shows a negative trend in the water quality of the PV aquifer.

In general, the ES index of groundwater from the PV aquifer indicates good quality for 48% of the samples. However, more than half of these samples are influenced by the effects of effective salinity. Conversely, the PS index suggests conditional use for most of the samples (58%). In Fig. 8b, it is evident that the water quality in the recharge areas of both Sierra Nevada and Malinche is good, while the water quality in urban areas and near the tributaries of the Atoyac River presents serious salinization issues.

On the other hand, with the chloro-alkaline indices, it is evidently shown that 5.2% of the groundwater samples are not active in the basic ion exchange (samples 28, 31, 56), and 94.8% of the groundwater samples have negative values (Table 3). This clearly indicates a chloro-alkaline imbalance, because Ca^{2+} and Mg^{2+} ions present in groundwater react with clay minerals to release Na^{+} ions.

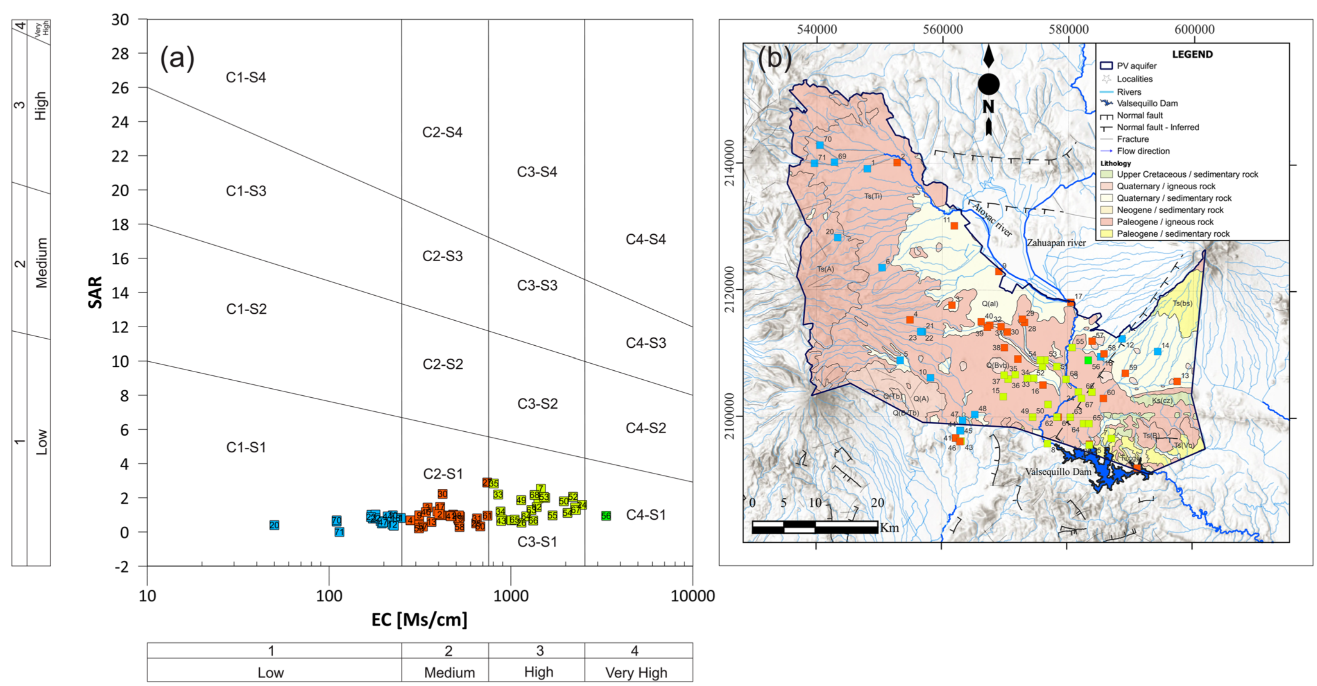

Fig. 7 Modified USSL diagram for groundwater in aquifer PV

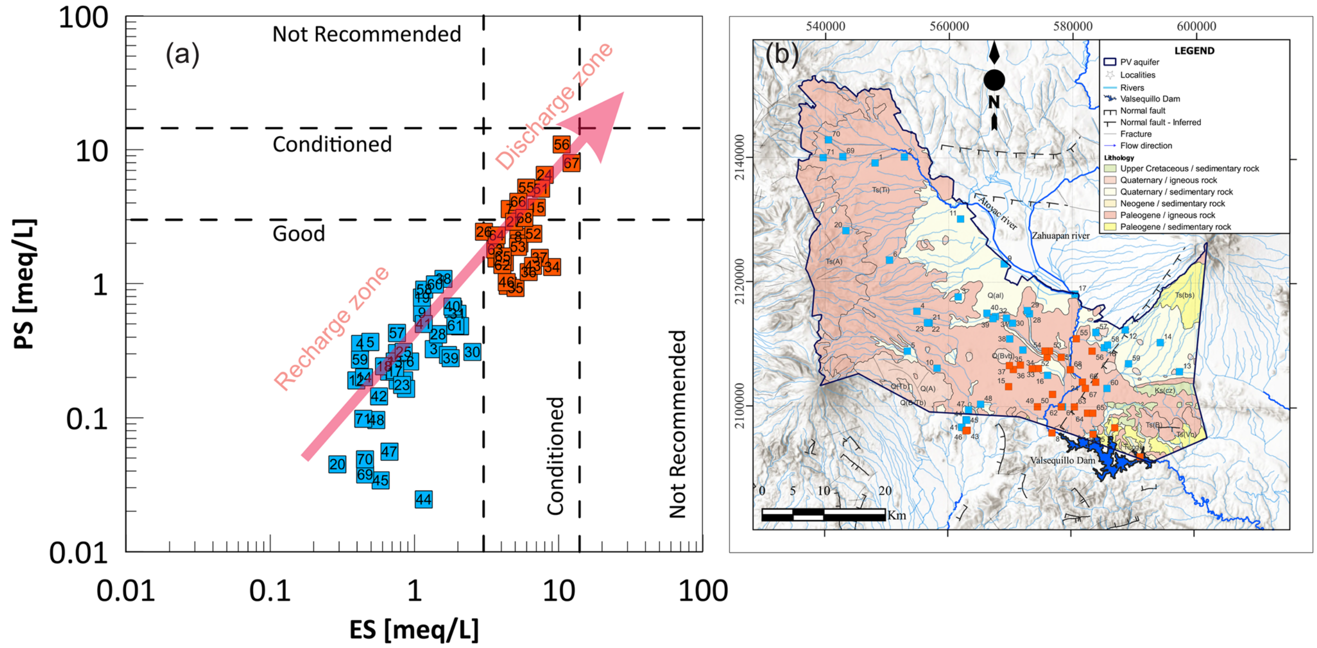

Fig. 8 Spatial distribution of the index effective salinity (ES) vs potential salinity (PS)

Evolution and quality groundwater

The predominant ion contents play a pivotal role in defining the basic hydrochemical characteristics of groundwater (Li et al. 2018). Figure 9 illustrates how the evolution of groundwater controls water quality. It is observed that in recharge areas, which are at higher altitudes, water quality is good, while in the discharge zone, salinity problems occur. Figure 9a shows the relationship between the altitudinal profile and the location of groundwater samples.

In Fig. 9b, the values of the PS, ES, and SAR indices are shown. These indices in recharge areas present low salt contents, so there is no alteration in water quality in these areas. However, high salt contents begin from samples 11 to 17; these samples are located in agricultural areas, so it is estimated that the water chemistry has been affected by the use of fertilizers, the SAR index values in this area show significant variations that must be taken into account in land use and vegetation. Nevertheless, there is a gradual increase in the PS and ES content from sample 35 to 27; this is related to the location of the wells, which are in the urban area, so anthropogenic contamination has significantly affected the water quality.

Based on Fig. 9, it can be concluded that the groundwater quality of the PV aquifer is directly influenced by the evolution of flows. The high values of agricultural indices such as PS, ES, and SAR suggest strong anthropogenic contamination, related to the use of fertilizers and the return of irrigation and wastewater through the tributaries of the Atoyac River. These results highlight the importance of addressing and controlling human activities that contribute to the degradation of water quality in the PV aquifer.

Conclusions

The geological characteristics of this volcano-sedimentary aquifer lead to the dissolution of minerals from the aquifer's rocky and sedimentary material, altering the chemical composition of the groundwater. The dominant hydrogeochemical facies are bicarbonate-magnesium and bicarbonate-calcium. Sulfate-magnesium waters originate from La Malinche, while the bicarbonate-magnesium-calcium waters come from Sierra Nevada.

In general, the groundwater of the PV aquifer is suitable for agricultural irrigation; according to the SAR, %Na, PI, and KR indices, it presents a low risk of sodicity, suggesting that it falls within permissible limits for agricultural use. However, the Wilcox and USSL diagrams suggest a potential risk of increasing salinity over time, mainly in areas near agricultural zones, urban areas, and the Atoyac River. Therefore, it is essential to maintain regular control and monitoring measures for this aquifer.

The chloro-alkaline indices reveal that ion exchange is the dominant process, where groundwater interacts with subsurface minerals, generating imbalances in the chloride-alkalinity relationship. Anthropogenic activities, particularly agriculture, exacerbate these imbalances.

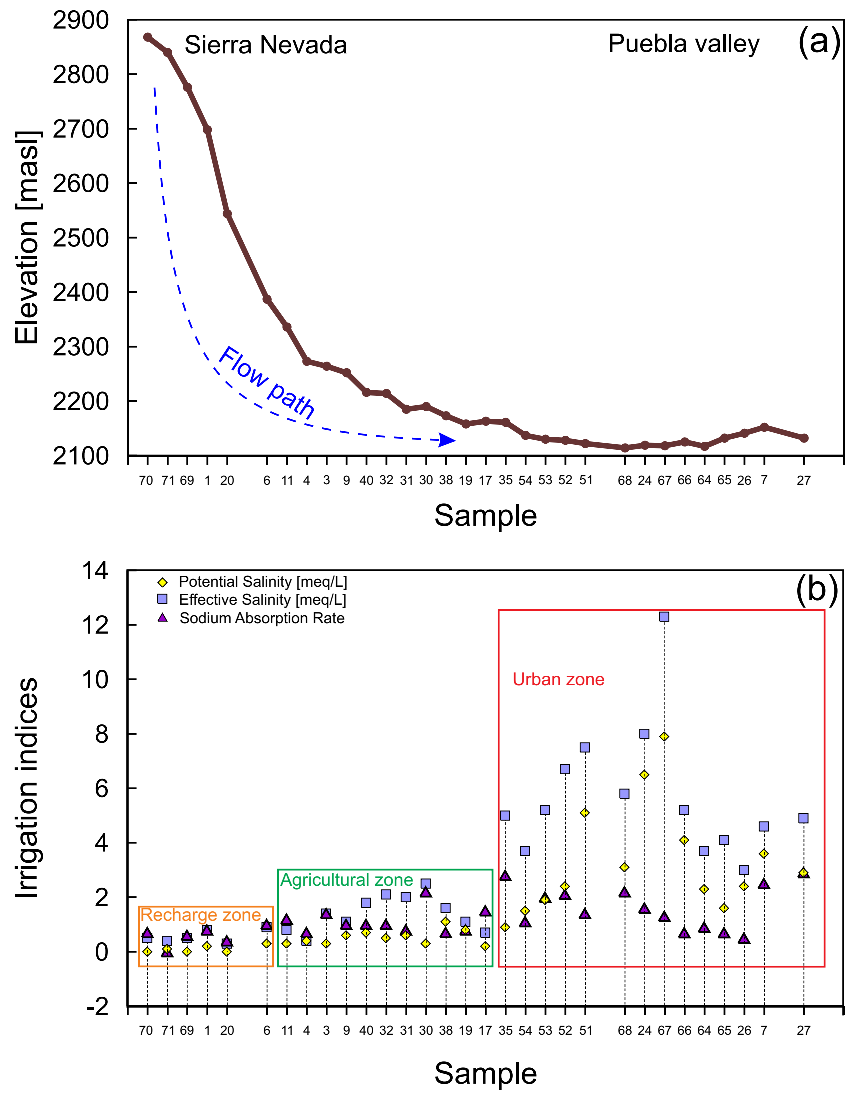

Fig. 9 Groundwater Evolution and Water Quality in the PV aquifer. **a** Relationship between altitude and groundwater evolution. **b** Groundwater evolution as a function of PS, ES, and SAR

The evolution of groundwater quality is influenced by anthropogenic activities, including the use of fertilizers and irrigation practices. These activities have led to an increase in salinity and have affected water quality, particularly in urban areas and near the Atoyac River. Therefore, proper management of the region's soils, mainly regosols, cambisols, and lithosols, is necessary because good management of these can prevent erosion, facilitate infiltration, and improve water retention capacity.

Although this study offers important insights into the hydrogeochemical characteristics of the PV aquifer, it is limited by the lack of long-term data, which may affect the understanding of temporal variations in water quality. Future research should incorporate extended monitoring and advanced modeling to better predict groundwater quality trends under varying land use and climate conditions. Despite these limitations, this research underscores the need for continuous monitoring and sustainable management practices to protect the aquifer from both natural and anthropogenic impacts.

Supplementary Information

Below is the link to the supplementary electronic material. It includes a figure showing the spatial distribution of the indices used to assess irrigation water quality in the PV aquifer.

Supplementary Information The online version contains supplementary material available at https://doi.org/10.1007/s11356-024-35346-8.

Author contribution All authors have equally contributed to the research and manuscript preparation. Material preparation, data collection, and analysis were performed by Janete Morán Ramírez, Ana Beatriz Rubio-Arellano, and José Alfredo Ramos-Leal. Víctor Manuel

Vázquez Báez's contribution is reviewing and supervision. The first draft of the manuscript was written by Ana Beatriz Rubio-Arellano, and all authors commented on previous versions of the manuscript. All authors have read and agreed to the published version of the manuscript.

Data availability The datasets used and/or analyzed during the current study are available from the corresponding author on reasonable request.

Declarations

Ethics approval Not applicable

Consent to participate Not applicable

Consent for publication Not applicable

Conflict of interest The authors declare no Conflict of interest.

References

Aboubaker M, Jalludin M, Razack M (2013) Hydrochemistry of a complex volcano-sedimentary aquifer using major ions and environmental isotopes data: Dalha basalts aquifer, southwest of Republic of Djibouti. Environ Earth Sci 70:3335–3349. https://doi.org/10.1007/s12665-013-2398-8

Abugu HO, Egbueri JC, Agbasi JC, Ezugwu AL, Omeka ME, Ucheana IA, Aralu CC (2024) A study on the mixing proportion in groundwater samples by using Piper diagram and Phreeqc model. Hydrochemical Characterization of Ground and Surface Water for Irrigation Application in Nigeria: A Review of Progress https://doi.org/10.1007/s42250-024-00917-2

Ahmed AH, Rayaleh WE, Zghibi A, Ouddane B (2017) Assessment of chemical quality of groundwater in coastal volcano-sedimentary aquifer of Djibouti, Horn of Africa. J Afr Earth Sci 131:284–300. https://doi.org/10.1016/j.jafrearsci.2017.04.010

Ayenew T, GebreEgziabher M, Kebede S, Mamo S (2013) Integrated assessment of hydrogeology and water quality for groundwater-based irrigation development in the Raya Valley, northern Ethiopia. Water Int 38(4):480–492. https://doi.org/10.1080/02508060.2013.821640

Ayub R, Messier K, Serre M et al (2019) Non-point source evaluation of groundwater nitrate contamination from agriculture under geologic uncertainty. Stoch Environ Res Risk Assess 33:939–956. https://doi.org/10.1007/s00477-019-01669-z

Baye AA, Boum-Nkot SN, Bello M (2024) Groundwater quality status in the Division of Fitri (Chad). Sustain Water Resour Manag 10:39. https://doi.org/10.1007/s40899-023-00994-0

Bozorg-Haddad O, Delpasand M, Loáiciga HA (2021) 10 - Water quality, hygiene, and health. In: Bozorg-Haddad O (ed) Economical, political, and social issues in water resources. Elsevier, pp 217–257. https://doi.org/10.1016/B978-0-323-90567-1.00008-5

Chadha DK (1999) A proposed new diagram for geochemical classification of natural waters and interpretation of chemical data. Hydrogeol J 7:431–439

CONAGUA (2020) Actualización de la disponibilidad media anual de agua en el acuífero Valle de Puebla (2104). Estado de Puebla. Tech. rep, CONAGUA

CONAGUA (2023) Estadísticas del Agua en México 2023. Tech. rep., Comisión Nacional del Agua, Coyoacán, Ciudad de México, https://sinav30.conagua.gob.mx:8080/port_publicaciones.html

Cruz-Fuentes T, del Carmen Cabrera M, Heredia J, Custodio E (2014) Groundwater salinity and hydrochemical processes in the volcano-sedimentary aquifer of La Aldea, Gran Canaria, Canary Islands, Spain. Sci Total Environ 484:154–166. https://doi.org/10.1016/j.scitotenv.2014.03.041

Dinka MO (2016) Quality composition and irrigation suitability of various surface water and groundwater sources at Matahara Plain. Water Resour 43:677–689. https://doi.org/10.1134/S0097807816040114

Doneen LD (1964) Notes on water quality in agriculture. University of California, Davis, Department of Water Science and Engineering

Durov SA (1948) Classification of natural waters and graphical representation of their composition. Dokl Akad Nauk USSR 59(1):87–90

Eaton FM (1950) Significance of carbonates in irrigation waters, vol 69. Soil science

El-Kholy RA, Zaghlool E, Isawi H, Soliman EA, Khalil MM, El-Aassar AHM, Said MM (2022) Groundwater quality assessment using water quality index and multivariate statistical analysis case study: East Matrouh, Northwestern coast. Egypt. Environ Sci Pollut Res 29(23):65699–65722. https://doi.org/10.1007/s11356-022-19761-3

Fentahun A, Mechal A, Karuppannan S (2023) Hydrochemistry and quality appraisal of groundwater in Birr River Catchment, Central Blue Nile River Basin, using multivariate techniques and water quality indices. Environ Monit Assess 195:655. https://doi.org/10.1007/s10661-023-11198-6

Gao D, Yan Y, Yao R et al (2024) Spatial analysis and GIS mapping of regional hydrochemistry, groundwater quality, and probabilistic health risk in western Sichuan Basin, southwestern China. Environ Earth Sci 83:41. https://doi.org/10.1007/s12665-023-11341-z

Gao Y, Qian H, Ren W, Wang H, Liu F, Yang F (2020) Hydrogeochemical characterization and quality assessment of groundwater based on integrated-weight water quality index in a concentrated urban area. J Clean Prod 260:121006. https://doi.org/10.1016/j.jclepro.2020.121006

Gárfias J, Arroyo N, Aravena R (2010) Hydrochemistry and origins of mineralized waters in the Puebla aquifer system, Mexico. Environ Earth Sci 59:1789–1805. https://doi.org/10.1007/s12665-009-0161-y

Gibbs RJ (1970) Mechanisms controlling world water chemistry. Sci 170(3962):1088–1090. https://doi.org/10.1126/science.170.3962.1088

INEGI (2014) Edafología. https://www.inegi.org.mx/temas/edafologia/

Jeevanandam M, Nagarajan R, Manikandan M, Senthilkumar M, Srinivasalu S, Prasanna MV (2012) Hydrogeochemistry and microbial contamination of groundwater from lower Ponnaiyar Basin, Cuddalore District, Tamil Nadu, India. Environ Earth Sci 67:867–887. https://doi.org/10.1007/s12665-012-1534-1

Kelley WP (1940) Permissible composition and concentration of irrigation water. Proc Am Soc Civ Eng 106(1):607–613. https://doi.org/10.1061/TACEAT.0005384

Kothari V, Vij S, Sharma S, Gupta N (2021) Correlation of various water quality parameters and water quality index of districts of Uttarakhand. Environ Sustain Indic 9:100093. https://doi.org/10.1016/j.indic.2020.100093

Krasilnikov P, Gutiérrez-Castorena MdC, Ahrens RJ, Cruz-Gaistardo CO, Sedov S, Solleiro-Rebolledo E (2013) The soils of Mexico. Springer Science & Business Media. https://doi.org/10.1007/978-94-007-5660-1

Krishna Kumar S, Bharani R, Magesh NS, Godson PS, Chandrasekar N (2014) Hydrogeochemistry and groundwater quality appraisal of part of south Chennai coastal aquifers, Tamil Nadu, India using WQI and fuzzy logic method. Appl Water Sci 4:341–350. https://doi.org/10.1007/s13201-013-0148-4

Kumar PR, Gowd SS, Krupavathi C (2024) Groundwater quality evaluation using water quality index and geospatial techniques in parts of

Anantapur District, Andhra Pradesh, South India. HydroResearch 7:86–98. https://doi.org/10.1016/j.hydres.2024.01.001

Lal B, Sengar SS, Singh R (2023) Hydrogeochemistry and groundwater quality assessment in Ambagarh Chowki, Chhattisgarh. India. Environ Monit Assess 195:43. https://doi.org/10.1007/s10661-022-10650-3

Li P, Wu J, Tian R, He S, He X, Xue C, Zhang K (2018) Geochemistry, hydraulic connectivity and quality appraisal of multilayered groundwater in the Hongdunzi Coal Mine. Northwest China. Mine Water Environ 37(2):222–237. https://doi.org/10.1007/s10230-017-0507-8

Marín Celestino AE, Ramos Leal JA, Martínez Cruz DA, Tuxpan Vargas J, De Lara Bashulto J, Morán Ramírez J (2019) Identification of the hydrogeochemical processes and assessment of groundwater quality, using multivariate statistical approaches and water quality index in a wastewater irrigated region. Water 11(8):1702. https://doi.org/10.3390/w11081702

Mosthaf K, Rosenberg L, Broholm MM, Fjordbøge AS, Lilbæk G, Christensen AG, Bjerg PL (2024) Quantification of contaminant mass discharge from point sources in aquitard/aquifer systems based on vertical concentration profiles and 3D modeling. J Contam Hydrol 260:104281. https://doi.org/10.1016/j.jconhyd.2023.104281

Motevalli A, Naghibi SA, Hashemi H, Berndtsson R, Pradhan B, Gholami V (2019) Inverse method using boosted regression tree and k-nearest neighbor to quantify effects of point and non-point source nitrate pollution in groundwater. J Clean Prod 228:1248–1263. https://doi.org/10.1016/j.jclepro.2019.04.293

Obiri-Nyarko F, Duah AA, Karikari AY, Ali NA (2023) Characterization of leachate, groundwater quality analysis, and evaluation of hydrogeochemical processes at the Kpone engineered landfill site. Ghana. Sustain Water Resour Manag 9:15. https://doi.org/10.1007/s40899-022-00794-y

Okan O, Güven A (2019) Hydrochemistry of groundwaters from alluvial and fractured igneous aquifers at the western region of Lake Hazar (Elazığ, Turkey). Arab J Geosci 12:52. https://doi.org/10.1007/s12517-018-4209-8

Ossai IC, Ahmed A, Hassan A, Hamid FS (2020) Remediation of soil and water contaminated with petroleum hydrocarbon: a review. Environ Technol Innov 17(1). https://doi.org/10.1016/j.eti.2019.100526

Palacios O, Aceves E (1970) Instructivo para el registro, muestreo e interpretación de datos de calidad del agua para riego. Colegio de Posgraduados, serie de apuntes (15)

Pashahkha P, Babazadeh H, Shahmohammadi-Kalalagh S et al (2022) Salinity-based spatial evaluation of groundwater quality for agricultural use. Int J Environ Sci Technol 19:6833–6844. https://doi.org/10.1007/s13762-021-03881-3

Raghunath HM (1987) Groundwater: hydrogeology, groundwater survey and pumping tests. Rural Water Supply and Irrigation Systems. John Wiley & Sons Inc, New Delhi, India

RamyaPriya R, Elango L (2018) Evaluation of geogenic and anthropogenic impacts on spatio-temporal variation in quality of surface water and groundwater along Cauvery River. India. Environ Earth Sci 77(2):1–17. https://doi.org/10.1007/s12665-017-7176-6

Richards LA (1954) Diagnosis and improvement of saline and alkali soils. US Department of Agriculture, Washington DC

Schoeller H (1977) Geochemistry of groundwater. In Groundwater Studies–An International Guide for Research and Practice. UNESCO pp 1–18

Semarnat (2019) Informe de la situación del medio ambiente en México. Compendio de Estadísticas Ambientales. Indicadores Clave, de Desempeño Ambiental y de Crecimiento Verde, Edición 2018. https://apps1.semarnat.gob.mx:8443/dgeia/informe18/index.html

Sharma N, Vaid U, Sharma SK (2021) Assessment of groundwater quality for drinking and irrigation purpose using hydrochemical studies in Dera Bassi town and its surrounding agricultural area of Dera Bassi Tehsil of Punjab. India. SN Appl Sci 3:245. https://doi.org/10.1007/s42452-021-04199-y

Shi J (2023) Identifying the influence of natural and human factors on seasonal water quality in China: current situation of China's water environment and policy impact. Environ Sci Pollut Res 30:104852–104869. https://doi.org/10.1007/s11356-023-29390-z

Subba Rao N, Das R, Sahoo H, Gugulothu S (2024) Hydrochemical characterization and water quality perspectives for groundwater management for urban development. Groundw Sustain Dev 24:101071. https://doi.org/10.1016/j.gsd.2023.101071

Todd DK, Mays LW (2004) Groundwater hydrology. John Wiley & Sons. https://doi.org/10.1002/0470871660

Torres Guerrero CA, Gutiérrez Castorena MDC, Ortiz Solorio CA, Gutiérrez Castorena EV (2016) Manejo agronómico de los Vertisoles en México: una revisión. Terra Latinoam 34(4):457–466

Votruba AM, Corman JR (2020) Definitions of water quality: a survey of lake-users of water quality-compromised lakes. Water 12(8):2114. https://doi.org/10.3390/w12082114

Vranešević M, Zemunac R, Grabić J, Salvai A (2024) Hydrochemical characteristics and suitability assessment of groundwater quality for irrigation. Appl Sci 14(2):615. https://doi.org/10.3390/app14020615

Wilcox L (1955) Classification and use of irrigation waters. US Department of Agriculture, Washington DC

Yang Y, Li P, Elumalai V et al (2023) Groundwater quality assessment using EWQI with updated water quality classification criteria: a case study in and around Zhouzhi County, Guanzhong Basin (China). Expo Health 15:825–840. https://doi.org/10.1007/s12403-022-00526-9

Zemunac R, Savic R, Blagojevic B et al (2021) Assessment of surface and groundwater quality for irrigation purposes in the Danube-Tisa-Danube hydrosystem area (Serbia). Environ Monit Assess 193:519. https://doi.org/10.1007/s10661-021-09294-6

Zhao H, Duan X, Stewart B, You B, Jiang X (2013) Spatial correlations between urbanization and river water pollution in the heavily polluted area of Taihu Lake Basin. China. J Geogr Sci 23(1):735–752. https://doi.org/10.1007/s11442-013-1041-7

Chapter 4

Water quality for human consumption and aquifer vulnerability

This research article was accepted in the journal *Groundwater for Sustainable Development* under the title *"Assessment of aquifer vulnerability and water quality: Validated using groundwater flow origin-based regression analysis"*.

The study aimed to evaluate the intrinsic vulnerability of the VP aquifer using the DRASTIC methodology adapted to the characteristics of a volcano-sedimentary environment and validate the results through simple linear regression analysis based on groundwater flow origin, correlating them with Water Quality Indices (WQI) and Contamination Indices (C_d).

The DRASTIC model was adjusted by modifying parameter weights to reflect local aquifer conditions, considering land use change (recharge, agricultural and urban areas) as the basis. Linear regression showed significant correlations ($p<0.001$) between vulnerability and WQI; for Sierra Nevada flows, an 84% fit was found between these two variables, and 83% for La Malinche.

DRASTIC classified 550 km^2 (25% of the area) as low vulnerability, 800 km^2 (36%) as moderate, and 690 km^2 (31%) as high. The most influential factors were recharge ($>$350 mm/year in critical zones), water table depth ($<$7 m) and topographic gradient ($>$5%). These results provide the first validation of an adapted DRASTIC with flow-origin-based regression for volcano-sedimentary aquifers. They emphasize the urgent need to protect recharge areas and regulate discharges into the Atoyac River. The methodology provides tools for sustainable management in subhumid environments under anthropogenic pressures.

Assessment of aquifer vulnerability and water quality: Validated using groundwater flow origin-based regression analysis

Ana Beatriz Rubio-Arellano †[a], José Alfredo Ramos-Leal†[a], Oscar Guadalupe Almanza-Tovar†[a], Víctor Manuel Vázquez-Báez*†[b], Janete Morán-Ramírez†[c]

[a]*División de Geociencias Aplicadas, Instituto Potosino de Investigación Científica y Tecnológica (IPICYT), Camino a la Presa de San José 2055, Lomas 4ta Secc., 78216, San Luis Potosí, México.*

[b]*Facultad de Ingeniería, Benemérita Universidad Autónoma de Puebla (BUAP), Blvd. Valsequillo y Av. San Claudio s/n, Ciudad Universitaria, Col. Jardines de San Manuel, Puebla, 72570, Puebla, México.*

[c]*Cátedras Conacyt, Instituto Potosino de Investigación Científica y Tecnológica (IPICYT), Camino a la Presa de San José 2055, Lomas 4ta Secc., 78216, San Luis Potosí, México.*

Abstract

The Puebla Valley aquifer (PV), a volcanosedimentary system located in central Mexico, faces increasing pressure due to land use change and groundwater contamination. However, its vulnerability had not been comprehensively assessed. This study aimed to evaluate the intrinsic vulnerability of the PV aquifer using the DRASTIC methodology adapted to the characteristics of a volcanosedimentary environment and validate the results using simple linear regression analysis based on the origin of groundwater flows, correlating them with water quality indices (WQI) and contamination indices (C_d).

The DRASTIC model was adjusted by modifying parameter weights to reflect local aquifer conditions, considering land use change (recharge, agricultural and urban zones) as the basis. Linear regression showed significant correlations ($p<0.001$) between vulnerability and WQI; for flows from Sierra Nevada, an 84% fit was found between these two variables, and 83% for La Malinche. The Atoyac River was identified as the main contamination source, with extreme values of WQI=35 (poor quality) and C_d >3 (high health risk) in adjacent areas.

DRASTIC classified 550 km^2 (25% of the area) as low vulnerability, 800 km^2 (36%) as moderate, and 690 km^2 (31%) as high. The most influential factors were recharge (>350 mm/year in critical zones), water table depth (<7 m) and topographic gradient (>5%).

These results validate for the first time a DRASTIC adapted with flow-origin-based regression for volcanosedimentary aquifers. They emphasize the need to: urgently protect recharge zones and regulate discharges into the Atoyac River. The methodology provides tools for sustainable management in subhumid environments, but under anthropogenic activities.

Keywords: DRASTIC, Aquifer Vulnerability, GIS, Water Quality Index, Contamination Index

*Corresponding author.

Email addresses: `ana.rubio@ipicyt.edu.mx` (Ana Beatriz Rubio-Arellano †), `jalfredo@ipicyt.edu.mx` (José Alfredo Ramos-Leal†), `oscar.almanza@ipicyt.edu.mx` (Oscar Guadalupe Almanza-Tovar†), `manuel.vazquez@correo.buap.mx` (Víctor Manuel Vázquez-Báez*†), `janete.moran@ipicyt.edu.mx` (Janete Morán-Ramírez†)

[1]These authors contributed equally to this work.

1. Introduction

The overexploitation and contamination of aquifers has become a global challenge, particularly in regions with high agricultural and urban demand (Egbueri et al., 2024; Yassin et al., 2024). Recent studies reveal the presence of microplastics in groundwater from 42 countries, including developed and developing nations (Agbasi et al., 2025); these emerging contaminants transport heavy metals and persistent organic compounds associated with health risks Boualem et al. (2025). Documented cases such as the Wadi Itwad aquifer in Saudi Arabia demonstrate the dual impact of human activity: large water table declines due to intensive extraction and nitrate contamination of agricultural origin Khan et al. (2023).

At a global scale, regions with subhumid climates face critical transformations in their water systems, derived from the combination of climate change and the growing overexploitation of aquifers (Opie et al., 2020; Taylor et al., 2022; Khan et al., 2023). The reduction in rainfall intensity, the increase in frequency of prolonged droughts, and the high water demand for agricultural use have reduced the natural recharge of aquifers (Huang et al., 2023; Elsaidy et al., 2025). Although extreme rainfall events occur that generate punctual recharge, these prove insufficient to compensate for the accumulated deficits.

In Mexico, the central region, characterized by a subhumid climate, experiences a similar situation. In the Guanajuato Bajío region, studies have reported average water table declines of 2 to 3 meters per year, causing land subsidence and progressive degradation of water quality, with the presence of contaminants such as arsenic and fluorides (Wester et al., 2011; Hoogesteger and Wester, 2017). Similar patterns, reported by Carrera-Hernández and Gaskin (2007), are observed in the Valley of Mexico, with drawdown rates of up to 3 m/year, and in the Querétaro Valley, where static level reductions of 2 to 3 m/year are recorded (Ochoa-González et al., 2013). The growing dependence on groundwater for various uses not only decreases its availability but also worsens quality-related risks, compromising regional water sustainability in the medium and long term.

This scenario highlights the need for studies that evaluate not only vulnerability but also groundwater availability and quality as inputs for sustainable management (Egbueri and Mgbenu, 2022). In this context, water quality indices such as the Water Quality Index (WQI) and Contamination Degree (C_d) have become fundamental tools for transforming physicochemical parameters and water ions into understandable indicators, facilitating decision-making (Egbueri and Mgbenu, 2020; Rahman et al., 2020). The WQI classifies water according to its suitability for human consumption, while the C_d quantifies contamination by comparing analytical concentrations with permissible limits (Egbueri and Mgbenu, 2022). Their combined application proves efficient for simultaneously characterizing overall water quality and detecting specific contamination hotspots.

The assessment of contamination vulnerability in aquifers has been addressed through multiple approaches, with overlay index-based methods like DRASTIC (Aller et al., 1987; Fannakh and Farsang, 2022) being particularly notable. This method considers seven hydrogeological parameters and applies weightings to identify areas with higher contamination susceptibility, integrating these data within Geographic Information System (GIS) environments to produce vulnerability maps (Daly et al., 2002; Taghavi et al., 2022). The incorporation of GIS has additionally enabled the integration of other indicators, such as WQI and C_d, into more comprehensive spatial analyses (Singha et al., 2019; Feng et al., 2020; Ourarhi et al., 2020).

However, the DRASTIC method has significant limitations, primarily related to subjectivity in weight assignment and lack of sensitivity to local aquifer conditions (Aslam et al., 2018; Agudelo Moreno et al., 2020). These weaknesses have led to the development of adjusted variants that seek to improve its predictive capacity and adaptation to specific hydrogeological contexts (Lad et al., 2019; Xiong et al., 2022; Miron Baki et al., 2024). Furthermore, DRASTIC does not establish a direct relationship between vulnerability and actual contamination, so its results must be validated through hydrogeochemical analyses (Jenifer and Jha, 2018).

In this study, adjustments are applied to the DRASTIC model to evaluate the intrinsic vulnerability of the Puebla Valley aquifer (PV), incorporating detailed hydrogeological information and geochemical data for a more robust interpretation. Unlike previous studies in Mexico, which have approached aquifer vulnerability from an exploratory perspective and at regional scales, this work proposes a more integrative approach by linking the DRASTIC model with water quality indices (WQI and C_d). It explicitly considers land-use change and vegetation cover as key factors in the spatial evolution of vulnerability and groundwater quality. This integration not only identifies zones with high contamination susceptibility but also establishes direct relationships between anthropogenic activities and the deterioration of water quality.

In this context, the overarching objective is to assess the intrinsic vulnerability of the aquifer PV using the DRASTIC methodology and validate the results with water quality indices. To achieve this goal, the following specific objectives are proposed: i) adapt the DRASTIC methodology to the local hydrogeological characteristics of a volcanic-sedimentary system; ii) calculate WQI and Cd indices to evaluate the suitability of groundwater for human consumption; iii) analyze the spatial relationship between vulnerability and water quality using Geographic Information Systems (GIS); and iv) propose recommendations to contribute to the sustainable management of this water resource.

2. Study area

The PV aquifer, located in the state of Puebla, Mexico (Fig. 1), encompasses a study area of 2025 km^2, with latitudes between 18°54' and 19°01' N, and longitudes between 98°01' and 98°39' E. This area is characterized by significant mountainous reliefs, including major elevations such as the Sierra Nevada and La Malinche, which serve as key contributors to the aquifer's recharge.

The topography of the region, ranging from 1,554 to 5,325 meters above sea level (Fig. 1), gives rise to a temperate sub-humid climate characterized by cold winters and rainy summers. Precipitation acts as a significant recharge source for the aquifer due to its physical characteristics.

The predominant soils in the region are Regosols, Cambisols, and Lithosols. Agricultural and livestock activities dominate much of the area, significantly contributing to contamination issues affecting the aquifer.

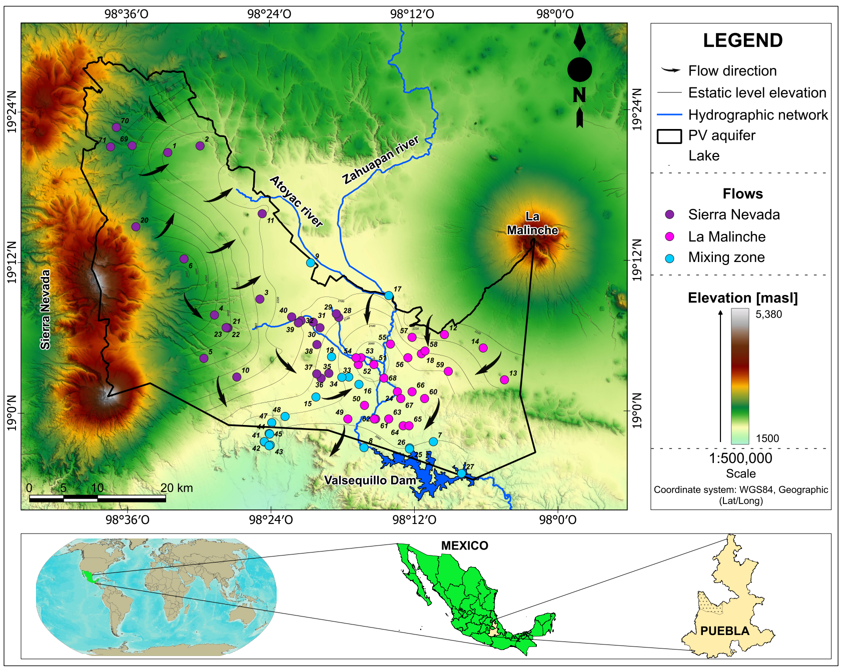

Fig. 1: Map showing the location of the PV aquifer and the distribution of water samples.

2.1. Geological setting

The Puebla Valley is of volcano-tectonic nature, derived from volcanic activity; this has been the main geological process that has allowed its formation with a high elevation (around 2200 meters above sea level). Additionally, it is crossed by the Trans-Mexican Volcanic Belt, which is a continental magmatic arc. This belt traverses the central-southern territory of Mexico, from the Pacific Ocean to the Gulf of Mexico.

The surface composition in the study area is varied and presents lateral irregularities. Alluvial, lacustrine, lava flows, lahars, pyroclastic materials, volcanic origin materials, and Cretaceous limestone deposits predominate (Salcedo-Sánchez et al., 2013), Fig. 2a. Flores-Márquez et al. (2006) report Pliocene lacustrine deposits (TpL), known as the first aquiclude, have been observed. These decrease in thickness from north to south, Fig. 2b. These deposits are approximately 50 meters thick in the valley, while alluvial thickness ranges from 150 to 200 meters.

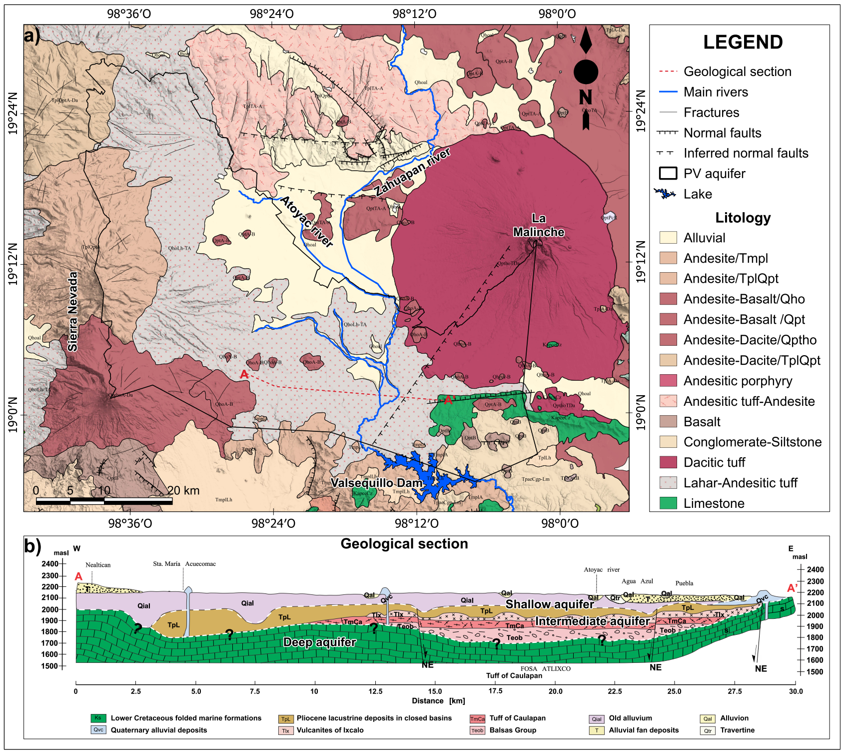

Fig. 2: Geology of the study area. a) Geological-structural map; b)Geological section of the VP aquifer.

2.2. Recharge and discharge

Groundwater recharge occurs primarily through direct rainfall infiltration and subsurface flow originating from runoff and infiltration from the east, north, and northeast. Groundwater discharge happens through underground flow towards the south and extraction via wells within the valley and the City of Puebla, resulting in the formation of cones of depression, Fig. 1.

2.3. Hydrogeological characteristics

Within the Puebla Valley, there are three aquifer systems. The first encompasses the entire study area except for the margins of the Atoyac River. It has a variable thickness ranging from 100 to 150 m, and the water it contains exhibits low salinity levels. Composed of Quaternary alluvial granular materials and

Tertiary lacustrine sands, except in the eastern zone of the City of Puebla, this high-potential aquifer supplies the majority of wells for potable water, irrigation, and industrial use.

The intermediate aquifer is distinguished from the shallow aquifer by the presence of sulfurous water with high salinity, particularly sulfates, as well as thermal water. This system is confined by a low-permeability clay layer that acts as an aquiclude. The average thickness of this aquifer is approximately 200 m. In the western part of the City of Puebla, this aquifer surfaces. Due to its depth and the low quality of its water, there are few extractions and representative measurements. Its base is composed of low-permeability limestone and marl.

The deep aquifer is bounded on its upper part by an aquiclude composed of low-permeability limestone and marl. This aquifer is mainly formed by calcareous marine deposits from the Lower Cretaceous. According to Silva Pérez (2003), this layer presents interconnected dissolution cavities that confer it secondary permeability. Additionally, Silva Pérez (2003) and Jiménez (2005) indicate that this aquifer underlies the metamorphic schist formations of the Acatlán complex.

The central region of the PV aquifer is intersected by the Atoyac River, acting as a drainage channel both on the surface and underground. The subsurface mainly comprises granular materials with variable permeability, influenced by compactness and clay content. Transmissivity varies across the area, with higher values near San Martin Texmelucan and lower values near Cholula. While the entire area is aquiferous, localized zones with low permeability restrict groundwater circulation.

2.4. Permeability and water use

Permeability varies across different locations, with the area between San Martin Texmelucan and Huejotzingo exhibiting high permeability. Areas around San Miguel Xoxtla have good aquifer characteristics but may contain locally impermeable zones. The western part of Puebla City has limited groundwater exploitation due to high saline content, whereas the eastern part has a large number of wells, primarily used by industries.

3. Materials and Methods

3.1. Sampling and analysis

In December 2021, a total of 71 groundwater samples were gathered from the PV aquifer, with the specific sampling locations shown in Fig. 1. Using the Hanna HI 98194 multiparameter instrument, various physicochemical parameters such as temperature, pH, electrical conductivity (EC), and Total Dissolved Solids (TDS) were measured at each sampling site. Additionally, alkalinity was determined in the field by conducting acid titration using phenolphthalein and bromophenol blue at a pH of 4.5.

The samples collected were stored in high-density polyethylene (HDLP) bottles. For anions analysis, 120 ml of each sample was collected, while for cations, 60 ml samples were acidified on-site to achieve a pH of 2. In the case of trace elements, 60 ml samples were obtained, and for organic matter analysis, 20 ml samples were taken. It is important to note that bottles designated for anions underwent a thorough cleaning process, being washed and rinsed seven times with deionized water. For cations and trace elements, a cleansing procedure involving 10% HCl was followed, and the bottles were subsequently rinsed seven times with deionized water. All collected samples were stored at a temperature below 4°C until they underwent laboratory analysis.

The analysis of cations was conducted using the ICP-OES (Inductively Coupled Plasma Optical Emission Spectroscopy) method. For the analysis of anions, the Colorimetry method was employed. Furthermore, an ion balance error was calculated to evaluate the accuracy of the results, all of which were within the range of ±10%. The chemical composition of the water samples was determined at the CGEO of the National Autonomous University of Mexico.

3.2. Indices for water characterization

3.2.1. Water quality index

The Water Quality Index (WQI) is used as a qualitative indicator of water condition. However, the results obtained through this index can be symbolic or a combination of variables that include both numeric and alphanumeric values (Jha et al., 2020; Uddin et al., 2021; Rajkumar et al., 2022). In countries like Mexico, the WQI is employed as a tool to assess the quality of water intended for human consumption (Rubio-Arias et al., 2012; Gaytán-Alarcón et al., 2022; Gómez-Mena et al., 2024). This indicator takes into account various chemical and physical parameters present in groundwater, providing a comprehensive measure of its suitability for consumption.

The calculations of the Water Quality Index (WQI) are derived from a chemical analysis of groundwater and the assignment of weights to the different solutes of interest (Egbueri and Mgbenu, 2020). The mathematical formula for WQI is presented as an equation in which the products of the percentages assigned to the parameters and the corresponding weights are summed, divided by the sum of the weights, as shown in Eq. 1.

$$WQI = K\frac{\sum C_i P_i}{\sum P_i} \tag{1}$$

where K is a weighting constant, and its value depends on the specific characteristics of the water. In this case, since it is apparently uncontaminated water, it was assigned a value of 1. C_i corresponds to the percentage value assigned to each parameter, while P_i indicates the weight of each parameter.

This index represents a weighted average of the importance of each water quality parameter, including considerations of odor and aesthetic aspects. Various physicochemical parameters were evaluated, such as major ions, total dissolved solids, electrical conductivity, temperature and pH. WQI values are standardized on a scale from 0 to 100. Groundwater is considered to have excellent quality when it achieves a WQI value of 100, while it is considered excessively polluted when the WQI score approaches zero.

3.2.2. Contamination index

The Water Contamination Index (C_d), is a metric used to establish a relationship between the concentrations of evaluated parameters, including major ions and physicochemical characteristics, and the maximum permissible limits established by national regulations, such as NOM127-SSA1-2021 in Mexico, as well as international regulations proposed by the Environmental Protection Agency (EPA). This index is applied individually to each analyzed sample.

The numerical values resulting from the index can be negative or positive, reflecting whether the concentrations are within or outside the limits established by the corresponding regulations. Negative values suggest that the permissible limits have not been exceeded, while positive values indicate the presence of contamination (Rajkumar et al., 2020; Bhardwaj et al., 2020). Its calculation is performed using the following mathematical expressions:

$$C_{fi} = \left(\frac{C_{Ai}}{C_{Ni}}\right) - 1$$

$$C_d = \sum_{i=1}^{n} C_{fi} \tag{2}$$

where C_{fi} corresponds to the contamination factor for the i-th parameter, C_{Ai} indicates the analytical value of the i-th component, C_{Ni} is the maximum permissible limit of the i-th parameter, and N is the normative value.

3.3. Collection, analysis and systematization of information for DRASTIC

For the development of the seven thematic layers of the DRASTIC model -depth to water **D**, net recharge **R**, aquifer media **A**, soil media **S**, slope **T**, impact of vadose zone **I**, and hydraulic conductivity **C**- databases from the National Water Commission (CONAGUA), the National Meteorological Service (SMN), the Mexican Geological Survey (SGM), and the National Institute of Statistics and Geography (INEGI) were utilized. The geospatial processing was performed using QGIS software version 3.22 Białowieża. Fig. 3 illustrates the workflow followed for generating the vulnerability map of the PV aquifer.

Each parameter considered in the DRASTIC model was rated on a scale from 1 to 10, where 10 indicates the highest vulnerability to contamination and 1 the lowest. These ratings were then multiplied by a specific weight reflecting the relative importance of each component within the model. The Eq. 3 integrates these values to calculate the final aquifer vulnerability level:

$$V_i = D_r D_w + R_r R_w + A_r A_w + S_r S_w + T_r T_w + I_r I_w + C_r C_w \tag{3}$$

Where the subscripts r correspond to intensity parameters and w are weight parameters. V_i corresponds to the DRASTIC index of aquifer vulnerability.

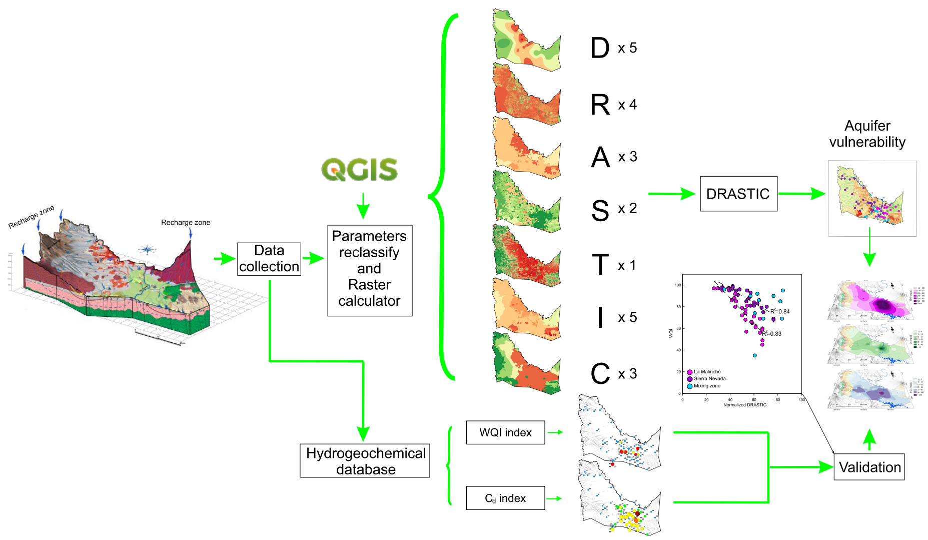

Fig. 3: Flow diagram of the DRASTIC methodology to prepare the vulnerability map of the PV aquifer

3.3.1. Depth of the static level [D]

Based on records from 56 piezometric wells from the year 2021, a distribution map of the static water level depth in the valley was generated using spatial interpolation through the Kriging method, with a resolution of 15 meters. Since the original DRASTIC methodology is designed for shallow aquifers, a correction was applied to the water depth values in order to adapt them to the local hydrogeological conditions, which are characterized by deeper aquifers, such as the PV aquifer (Ramos-Leal and Castillo, 2003). The reassigned weights for this layer are shown in Table 1.

3.3.2. Net recharge [R]

Net recharge was calculated based on the water balance of the aquifer. To this end, 24 climatological stations from the SMN were used, supplemented by three hypothetical stations located on the Popocatépetl, Iztaccíhuatl, and La Malinche volcanoes. Missing data from the stations were estimated using the Inverse Distance Weighted Method (IDWM), employing at least three neighboring stations as a reference. The mean annual precipitation was determined using the Thiessen polygon method in QGIS, assigning areas of influence to each station and validating the results through statistical tests of homoscedasticity.

The mean annual temperature was estimated using the same 26 stations, applying IDWM to complete the missing data. For the calculation of actual evapotranspiration (ET), the Turc formula (Eq. 4) was used, selected for its robustness under conditions of limited meteorological data availability. This formula considers both precipitation (P) and mean annual temperature (T):

$$ETR = \frac{P}{\sqrt{0.9 + \frac{P^2}{L^2}}},$$
$$L = 300 + 25T + 0.05T^3 \tag{4}$$

In Eq. 4, P is expressed in millimeters and T in °C. When using this formula, it is important to consider a theoretical limitation: if $P < 0.31L$, then $ETR = P$. This is because, under this condition, the ETR would otherwise exceed precipitation, which is not physically plausible.

Surface runoff was estimated using dimensionless coefficients that take into account the terrain slope and vegetation cover, determined from the Normalized Difference Vegetation Index (NDVI) obtained from Landsat-8 imagery, reclassified into three categories: dense vegetation, moderate vegetation, and bare soil.

Finally, net recharge was calculated using a modified water balance (Eq. 5), which incorporates precipitation, evapotranspiration, runoff, and contributions from irrigation return flow (5 of the water used) and infiltration due to leaks in urban water supply networks (22.5% of public supply), according to data reported by CONAGUA:

$$R = P - ETR - Esc + R_r + R_i \tag{5}$$

Where R corresponds to recharge, P is precipitation, ETR is actual evapotranspiration, Esc indicates runoff, R_r represents irrigation return flow, and R_i denotes recharge from urban leakage infiltration - all these parameters have units of mm/year. Once the net recharge layer was obtained, it was classified according to the values established in Table 1.

3.3.3. Aquifer media [A]

This thematic map was derived from the lithological information provided by the SGM, where igneous and sedimentary rocks predominate. As the lithological units are categorical and not expressed in numerical terms, a representative rating was assigned to each geological formation based on its characteristics. The ranges and weights for this parameter can be viewed in Table 2.

3.3.4. Soil Media [S]

The soil type corresponds to the description of the upper layer, specifically within the first two meters of depth. In this study, the 2021 land use and vegetation map provided by INEGI was used as the basis for classification. This approach represents a variation from the original methodology, in which numerical values were assigned to different types of land use and vegetation to quantify their contribution to aquifer vulnerability (see Table 3).

3.3.5. Topography "Slope" [T]

The topographic gradient refers to the inclination or slope of the terrain concerning the horizontal distance, expressed in degrees. This parameter was obtained using a digital elevation model from the CEM-INEGI, and the slopes were reclassified using GRASS-GIS. The weights and ratings can be consulted in Table 1.

3.3.6. Impact of the vadose zone [I]

The vadose zone is the unsaturated region of the subsurface that extends from the soil surface to the water table, where the soil contains air and water but is not fully saturated. For this parameter, lithological information from the SGM was used. The weights and the assigned weight for this layer can be consulted in Table 2.

3.3.7. Conductivity Hydraulic [C]

The hydraulic conductivity is defined as the subsurface's capacity to allow water flow. This parameter is obtained by evaluating the speed at which water can move through the soil. In this case, pumping tests conducted in the valley area by CONAGUA were used, along with well logs and lithological maps from the SGM. The weights and weighting of this parameter can be consulted in Table 1.

3.4. Normalization of the aquifer vulnerability map

To estimate the vulnerability of the PV aquifer, the DRASTIC method was applied by integrating the seven hydrogeological parameters previously calculated. The DRASTIC index was computed using Eq. 3, which assigns specific weights to each parameter to obtain a cumulative vulnerability value.

In order to facilitate comparison and interpretation, the resulting DRASTIC index values were normalized to a scale from 0 to 100, following the procedure described in Eq. 6:

$$V_{\text{in}} = 100 \times \left(\frac{V_i - V_{\text{imin}}}{V_{\text{imax}} - V_{\text{imin}}} \right) \tag{6}$$

Where, V_{in} corresponds to the normalized vulnerability index, V_i indicates the calculated vulnerability index, V_{imin} is the minimum value observed, and V_{imax} is the maximum vulnerability index. This normalization allows for a standardized representation of vulnerability levels across the aquifer.

4. Results

4.1. Evaluation of DRASTIC parameters

4.1.1. Depth of the static level [D]

The depth of the water table ranges from 5 to 155 meters, with the greatest depths recorded near the mountains (Nevada and La Malinche), as well as in the central-southern area of the Puebla metropolitan area. On the other hand, the shallowest portions are found in the valley, mainly in agricultural areas of the west-central region. Fig. 4a shows that the areas of highest vulnerability are located in the valley, while the lowest vulnerability areas correspond to the topographically elevated zones.

4.1.2. Net recharge [R]

The highest recharge comes from the slopes of Sierra Nevada, with values ranging from 675-915 mm/year. Similarly, in most of the valley, recharge ranges from 225-450 mm/year. This parameter was classified based on the DRASTIC metric, generally indicating net recharge values with a prevalence of weights greater than 8. Fig. 4b shows that recharge zones are associated with high vulnerability.

4.1.3. Aquifer media [A]

The valley area is composed of unconsolidated alluvial material, including gravel, sand, and clay, with an average thickness of 130 meters and low permeability. In contrast, the highest weights are assigned to areas with fractured volcanic rock, mainly distributed on the slopes of the volcanoes. The weights also remain high on the slopes of the mountains where there is presence of consolidated volcanic material, as illustrated in Fig. 4c.

4.1.4. Soil Media [S]

The highest weights for this parameter are associated with forested areas, primarily on the slopes of the Sierra Nevada, as well as regions with intensive agricultural activity. Conversely, the lowest weights correspond to bare or sparsely vegetated soils and urban zones, as illustrated in Fig. 4d.

4.1.5. Topography "Slope" [T]

The characteristic topographic gradient of this area indicates a very steep slope in the volcano zone, which favors runoff but not infiltration. On the other hand, the gentle slopes of the valley allow for greater water infiltration.

In general, the volcano zone (Popocatépetl, Iztaccíhuatl, and La Malinche) presents a low degree of vulnerability due to the steep slopes. In contrast, the valley area has a high risk of contamination, as shown in Fig. 4e.

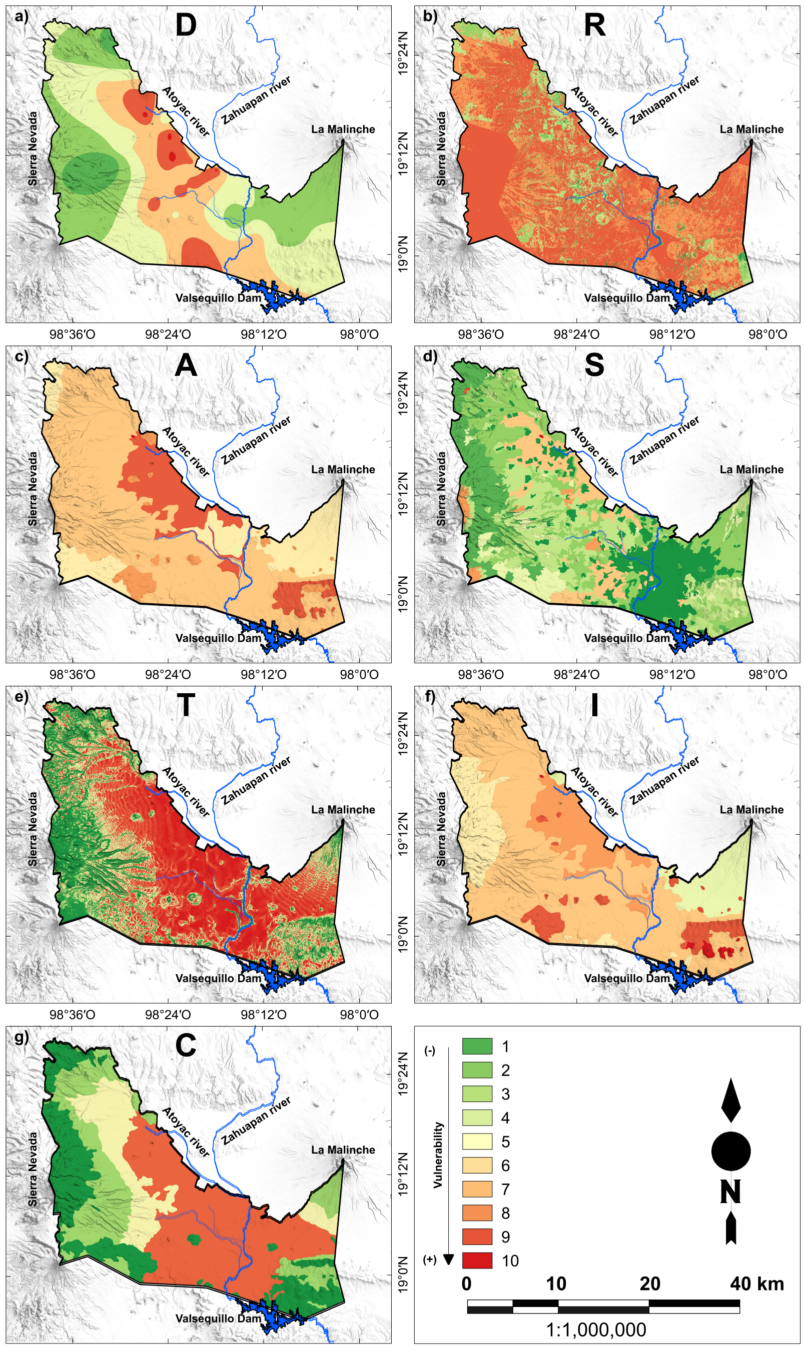

Fig. 4: Spatial Distribution of DRASTIC Parameters in the VP Aquifer. a) Water Table Depth; b) Net Recharge; c) Aquifer Media; d) Soil Type; e) Topographic Gradient; f) Vadose Zone Impact; g) Hydraulic Conductivity.

4.1.6. Impact of the vadose zone [I]

The highest vulnerability values are associated with recharge areas, primarily in Sierra Nevada, caused by the presence of andesitic tuffs with a high degree of fracturing. Low vulnerability is found in sedimentary rocks consisting mainly of conglomerates and limestone. Additionally, in the foothills of the volcanoes, there are areas of intermediate vulnerability. On the other hand, in the valley area, the predominant lithology consists of unconsolidated alluvial material, including gravel, sand, and clay, where there are low vulnerability values, as illustrated in Fig. 4f.

4.1.7. Conductivity Hydraulic [C]

Fig. 4g shows that the highest hydraulic conductivity values are primarily located in the central and southern parts of the valley, coinciding with alluvial deposits, agricultural areas, and metropolitan zones, suggesting a greater capacity for groundwater flow. In contrast, areas with lower conductivity, located to the north and west in the elevated regions near Sierra Nevada and La Malinche, indicate the presence of less permeable materials associated with consolidated volcanic rocks.

4.2. Aquifer Vulnerability Map [DRASTIC]

The normalized vulnerability index of the Puebla Valley aquifer exhibits a distinct spatial distribution, with medium-to-high vulnerability values (exceeding 50%) concentrated primarily in the central and southeastern sectors of the study area (Fig. 5). These vulnerable zones correlate with favorable hydrogeological conditions for contaminant transport, including shallow groundwater depths, elevated recharge rates, and gentle topographic slopes. In contrast, reduced vulnerability occurs in topographically elevated areas characterized by lower-permeability geological formations. This spatial heterogeneity underscores the critical influence of local hydrogeological settings on aquifer contamination susceptibility.

Regarding the water table depth, high values are recorded because it is a shallow aquifer, with the water table approximately at 30 meters, making it highly vulnerable to contamination problems. Additionally, the net recharge in the valley area also suggests high values, mainly due to the subhumid temperate climate of the region. The topographic gradient layer indicates high values in the valley, as the aquifer is surrounded by large elevations such as Sierra Nevada and La Malinche. It is also relevant to consider that much of the valley is an agricultural zone, which has significantly modified land use and increased its vulnerability.

On the other hand, low to medium vulnerability is distributed mainly on the slopes of Sierra Nevada and to a lesser extent in La Malinche. Although the parameters of aquifer media, soil type, vadose zone impact, and hydraulic conductivity suggest high values in these areas, volcanic rocks with fracturing do not significantly influence the vulnerability of this aquifer.

The vulnerability of La Malinche is more affected compared to Sierra Nevada due to the lower topographic slope and the lithology present in the area, resulting in lower hydraulic conductivity values. Recharge zones show low vulnerability values and are associated with large elevations, as they present unique conditions that make them less susceptible to contamination.

The interaction between the aquifer and the Atoyac River exerts a significant influence on some DRASTIC parameters. Near the channel, the water table becomes shallower due to direct recharge, while net Recharge increases through surface water infiltration. The associated floodplains exhibit gentle Topographic slope, enhancing infiltration. Additionally, Hydraulic conductivity is elevated due to highly permeable alluvial deposits, which facilitate water flow and contaminant transport.

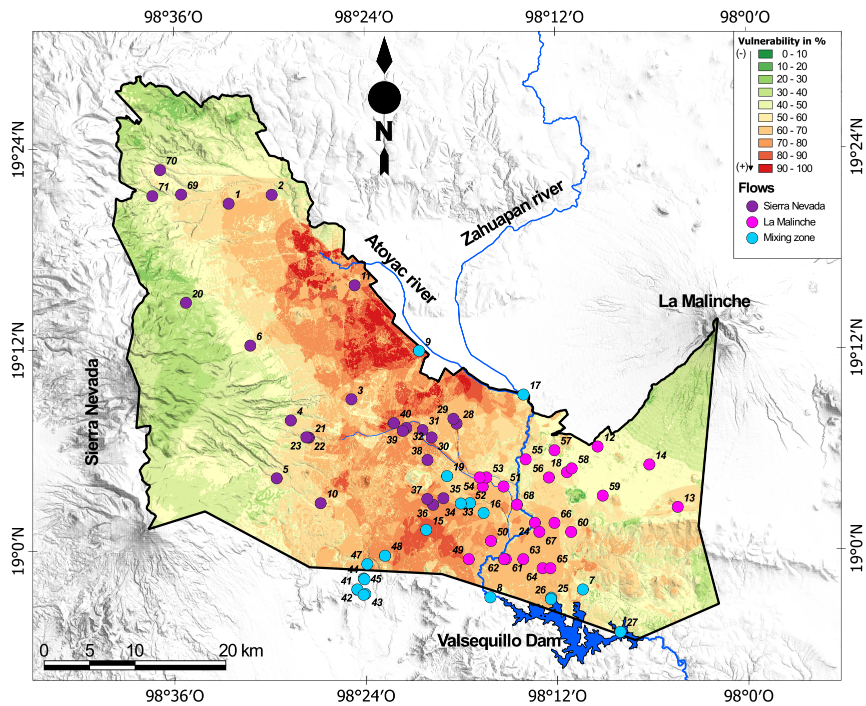

Fig. 5: Correlation between aquifer vulnerability and water quality in two different groundwater flow sources.

4.3. Indices for water characterization

The PV aquifer, being shallow, makes the Water Quality Index (WQI) an effective tool for comprehensive water quality assessment. Samples obtained indicate WQI values ranging from 33% to 99%, with higher percentages indicative of better quality. Of these samples, 27 samples are classified as excellent, 16 as acceptable, 11 as slightly contaminated, 14 as contaminated, 2 as heavily contaminated, and 1 as excessively contaminated, as shown in Fig. 6a.

On the other hand, according to the methodology of the water Contamination Index Cd, values can range from negative to positive. Negative values indicate samples without signs of contamination. In the case of the PV aquifer, 61 samples have a low C_d, 4 have a medium C_d, and 7 present a high C_d, as illustrated in Fig. 6b.

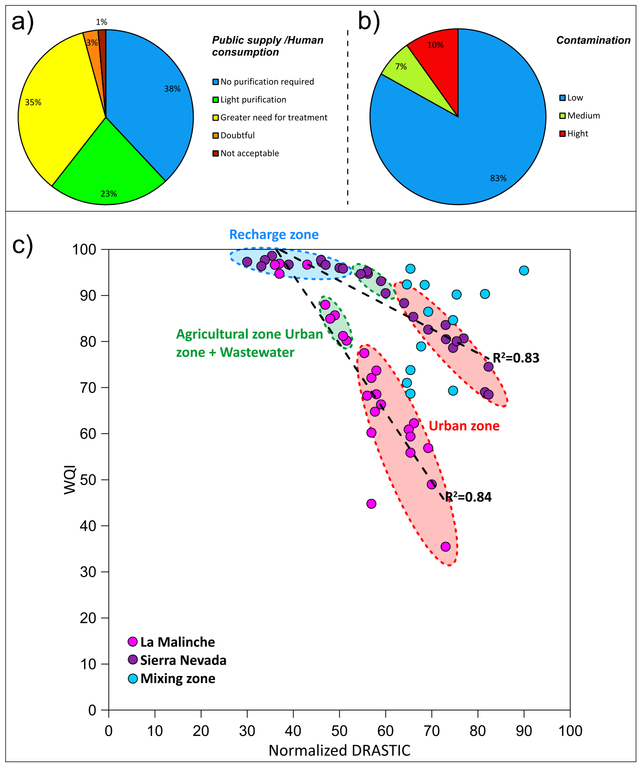

Fig. 6: Distribution of percentage values of water characterization indices. a) Water Quality Index; b) Water Contamination Index: c) Relationship between DRASTIC and WQI indices considering land use change.

4.4. Validation of the vulnerability map

Our results demonstrate a significant improvement in the correlation between DRASTIC and WQI compared to previous studies. For instance, Jang et al. (2025) in the Pingtung Plain (Taiwan) reported moderate correlations (r = 0.69) between DRASTIC and nitrate-nitrogen when incorporating parameters like land use and dissolved oxygen, while İpek and Türker (2024) in the Yesilköy aquifer initially found weak correlation (r = 0.2) that required AHP method adjustments to achieve moderate correlation (r = 0.65). In contrast, this study achieved high correlation (r = 0.9) in a volcanic-sedimentary aquifer through contextualized DRASTIC weight adjustments based on local hydrogeological characteristics. While the modified DRASTIC method applied in this study provides a good spatial assessment of vulnerability, recent approaches integrating hydrological modeling and water quality parameters (Dang et al., 2022) could offer an even more detailed analysis, particularly in highly complex hydrogeological settings.

The DRASTIC vulnerability map was validated through Pearson correlation analysis between the vulnerability index and water quality parameters (Table 4). Results showed a strong negative correlation between DRASTIC and WQI (R^2 = -0.82, $p < 0.001$), indicating that areas with higher vulnerability consistently exhibited poorer water quality. A moderate positive correlation was observed between DRASTIC and Cd (R^2 = 0.54, $p < 0.005$), suggesting that more vulnerable zones often had elevated contamination levels, though with notable exceptions. As expected, WQI and Cd showed a significant negative correlation (R^2 = -0.78, $p < 0.001$), confirming the inverse relationship between overall water quality and contamination intensity.

To account for anthropogenic influences on natural hydrogeological processes, we stratified the analysis by recharge source. For La Malinche-derived flows, linear regression revealed a strong negative DRASTIC-WQI relationship (R^2 = 0.83, $p < 0.001$), demonstrating that high-recharge areas maintained better water quality. Similarly, Sierra Nevada flows showed an even stronger correlation (R^2 = 0.84, $p < 0.001$), with DRASTIC explaining 84% of WQI variability. These results confirm that vulnerability mapping reliably reflects water quality degradation along groundwater evolutionary pathways.

No significant correlation was found between DRASTIC and WQI in the valley area and near the Atoyac River, where groundwater flows from Sierra Nevada and La Malinche converge, and which is also a zone of high human activity. Based on the above, three groups were identified : Sierra Nevada (26 samples), La Malinche (27 samples), and the mixing zone (11 samples), as shown in Fig. 6c. The lowest WQI values were recorded near the tributaries of the Atoyac River, suggesting contamination caused by irrigation return flow and urban wastewater. This spatial pattern confirms that while DRASTIC effectively predicts natural vulnerability, anthropogenic factors can decouple vulnerability from water quality trends in urbanized areas.

A strong inverse relationship was observed between WQI and TDS, with the linear regression model explaining 81% of the variability (Fig. 7a). This demonstrates that water quality systematically declines with increasing mineralization, particularly in discharge zones adjacent to the Atoyac River. The pronounced TDS peak in the valley area clearly reflects cumulative impacts from irrigation return flows and untreated wastewater discharges, as shown in Fig. 8a.

The WQI-Cl^- relationship showed a moderately strong negative correlation (Fig. 7b), revealing a distinct spatial pattern. While recharge zones maintained low chloride concentrations (<50 mg/L), values increased progressively through agricultural areas before peaking in the valley (Fig. 8b). Land use practices and natural water-rock interactions likely drive this spatial pattern.

Sulfate exhibited the most complex behavior, with a strong WQI correlation (Fig. 7c) but dual control mechanisms. The convergence zone of Sierra Nevada and La Malinche flows showed maximum SO_4^{2-} concentrations (>150 mg/L), attributable to both natural geological sources and anthropogenic inputs from urban/industrial wastewater (Fig. 8c). This bimodal origin is supported by: 1) elevated background levels in Sierra Nevada groundwater (geogenic), and 2) point source peaks near industrial facilities along the Atoyac River.

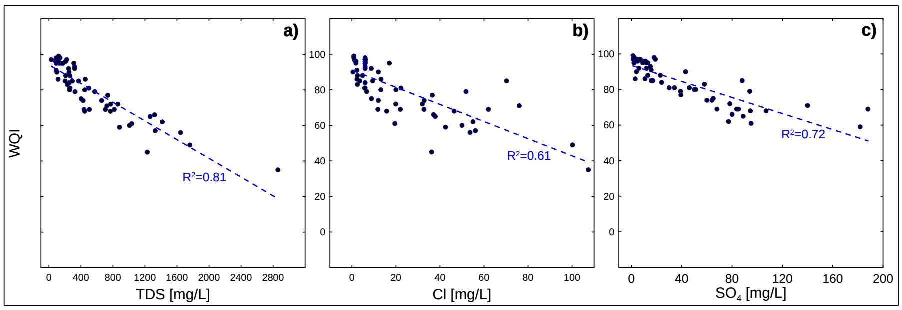

Fig. 7: Correlation of the Water Quality Index (WQI. a) WQI vs TDS; b) WQI vs Cl; c) WQI vs SO_4.

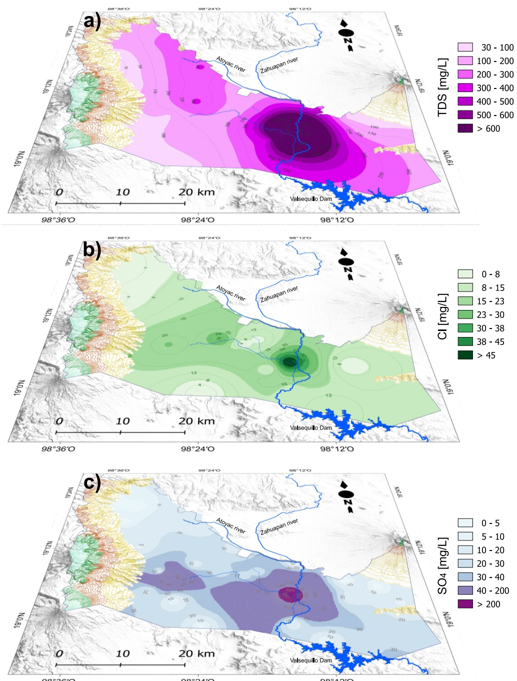

Fig. 8: Spatial distribution of vulnerability and physicochemical parameters in the PV aquifer. a) TDS; b) Cl; c) SO_4.

5. Discussion of results

In this case study, the accuracy of the DRASTIC model was evaluated in relation to WQI, with groundwater flow origins considered as a key factor. Fig. 9a displays the topographic profile extending from Sierra Nevada to the valley. The central portion of the PV aquifer is traversed by the Atoyac River, which drains both surface water and groundwater flow toward the Valsequillo Dam, located south of the aquifer. Recharge occurs through direct infiltration in the valley and via groundwater flow from the east, north, and northeast, moving toward the Atoyac River and south of Puebla. Discharge takes place through southward groundwater flow and well extraction.

Fig. 9b shows aquifer vulnerability in relation to land use changes. The first 24 km correspond to the recharge zone in Sierra Nevada, with vulnerability values below 65%. Subsequently, the agricultural area extends to km 48, showing vulnerability between 60% and 80%. Finally, the urban zone displays highly variable vulnerability values, ranging from 20% to 90%.

Fig. 9c illustrates distinct hydrochemical patterns along the groundwater flow path. The Sierra Nevada recharge zone exhibits baseline water quality conditions with low TDS (<150 mg/L) and NO_3 concentrations (< 5 mg/L). This transitions abruptly in agricultural areas (24-48 km), where intensive farming practices elevate TDS (350-600 mg/L) and NO_3 (15-45 mg/L) due to fertilizer and pesticide leaching. A secondary contamination threshold occurs beyond 38 km, where tributaries of the Atoyac River contribute wastewater-derived solutes, increasing TDS by 30-40% and NO_3 by 25-35% above agricultural background levels. The urban zone shows the most severe degradation, with TDS (800-1200 mg/L) and NO_3 (50-80 mg/L) levels reflecting combined impacts from: 1) irrigation return flows, 2) untreated domestic and industrial wastewater, and 3) direct input from informal settlements lacking sanitation infrastructure, all transported through the Atoyac River system.

Fig. 9d reveals a marked spatial pattern in water quality indices. The recharge zone maintains excellent water quality (WQI >90), characteristic of pristine groundwater conditions. However, a progressive WQI deterioration occurs through agricultural areas (WQI 80-85), strongly correlated with: 1) fertilizer/pesticide leaching, and 2) contamination inputs from Atoyac River tributaries. Concurrently, the C_d exceeds permissible limits (C_d >0). The urban zone displays critically low WQI values (<40), followed by secondary anthropogenic sources (industrial discharges y urban runoff).

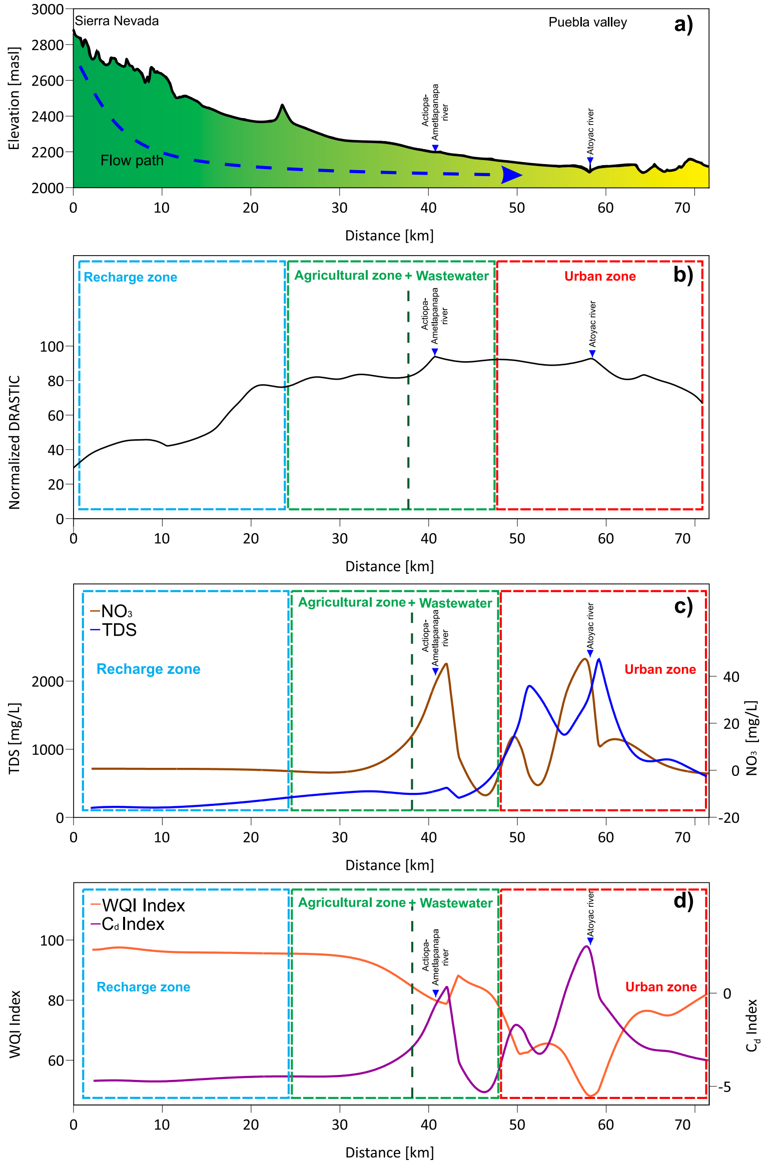

Fig. 9: Distribution of groundwater quality and contamination in Sierra Nevada. a) Topographic profile; b) Normalized DRASTIC; c) TDS [mg/L]; d) WQI Index.

Furthermore, Fig. 10a displays the topographic profile extending from La Malinche toward the valley. This region is partially bisected by the Atoyac and Actiopa-Ametlapanapa rivers, with La Malinche constituting a major recharge source for the PV aquifer. Fig. 10b presents vulnerability values associated with groundwater flow dynamics, revealing three distinct zones: 1) the urban valley area, exhibiting high vulnerability (90-60%); 2) the rainfed agricultural zone with moderate vulnerability (60-40%); and 3) the recharge area with lower vulnerability (<35%).

The TDS and NO_3 concentrations (Fig. 10c) are elevated in urban zones, indicating wastewater contamination transported by the Atoyac River and its tributaries. In contrast, the agricultural area at the base of La Malinche shows low concentrations, demonstrating minimal contaminant presence. As expected, recharge areas exhibit the lowest recorded levels.

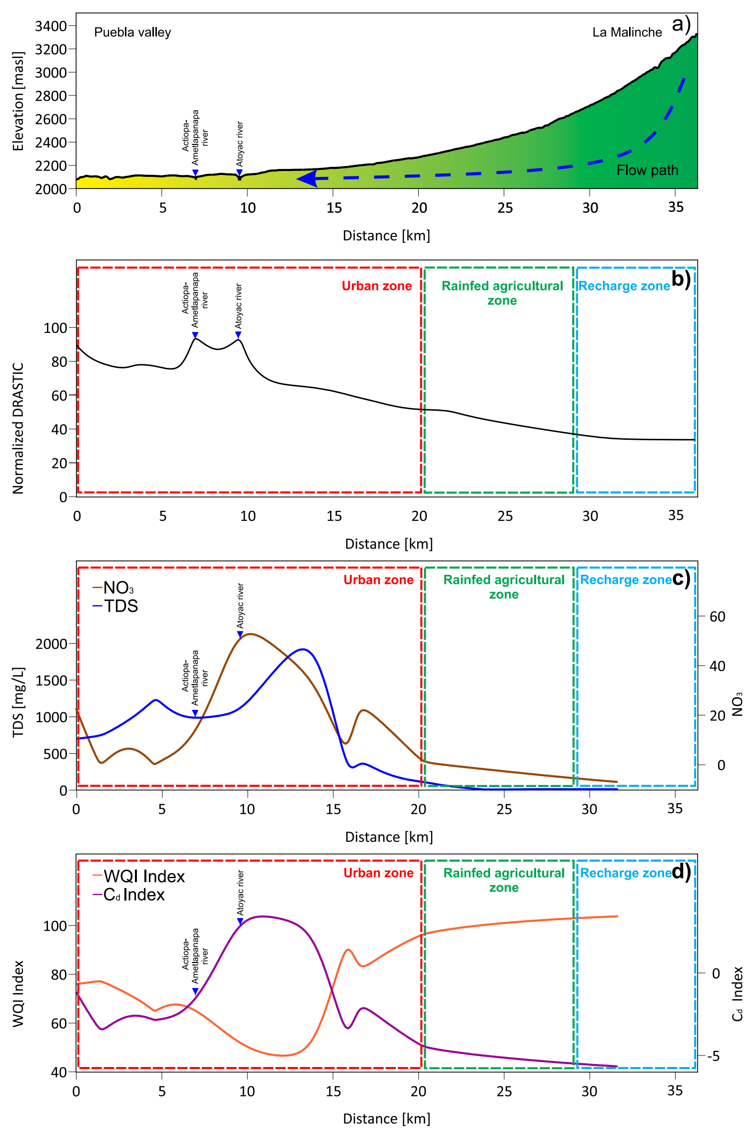

Fig. 10: Distribution of groundwater quality and contamination in La Malinche. a) Topographic profile; b) Normalized DRASTIC; c) TDS [mg/L]; d) WQI Index.

Fig. 10d demonstrates that both the WQI and C_d indices reveal significant contamination in the valley, particularly downstream of Puebla's urban and industrial zones (WQI >85, C_d >0). Water quality progressively deteriorates toward the Atoyac and Actiopa-Ametlapanapa rivers, exceeding permissible limits for human consumption. In contrast, recharge areas and agricultural zones maintain good water quality (WQI >95, Cd <0).

Fig. 11a confirms degraded water quality near the Atoyac, Prieto, and Actiopa-Ametlapanapa rivers, resulting from intensive agricultural practices and the discharge of irrigation return flows and untreated wastewater into the hydrological system. The WQI classification identified a deep well (100 m) with severe SO_4 contamination, linked to surface runoff from the Atoyac River and industrial effluents infiltrating through geological faults (Sánchez et al., 2017). In contrast, recharge zones (Sierra Nevada and La Malinche) maintain optimal water quality (WQI >90; Fig. 11a), highlighting the direct impact of human activities on aquifer degradation. Spatial analysis of the Cd index (Fig. 11b) reveals pronounced contamination in the valley (Cd >0), while recharge areas remain pristine (Cd <0). Critical parameters in discharge zones including TDS, NO_3 and SO_4 consistently exceed regulatory limits for potable water, underscoring the need for targeted remediation strategies in anthropogenically affected areas.

The distribution of VP aquifer vulnerability is illustrated in Table 5. Over a quarter of the aquifer exhibits low or very low vulnerability, while the largest proportion falls under the moderate category. Notably, more than half of the aquifer comprises relatively contamination-free areas, though these regions remain persistently vulnerable to potential contamination. A significant portion of the aquifer was classified as having high or very high vulnerability, underscoring the need for targeted protective measures.

These findings have critical implications for the region's water security. The marked degradation of water quality along the groundwater flow path, particularly in urban and industrial zones near the Atoyac River, demonstrates an imminent risk to potable water supplies. The progressive increase in contaminants (NO_3 and SO_4) associated with agricultural activities, industrial discharges, and inadequate sanitation not only reduces safe water availability but also increases treatment costs, compromising long-term resource sustainability (Agbasi et al. , 2024).

However, the preservation of recharge zones in both Sierra Nevada and La Malinche presents a key opportunity for sustainable management strategies. To ensure water security, three critical measures are required: 1) strict protection of recharge areas where vulnerability is naturally low and water quality remains optimal; 2) rigorous control of contamination sources along the Atoyac River corridor, prioritizing treatment of urban and industrial wastewater; and 3) continuous monitoring of agricultural zones where moderate vulnerability may worsen due to intensive fertilizer use. These measures are essential not only to mitigate immediate risks but also to balance efficient water resource use with the social and economic well-being of populations directly dependent on this vital resource.

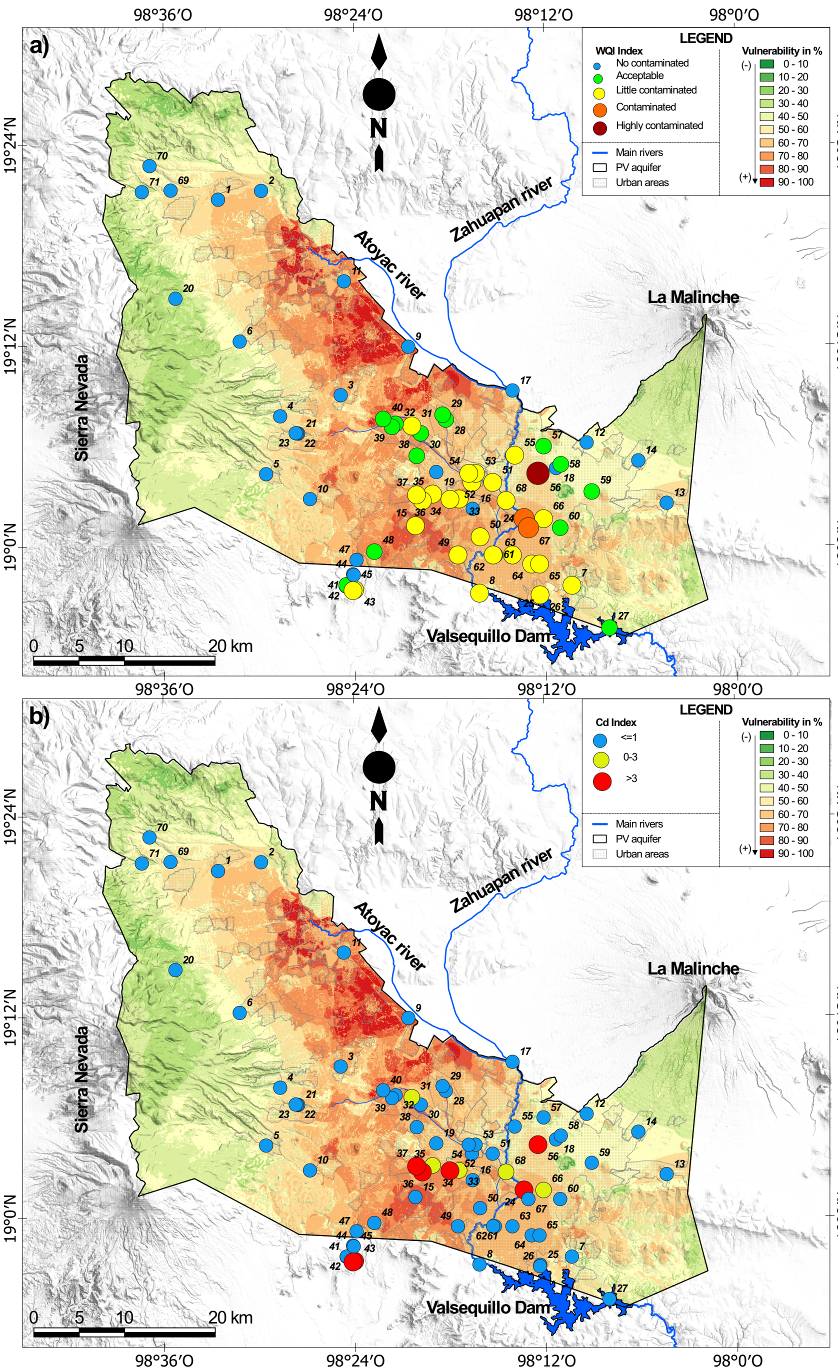

Fig. 11: Aquifer vulnerability validation map. a) Spatial distribution of the water quality index; b) Spatial distribution of the water contamination index.

6. Limitations and Future Research Directions

While our study provides robust evidence of vulnerability in the VP (volcanic-sedimentary) aquifer, four key limitations must be considered: 1) the fixed DRASTIC weights may underestimate vulnerability in hydrogeological transition zones, requiring specific adjustments where permeability changes abruptly, thus, integrating geophysical methods and hydrochemical analyses is essential to track contaminant migration in heterogeneous media (Alao et al., 2023); 2) the low DRASTIC-WQI/C_d correlation in the valley suggests anthropogenic contamination (point-source industrial discharges) dominates over natural vulnerability; 3) the 71 sampling points, while adequate for regional scale, do not capture high spatial variability near the Atoyac River confluence; and 4) only the shallow aquifer was evaluated, necessitating characterization of both intermediate and deep aquifers.

For future research, we propose: a) optimizing DRASTIC for urban areas by incorporating impervious surfaces and sewer networks; b) local studies in agricultural areas to quantify irrigation return flows and their relationship with NO_3; and c) depth sampling to evaluate vertical connectivity and multi-aquifer vulnerability. These advances would enable more precise water resource management in complex systems like the VP.

7. Conclusions

In this study, a vulnerability map was constructed for the PV aquifer using GIS and the DRASTIC methodology. The results suggest lower vulnerability in recharge areas such as Sierra Nevada and La Malinche, while the most vulnerable areas are located in the valley, where a significant portion of agriculture in the region occurs, along with urbanization and the flow of the Atoyac river. In total, 34% of the total aquifer area is highly vulnerable, highlighting the need for land use planning in the region.

The overlay of the spatial distribution of the WQI index and the DRASTIC vulnerability map revealed the necessity of studying groundwater from the perspective of flow origins, as the physical conditions of the two recharge systems are completely different.

A relationship was observed between water contamination in high-vulnerability areas and good water quality associated with low-vulnerability areas. Additionally, by overlaying the C_d index, based on permissible limits established in the study area, with DRASTIC, it was found that recharge areas show no contamination, while samples distributed in the valley exhibit signs of contamination.

The moderate to high vulnerability is attributed to the presence of granular materials with variable permeability and clay content. Most of the recharge comes from rainfall, which infiltrates and flows through subsurface materials. Recharge occurs both by direct infiltration in the valley and by groundwater flow from runoff and infiltrations from the east, north, and northeast, flowing towards the Atoyac river and south towards the city of Puebla. The DRASTIC parameters that significantly influence the vulnerability of this aquifer are net recharge, depth to the water table, and topographic gradient.

Through simple linear regression analysis, the relationship between the water quality index (WQI) and the vulnerability map of the aquifer created using the DRASTIC methodology was evaluated. Although a strong correlation was not found across the entire aquifer, two distinct trends were identified in the statistical analysis, which were related to the origin of the groundwater flows recharging the aquifer.

The validation of the vulnerability-quality water relationship in Sierra Nevada showed a correlation of 84%, while the flow from La Malinche was 83%. Linear regression was not applied to the valley area because water quality has been altered by fertilizer use in the agricultural zone and the return of irrigation combined with wastewater in the industrial and urban areas. Therefore, the mixture of flows from La Malinche and Sierra Nevada combined with anthropogenic contamination alters water quality.

This research demonstrates how water quality varies with the evolution of groundwater, emphasizing the importance of considering the origin and distribution of groundwater flows in its analysis.

Author contributions

All authors have contributed equally to the research and preparation of the manuscript. Material preparation, data collection, and analysis were conducted by Janete Moran Ramírez, Ana Beatriz Rubio Arellano, and José Alfredo Ramos Leal. The contributions of Oscar Guadalupe Almanza Tovar and Víctor Manuel Vázquez Báez involved review and supervision. The first draft of the manuscript was written by Ana Beatriz Rubio Arellano and José Alfredo Ramos Leal; all authors provided comments on previous versions of the manuscript. All authors have read and agreed to the published version of the manuscript.

Declarations

Funding sources

This research did not receive any specific grant from funding agencies in the public, commercial, or not-for-profit sectors.

Data availability statement

All data that was used in this study are in the manuscript. Any other data that may be required from the author's will be available on request.

References

Agbasi, J.C., Abu, M., Egbueri, J.C., 2024. Towards sustainable industrial development: modelling the quality, scaling potential and corrosivity of groundwater using GIS, spatial statistics, soft computing and index-based methods. Environ. Dev. Sustain. 1-41. https://doi.org/10.1007/s10668-024-05105-3.

Agbasi, J.C., Egbueri, J.C., Pande, C.B., Khan, M.Y.A., Ighalo, J.O., Uwajingba, H.C., Abba, S.I., 2025. Review of the potential effects and remediation strategies of microplastic pollutants in drinking water sources. Anal. Lett. 58 (5), 799–839. https://doi.org/10.1080/00032719.2024.2343366.

Agudelo Moreno, L.J., Zuleta Lemus, D., Lasso Rosero, J., Agudelo Morales, D.M., Sepúlveda Castaño, L.M., Paredes Cuervo, D., 2020. Evaluation of aquifer contamination risk in urban expansion areas as a tool for the integrated management of groundwater resources. Case: Coffee Growing Region, Colombia. Groundw. Sustain. Dev. 10, 100298. https://doi.org/10.1016/j.gsd.2019.100298.

Alao, J.O., Abdo, H.G., Ayejoto, D.A., Mohammed, M.A.A., Danladi, E., Saqr, A.M., Almohamad H., Fahad, A. 2023. Evaluation of Groundwater contamination and the Health Risk Due to Landfills using integrated geophysical methods and Physiochemical Water Analysis. Case Stud. Chem. Environ. Eng. 8, 100523. https://doi.org/10.1016/j.cscee.2023.100523.

Aller, L., Lehr, J.H., Petty, R., 1987. DRASTIC: A standardized system to evaluate groundwater pollution potential using hydrogeologic settings. National Water Well Association, Worthington, Ohio, 1987. Truman Bennett, Bennett and Williams, Inc. Columbus, Ohio, 43229.

Aslam, R.A., Shrestha, S., Pandey, V.P, 2018. Groundwater vulnerability to climate change: A review of the assessment methodology. Sci. Total Environ. 612, 85–875. https://doi.org/10.1016/j.scitotenv.2017.08.237.

Bhardwaj, S., Soni, R., Gupta, S.K., Shukla, D.P., 2020. Mercury, arsenic, lead and cadmium in waters of the Singrauli coal mining and power plants industrial zone, Central East India. Environ. Monit. Assess. 192(4), 251. https://doi.org/10.1007/s10661-020-8225-2.

Bouselsal, B., Satouh, A., Egbueri, J.C., Hashim, M.A., Arafat, A.A., Paramasivam, P. Alzaed, A., Hussein, E.E., 2025. Groundwater for drinking and sustainable agriculture and public health hazards of nitrate: Developmental and sustainability implications for an arid aquifer system. Results Eng. 25, 104160. https://doi.org/10.1016/j.rineng.2025.104160.

Carrera-Hernández, J.J., Gaskin, S.J., 2007. The Basin of Mexico aquifer system: regional groundwater level dynamics and database development. Hydrogeol J. 15, 1577–1590. https://doi.org/10.1007/s10040-007-0194-9.

Daly, D., Dassargues, A., Drew, D., Dunne, S., Goldscheider, N., Neale, S., Popescu, I., Zwahlen, F., 2002. Main concepts of the "European approach" to karst-groundwater-vulnerability assessment and mapping. Hydrogeol J. 10, 340–345. https://doi.org/10.1007/s10040-001-0185-1.

Dang, X., Gao, M., Wen, Z., Hou, G., Jakada, H., Ayejoto, D., Sun, Q., 2022. Saline groundwater evolution in the Luanhe River delta (China) during the Holocene: hydrochemical, isotopic, and sedimentary evidence. Hydrol. Earth Syst. Sci. 26 (5), 1341–1356. https://doi.org/10.5194/hess-26-1341-2022.

Egbueri, J.C., Mgbenu, C.N., 2020. Chemometric analysis for pollution source identification and human health risk assessment of water resources in Ojoto Province, southeast Nigeria. Appl. Water Sci. 10 (4), 1–18. https://doi.org/10.1007/s13201-020-01180-9.

Egbueri, J.C., Mgbenu, C.N., 2022. Assessment of groundwater vulnerability mapping methods for sustainable water resource management: An overview. J. Water Land Dev. 52, 186–198. https://doi.org/10.24425/jwld.2022.140389.

Egbueri, J.C., Agbasi, J.C., Ezugwu, A.L., Omeka, M.E., Ucheana, I.A., Aralu, C.C., Abugu, H.O., 2024. Metal(loid)s, nitrate, polycyclic aromatic hydrocarbons, and radioactive contaminants in Nigerian water resources: state-of-the-art of their ecological and health risk assessments. Environ. Dev. Sustain. 1–50. https://doi.org/10.1007/s10668-024-05423-6.

Elsaidy, A., Yimer, E.A., Mogheir, Y., Huysmans, M., Villani, L., Van Griensven, A., 2025. Groundwater drought and anthropogenic amplifiers: A review of assessment and response strategies in arid and semi-arid areas. Sci. Total Environ. 978, 179406. https://doi.org/10.1016/j.scitotenv.2025.179406.

Fannakh, A., Farsang, A., 2022. DRASTIC, GOD, and SI approaches for assessing groundwater vulnerability to pollution: a review. Environ. Sci. Eur. 34(1), 77. https://doi.org/10.1186/s12302-022-00646-8.

Feng, B., Wang, J., Zhang, Y., Hall, B., Zeng, C., 2020. Urban flood hazard mapping using a hydraulic–GIS combined model. Nat Hazards. 100, 1089–1104. https://doi.org/10.1007/s11069-019-03850-7.

Flores-Márquez, E.L., Jiménez-Suárez, G., Martínez-Serrano, R.G., Chávez, R.E. and Pérez, D.S., 2006. UStudy of geothermal water intrusion due to groundwater exploitation in the Puebla Valley aquifer system, Mexico. Hydrogeol J. 14, 1216–1230. https://doi.org/10.1007/s10040-006-0029-0.

Gaytán-Alarcón, A.P., González-Elizondo, M.S., Sánchez-Ortíz, E., Alarcón-Herrera, M.T., 2022. Comparative assessment of water quality indices—a case study to evaluate water quality for drinking water supply and irrigation in

Northern Mexico. Environ. Monit. Assess. 194(8), 588. https://doi.org/10.1007/s10661-022-10198-2.

Gómez-Mena, B., Morán-Ramírez, J., Almanza-Tovar, O.G., López Álvarez, B., Martínez-Morales, M., Ramos-Leal, J.A., 2024. Aquifer vulnerability assessment in the oaxacan complex: integrating the DRASTIC methodology, TEM, and water quality analysis. Environ. Earth Sci. 83(24), 667. https://doi.org/10.1007/s12665-024-11983-7.

Hoogesteger, J., Wester, P., 2017. Regulating groundwater use: The challenges of policy implementation in Guanajuato, Central Mexico. Environ. Sci. Policy. 77, 107–113. https://doi.org/10.1016/j.envsci.2017.08.002.

Huang, J., Cao, L., Wang, L., Liu, L., Yu, B., Han, L., 2023. Identification and Spatiotemporal Migration Analysis of Groundwater Drought Events in the North China Plain. Atmosphere. 14, 961. https://doi.org/10.3390/atmos14060961.

Jang C.S., Chen, S.K., Chang, L.F., 2025. Evaluation of groundwater vulnerability to nitrate-nitrogen by using probability-based modssified DRASTIC models with source and attenuation factors. J. Hydrol. 655, 132951. https://doi.org/10.1016/j.jhydrol.2025.132951.

Jenifer, M.A., Jha, M.K., 2018. Comparative evaluation of GIS-based models for mapping aquifer vulnerability in hard-rock terrains. Environ. Earth Sci. 77, 672. https://doi.org/10.1007/s12665-018-7821-8.

Jha, M.K., Shekhar, A., Jenifer, M.A., 2020. Assessing groundwater quality for drinking water supply using hybrid fuzzy-GIS-based water quality index. Water Res. 179, 115867. https://doi.org/10.1016/j.watres.2020.115867.

Jiménez, G., 2005. Exploración de modelo de flujo y transporte en el acuífero del Valle de Puebla. Ph.D. Universidad Nacional Autónoma de México, Instituto de Geofísica, Posgrado en Ciencias de la Tierra. Distrito Federal, México

Khan, M.Y.A., ElKashouty, M., Abdellattif, A., Egbueri, J.C., Taha, A.I., Al Deep, M., Shaaban, F., 2023. Influence of natural and anthropogenic factors on the hydrogeology and hydrogeochemistry of Wadi Itwad Aquifer, Saudi Arabia: Assessment using multivariate statistics and PMWIN simulation. Ecol. Indic. 151, 110287. https://doi.org/10.1016/j.ecolind.2023.110287.

Lad, S., Ayachit, R., Kadam, A., Umrikar, B., 2019. Groundwater vulnerability assessment using DRASTIC model: a comparative analysis of conventional, AHP, Fuzzy logic and Frequency ratio method. Model. Earth Syst. Environ. 5, 543–553. https://doi.org/10.1007/s40808-018-0545-7.

Miron Baki, A., Ghavami, S.M., Qureshi, S.A.M., Ghaffari, O., 2024. A three-step modification of the DRASTIC model using spatial multi criteria decision making methods to assess groundwater vulnerability. Groundw. Sustain. Dev. 26, 101277. https://doi.org/10.1016/j.gsd.2024.101277.

Ochoa-González, G. H., Teatini, P., Carreón-Freyre, D., Gambolati, G., 2013. Modeling the deformation of faulted volcano-sedimentary sequences associated to groundwater withdrawal in the Queretaro Valley, Mexico. MODSIM. 2737–2743. https://doi.org/10.1016/j.gsd.2024.101277.

Opie, S., Taylor, R.G., Brierley, C., Shamsudduha, M., Cuthbert, M., 2020. Climate–groundwater dynamics inferred from GRACE and the role of hydraulic memory. Earth Syst. Dyn. 11, 775–791. https://doi.org/10.5194/esd-11-775-2020.

Ourarhi, S., Barkaoui, A.E., Zarhloule, Y., Kadiri, M., Bouiss, H., 2020. Groundwater vulnerability assessment in the Triffa Plain based on GIS combined with DRASTIC, SINTACS, and GOD models. Model. Earth Syst. Environ. 10 (1), 619–629. https://doi.org/10.1007/s40808-023-01801-7.

Rahman, M.A., Paul, M., Bhoumik, N., Hassan, M., Alam, M.K., Aktar, Z., 2020. Heavy metal pollution assessment in the groundwater of the Meghna Ghat industrial area, Bangladesh, by using water pollution indices approach. Appl. Water Sci. 10 (8), 1–15. https://doi.org/10.1007/s13201-020-01266-4.

Rajkumar, H., Naik, P.K., Rishi, M.S., 2020. A new indexing approach for evaluating heavy metal contamination in groundwater. Chemosphere. 245, 125598. https://doi.org/10.1016/j.chemosphere.2019.125598.

Rajkumar, H., Naik, P.K., Rishi, M.S., 2022. A comprehensive water quality index based on analytical hierarchy process. Ecol. Indic. 145, 109582. https://doi.org/10.1016/j.ecolind.2022.109582.

Ramos-Leal, J.A., Castillo, R., 2003. Aquifer vulnerability mapping in the Turbio river valley, Mexico: a validation study. Geofis. Int. 42(1),141–156. https://doi.org/10.22201/igeof.00167169p.2003.42.1.367.

Rubio-Arias, H., Contreras-Caraveo, M., Quintana, R.M., Saucedo-Teran, R.A., Pinales-Munguia, A., 2012. An Overall Water Quality Index (WQI) for a Man-Made Aquatic Reservoir in Mexico. Int. J. Environ. Res. Public Health. 9 (5), 1687–1698. https://doi.org/10.3390/ijerph9051687.

Salcedo-Sánchez, E.R., Esteller, M.V., Garrido Hoyos, S.E., Martínez-Morales, M., 2013. Groundwater optimization model for sustainable management of the Valley of Puebla aquifer, Mexico. Environ. Earth Sci. 70, 337–351. https://doi.org/10.1007/s12665-012-2131-z.

Silva Pérez, D., 2003. Modelo evolutivo del acuífero del Valle de Puebla. Ph.D. Universidad Nacional Autónoma de México. Distrito Federal, México

Singha, S.S., Pasupuleti, S., Singha, S., Singh, R., Venkatesh, A.S., 2019. A GIS-based modified DRASTIC approach for geospatial modeling of groundwater vulnerability and pollution risk mapping in Korba district, Central India. Environ. Earth Sci. 78, 1–19. https://doi.org/10.1007/s12665-019-8640-2.

Sánchez, E.R.S., Hoyos, S.E.G., Esteller, M.V., Morales, M.M., Astudillo, A.O., 2019. Hydrogeochemistry and water-rock interactions in the urban area of Puebla Valley aquifer (Mexico). J. Geochem. Explor. 181, 219–235. https://doi.org/10.1016/j.gexplo.2017.07.016.

Taghavi, N., Niven, R.K., Paull, D.J., Kramer, M., 2022. Groundwater vulnerability assessment: A review including new statistical and hybrid methods. Sci. Total Environ. 822, 153486. https://doi.org/10.1016/j.scitotenv.2022.153486.

Taylor, R., Aureli, A., Allen, D., Banks, D., Villholth, K., Stigter, T., 2022. Chapter 7: Groundwater, aquifers and climate change, in: Connor, R. (Ed.), The United Nations World Water Development Report 2022: Groundwater: Making the Invisible Visible. UNESCO, Paris, France, pp. 101—114.

Uddin, M.G., Nash, S., Olbert, A.I., 2021. A review of water quality index models and their use for assessing surface water quality. Ecol. Indic. 122, 107218. https://doi.org/10.1016/j.ecolind.2020.107218.

Wester, P., Sandoval Minero, R., Hoogesteger, J., 2011. A review of water quality index models and their use for assessing surface water quality. Hydrogeol J. 19, 889–899. https://doi.org/10.1007/s10040-011-0733-2.

Xiong, H., Wang, Y., Guo, Han, J., Ma, C., Zhang, X., 2022. Current status and future challenges of groundwater vulnerability assessment: A bibliometric analysis. J. Hydrol. 615, 128694. https://doi.org/10.1016/j.jhydrol.2022.128694.

Yassin, M.A., Abba, S.I., Shah, S.M.H., Usman, A.G., Egbueri, J.C., Agbasi, J.C., Khogali, A., Baalousha, H.M., Aljundi, I.H., Sammen, S.S., Scholz, M., 2024. Toward Decontamination in Coastal Regions: Groundwater Quality, Fluoride, Nitrate, and Human Health Risk Assessments within Multi-Aquifer Al-Hassa, Saudi Arabia. Water. 16 (10), 1401. https://doi.org/10.3390/w16101401.

İpek, C., Türker, U., 2024. Geospatial-Based Groundwater Resources Susceptibility and Contamination Risk Mapping for Yeşilköy Aquifer, Cyprus. "Environ. Earth Sci. 83 (15), 446. https://doi.org/10.1007/s12665-024-11761-5.

Table 1: Ranges and ratings for Depth to Water, Net Recharge, Topography, and Hydraulic Conductivity.

Parameter		**Range**	**Rating**
Depth to Water [D]	Weight = 5	0–7.5	10
		7.5–23	9
		23–45.5	7
		45.5–76.0	5
		76.0–114.5	3
		114.5–152.5	2
		>152.5	1
		Units: m	
Net Recharge [R]	Weight = 4	0–50.8	1
		50.8–101.6	3
		101.6–177.8	7
		177.8–254.0	8
		>254	9
		Units: mm	
Topography [T]	Weight = 1	0–2	10
		2–6	9
		6–12	5
		12–18	3
		>18	1
		Units: %	
Hydraulic Conductivity [C]	Weight = 3	0.04–4.08	1
		4.08–12.22	2
		12.22–28.55	4
		28.55–40.75	6
		40.75–81.49	8
		>81.49	10
		Units: m/day	

Table 2: Ranges and Ratings for Aquifer Media (A) and Vadose Zone Media (I)

Aquifer Media [A] (Weight = 3)	**Rating**		**Vadose Zone [I] (Weight = 5)**
	A	**I**	
Massive shale	2	1	Silt/clay
Metamorphic/igneous	3	3	Shale
Weathered metamorphic/igneous	4	4	Metamorphic/igneous
Thin-bedded sandstone, limestone–shale sequences	6	6	Sand and gravel with significant silt and clay
Massive sandstone	6	6	Bedded limestone, sandstone, shale
Massive limestone	8	6	Sandstone
Sand and gravel	8	6	Limestone
Basalt	9	8	Sand and gravel
Karst limestone	10	9	Basalt
–	–	10	Karst limestone

Table 3: Ranges and ratings for Soil Media used in the VP aquifer

Soil Media [S]	**Weight = 2**	**Rating**
No apparent vegetation		1
Permanent rainfed agriculture		2
Cultivated forest / Oak-pine forest		2
Annual and semi-permanent rainfed agriculture		3
Annual rainfed agriculture		3
Secondary arboreal vegetation of Táscate forest		3
Annual and perennial rainfed agriculture		4
Induced grassland		4
Secondary arboreal vegetation of temperate forest (low coverage)		4
Secondary arboreal vegetation of temperate forest		5
Semi-permanent irrigation agriculture		5
Annual and semi-permanent irrigation agriculture		7
High mountain prairie		7
Annual and perennial irrigation agriculture		8
Bodies of water		10

Table 4: Correlation matrix analyzing the relationships among DRASTIC, WQI, and Cd.

	DRASTIC	**WQI**	**Cd**
DRASTIC	1.0		
WQI	-0.9	1.0	
Cd	0.5	-0.7	1.0

Table 5: Area of vulnerability identified by DRASTIC in the PV aquifer.

Vulnerability	**Area [km^2]**	**Percentage [%]**
Very low	19.4	1.0
Low	533.4	26.2
Moderate	788.7	38.8
High	574.7	28.3
Very high	116.0	5.7

Chapter 5

Hydrogeochemical modeling

This research article was published in *Modeling Earth Systems and Environment* under the title *"Identification of natural water sources and anthropogenic contamination applying the VISHMOD methodology in a volcano-sedimentary aquifer"*. The publication aimed to study the origin, distribution, and circulation of groundwater through hydrogeochemical modeling.

The research detected that water-rock interaction processes govern groundwater composition. The VISHMOD methodology was implemented to identify and simulate mixing processes and water-rock interactions in the VP aquifer. Results identified three end members: the first associated with local flow, the second with intermediate flow in a volcanic environment, and the third with regional flow in a carbonate environment.

VISHMOD modeling suggests groundwater chemical composition has been affected by anthropogenic contamination associated with influence from the Atoyac River, irrigation return flows, and wastewater from the Puebla metropolitan area. Ternary mixing processes define the flows, where the local end member contributes 74%, indicating recharge zone dominance. Regional members (located in carbonate rocks) contribute 9%, while the intermediate member (in volcanic rocks) accounts for the remaining 17%.

Modeling Earth Systems and Environment (2024) 10:4845–4861
https://doi.org/10.1007/s40808-024-02032-0

ORIGINAL ARTICLE

Identification of natural water sources and anthropogenic contamination applying the VISHMOD methodology in a volcano-sedimentary aquifer

Ana Beatriz Rubio-Arellano[1] · Janete Morán-Ramírez[2] · Jose Alfredo Ramos-Leal[3]

Received: 14 December 2023 / Accepted: 28 April 2024 / Published online: 24 May 2024

Abstract

This study employs hydrogeochemical modeling as a tool for the hydrogeological investigation of the Puebla Valley aquifer (PV). The aim is to gain insights into the origin, distribution, and circulation of groundwater. The objective is to identify the water-rock interaction processes that govern the composition of groundwater, contributing to a comprehensive understanding of the PV aquifer's chemical variations in the study area. The VISHMOD methodology is implemented to identify and simulate water-rock mixing and interaction processes in the study aquifer. Three end-members were identified: one associated with local flow, intermediate flow in a volcanic environment and regional flow in a carbonate environment. The results suggest that the groundwater chemistry has been affected due to anthropogenic contamination associated with the influence of the Atoyac River, the return of irrigation water, and wastewater from the metropolitan area of the city of Puebla. Ternary mixing processes define the flows, where the local extreme member contributes 74%, indicating the dominance of recharge zones. On the other hand, the regional members (located in carbonate rocks) contributes 9%, and the intermediate member (located in volcanic rocks) contributes the remaining 17%.

Keywords Hydrogeochemical modeling · VISHMOD · Water–rock interaction · Groundwater · End member · Mixing groundwater

Ana Beatriz Rubio-Arellano, Janete Morán-Ramírez and Jose Alfredo Ramos-Leal have contributed equally to this work.

✉ Jose Alfredo Ramos-Leal
jalfredo@ipicyt.edu.mx

Ana Beatriz Rubio-Arellano
ana.rubio@ipicyt.edu.mx

Janete Morán-Ramírez
janete.moran@ipicyt.edu.mx

[1] Posgrado en Geociencias Aplicadas, Instituto Potosino de Investigación Científica y Tecnológica (IPICYT), Camino a la Presa de San José 2055, Lomas 4ta Secc., San Luis Potosí 78216, San Luis Potosí, Mexico

[2] Cátedras Conacyt, Instituto Potosino de Investigación Científica y Tecnológica (IPICYT), Camino a la Presa de San José 2055, Lomas 4ta Secc., San Luis Potosí 78216, San Luis Potosí, Mexico

[3] División de Geociencias Aplicadas, Instituto Potosino de Investigación Científica y Tecnológica (IPICYT), Camino a la Presa de San José 2055, Lomas 4ta Secc., San Luis Potosí 78216, San Luis Potosí, Mexico

Introduction

Hydrogeochemistry is a scientific discipline that investigates the distribution of groundwater with varying properties and compositions. It also examines the conditions of the geological medium through which it circulates and the causes and effects of changes in these properties and compositions (Lakshmanan et al. 2003; Tikhomirov 2016). Hydrogeochemistry draws upon fundamental sciences such as mathematics, chemistry, physics, geology, and biology; however, mathematical modeling has become an essential component in contemporary hydrogeochemistry (Laaksoharju et al. 2008).

Groundwater possesses distinct advantages over surface water; notably, it is less affected by evaporation, pollution, and climate change (Epting et al. 2021). Furthermore, the widespread spatial distribution and absence of storage capacity loss in aquifers are essential benefits of groundwater (Jakeman et al. 2016).

Understanding the geochemical evolution of groundwater characteristics is crucial for achieving sustainable development and effective water resource management (Varol and Sekerci 2018). Hydrogeochemical modeling serves as a tool for hydrogeochemical characterization and the identification of evolutionary processes, mixtures, and rock-water interactions contributing to the final chemical signature of groundwater.

VISHMOD is a comprehensive methodology designed to interpret the evolutionary history of groundwater chemical characteristics through a series of steps. The goal is to calibrate and validate the proposed model to obtain analytical errors or ionic deltas (Moran-Ramírez and Ramos-Leal 2014; Moran-Ramírez 2016; Moran-Ramírez et al. 2018; Morán-Ramírez et al. 2020). The VISHMOD methodology bears similarity to the sequence of steps in flow models, as both involve a comparison between modeled and field data.

In this study, we employ the VISHMOD (Virtual Samples in Hydrochemical Modeling) methodology as a tool to elucidate the evolutionary process of groundwater in the Puebla Valley aquifer (PV). The VISHMOD methodology standardizes hydrogeochemical modeling to ensure the model can reproduce field measurements uniformly (Moran-Ramírez and Ramos-Leal 2014; Moran-Ramírez 2016; Moran-Ramírez et al. 2018; Morán-Ramírez et al. 2020).

Volcano-sedimentary aquifers result from a complex geological history, leading to a heterogeneous distribution of fractures (Manciati et al. 2021). These aquifers are characterized by the interdigitation of volcanic and sedimentary material (Moran-Ramírez et al. 2018). Generally, aquifers exhibit some degree of heterogeneity, but fractured rock aquifers often have highly anisotropic hydraulic properties such as hydraulic conductivity, influencing infiltration rates (Cook 2003).

Numerous investigations delve into hydrogeochemical processes in volcano-sedimentary aquifers, covering hydrogeochemical characterization, identification of hydrogeochemical processes, and the origin, composition, and evolution of groundwater (Esteller et al. 2017; Fonseca-Montes et al. 2020; Morán-Ramírez et al. 2020; Tay 2021; Che et al. 2021; Morán-Ramírez et al. 2022).

In the last four decades, global publications on hydrogeochemical modeling have increased. However, in Mexico, this trend is not mirrored, with limited publications leading to a lack of knowledge about water interaction processes with the geological environment in the Mexican territory.

Mexico boasts 653 aquifers for evaluation, management, and national water administration in the subsoil (CONAGUA 2022). In countries like Mexico, groundwater is of vital importance, often serving as the primary and only permanent water source in arid regions. The quality and quantity of water resources are currently considered national security concerns worldwide (Spring 2014). Hence, the study and proper management of water are priorities in integral water systems management.

In recent decades in Mexico, hydrogeological studies focused on specific areas, such as pumping zones, with little consideration for recharge zones. Consequently, these studies only address immediate needs rather than long-term concerns. A comprehensive survey of the hydrogeological system, including recharge and discharge zones, provides detailed insights into the aquifer's response to various hydrogeological-administrative situations.

This research aims to identify and quantify the hydrogeological processes in the Puebla Valley aquifer through hydrogeochemical modeling with VISHMOD methodology. The objective is to understand the origin, circulation and distribution of groundwater flow, its interaction with the geological environment and anthropogenic alteration.

Study area and regional geology

General settings

The study area is situated in the Trans-Mexican Volcanic Belt (TMVB) physiographic province, specifically within subprovince 57, known as "Lagos y volcanes de Anáhuac". This region is characterized by imposing volcanic mountains, including Mexico's highest volcanoes: Popocatépetl, Iztaccíhuatl, and La Malinche. The study area encompasses a diverse topography, ranging from plains and plateaus to volcanic mountains.

The PV aquifer is centrally located in the State of Puebla, between latitudes 18°54' to 19°01' N and longitudes 98°01' to 98°39' W, covering approximately 2,025 km^2, Fig. 1a. Geopolitically, it spans 26 municipalities of the State of Puebla, 20 entirely and six partially. As of August 2021, the average annual water availability in this aquifer is estimated at 20,667,700 hm^3/year (CONAGUA 2020).

Using data from the CLICOM database (CLICOM 2000), we analyzed 21 climatological stations to calculate the precipitation and temperature of the aquifer. The valley experiences an annual mean temperature of 15.3°C, with yearly rainfall ranging from 650 to 900 mm. The highest rainfall is recorded on the tops of the surrounding volcanoes, with average values of 1350 mm/year for Popocatépetl and Iztaccihuatl, and 1000 mm/year for La Malinche.

The study area falls within the Atoyac River basin, with the Atoyac River being the primary collector. This river originates from the northern slope of the Iztaccíhuatl volcano and is fed by various tributaries, including Tlahuapan, Turin, Otlati, Atotonilco, and San Jerónimo rivers. Downstream, it passes through the city of Puebla,

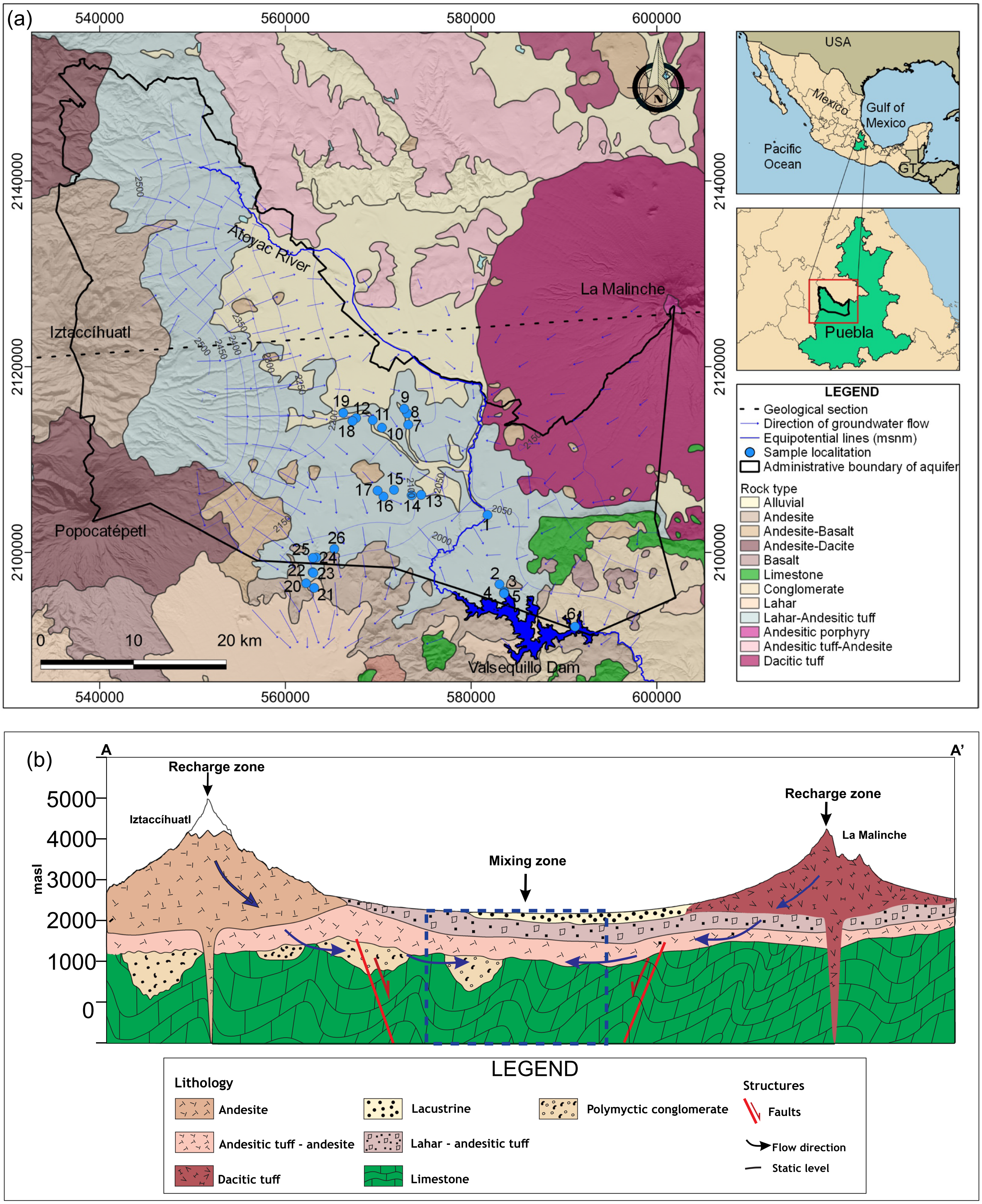

Fig. 1 Geology of the study area. **a** Location of testing wells and groundwater flow directions; **b** Hydrogeological conceptual model of the VP aquifer

receiving contributions from the Coronado and Malinche rivers and wastewater from Puebla and Cholula, ultimately reaching the Valsequillo dam.

The geology of the Puebla Valley is complex and variable, encompassing metamorphic terrains of Precambrian, Paleozoic, and Mesozoic ages. The geological materials exhibit heterogeneity, with prevalent lava flows, lahars, alluvial and lacustrine deposits, volcanic materials, and Cretaceous limestones.

Mooser (1996) described the tectonism of the Puebla basin, identifying faults and fractures with significant impacts on land subsidence. These subsided areas now serve as groundwater storage, with medium to medium-high permeability in alluvial and volcanic fillings. Fracturing and faulting have played a crucial role in facilitating water circulation.

The formation of the Puebla Valley began in the Cambrian with the construction of the Acatlán complex, representing the oldest deposits in the area (Cserna 1989). During the Triassic period, a detrital and carbonate marine sedimentary sequence evidenced oceanic invasion. In the Cenozoic era, volcanism developed in the Trans-Mexican volcanic belt. The calcareous rocks at the basin's lower part serve as the hydrogeological basement, reflecting the hydrogeological impact of the complex geological events in the Puebla basin (Siebe et al. 1996; Flores-Márquez et al. 2006).

This research aims to identify and quantify hydrogeological processes in the Puebla Valley aquifer through hydrogeochemical modeling. The goal is to understand the origin, circulation, and distribution of groundwater flow and its interaction with the geological environment.

The zones with the highest elevations correspond to volcanic structures and play a crucial role in the initial recharge of the aquifer. To the west is the Sierra Nevada, and to the northeast is La Malinche, Fig. 1a. Two primary aquifer recharge zones are identified: the first from the Popocatépetl and Iztaccíhuatl volcanoes (South Zone of Sierra Nevada), and the second from the La Malinche volcano. The flows eventually converge and mix in the Valley area, heading towards the central part of the Atoyac River.

According to the Comisión Nacional del Agua (CONAGUA), in 1997, groundwater depths in the valley zone varied between 5 and 35 m. The highest elevation zones had greater static level depths, gradually changing from 60 to 155 m. In 2002, the depth of the static level generally increased throughout the area, more prominently near the mountains (Sierra Nevada and La Malinche). By 2010, the shallowest static levels were found at a depth of 25 m in the valley zone, while in the highest elevation zones, they reached a depth of 125 m. Overall, the topography of the valley controls the flow directions.

As depicted in Fig. 1a, the study area is locally constituted by sedimentary and extrusive igneous rocks with ages ranging from Cretaceous to Recent, distributed in the metavolcanosedimentary sequence of the Terreno Guerrero. The cross-section illustrates the subsoil of the aquifer, primarily formed by extrusive volcanic material and, to a lesser extent, by sedimentary rock. Generally, the predominant lithology consists of andesites, andesitic tuffs, dacitic tuff, basalt, alluvial material, limestones, and conglomerates, Fig. 1b.

Within the aquifer, there is an upper portion composed of unconsolidated fluvial and alluvial material, including gravels, silt, clays, sands, and lahar material. It has an approximate thickness of 130 ms and exhibits medium to high permeability, enabling groundwater recharge and flow. Conversely, the lower portion consists of fractured extrusive igneous rocks, such as basalts and andesites, with a thickness of several hundred meters. Bounded by calcareous rocks at the base, considered the hydrogeological basement of the basin. The geological faults and fractures of the region contribute to the contamination of the shallow aquifer by vertical flows from the deep aquifer and the contribution of minerals in the shallow aquifer, see Fig. 1b. On the other hand, intense agricultural activity contributes to the return of irrigation with poor quality water to the shallow aquifer.

Sampling and analytical methods

Twenty-six groundwater samples were collected within the valley zone of aquifer from December 13 to 15, 2021; the sampling locations are shown in Fig. 1a. To ensure sample integrity, all accessories, including bottles and containers, were thoroughly washed with groundwater from the respective wells before use. Nitrile gloves were worn during the sampling process to prevent contamination.

In wells equipped with a pump, water was allowed to run for approximately 30 s before sample collection. In wells without a pump, water was manually obtained by introducing a container into the well.

During each sampling event, in situ measurements of temperature, pH, electrical conductivity (EC), dissolved oxygen (DO), oxidation-reduction potential (ORP), and total dissolved solids (TDS) were conducted using a HANNA HI 98194 multiparameter instrument. Alkalinity was also measured in the field through acid titration using phenolphthalein and bromophenol blue at pH 4.5.

Polyethylene bottles (HDLP) were used for sample collection, with 60 ml for cation analysis, 120 ml for anions, and 55 ml for trace elements. Bottles were pre-rinsed with filtered sample water (0.45 µm) from each well. For anion bottles, a meticulous cleaning process was followed, involving seven washes with deionized water. Cation and trace element bottles were washed with 10% HCl and then rinsed seven times with deionized water.

Samples designated for cations and trace element analysis underwent in situ acidification to achieve pH<2 using ultra-pure nitric acid. Conversely, samples for anion analysis were not acidified. The ICP method was employed for anion and cation analysis at the CGEO UNAM (National Autonomous University of Mexico) laboratory, while the colorimetric method, applied at the IPICYT (Potosino Institute of Scientific and Technological Research), was used for anion analysis.

Methodology

In Moran-Ramirez and Ramos-Leal, 2014 research (Moran-Ramírez and Ramos-Leal 2014; Moran-Ramírez et al. 2018), shows and details each of the steps that must be implemented to use the VISHMOD methodology (Fig. 2). We have used this methodology in the study area, each step is described in detail below.

Conceptual model

A conceptual model of the study area is essential for a comprehensive hydrogeological characterization. This model will encompass existing rock types, flow directions, and structural features such as fractures, faults, and folding. Additionally, it will account for lithological changes to support an accurate depiction of the hydrogeological setting.

Hydrogeochemical characterization

Analyzing hydrogeochemical data yields valuable insights into the origin, flow trajectory, residence time, and hydrochemical evolution of groundwater. This information is primarily controlled by water–rock interaction and the evaporation-crystallization process (Xiao et al. 2017).

In the study of the groundwater's origin, evolution, and circulation, graphic visualization tools play a crucial role. Diagrams such as Piper and Mifflin are employed to visually represent and interpret the chemical evolution of water.

Foreward model

The analysis of physical and chemical characteristics, including the concentration of major and minor ions, trace elements, and isotopes, provides valuable insights into the chemical composition of groundwater, its origin, and the processes affecting it (Mora et al. 2017). Groundwater, following predictable flow patterns determined by topography, exhibits physicochemical properties associated with features along its flow path (Peel et al. 2022). During this flow path, some minerals precipitate and dissolve, while others remain in equilibrium. The PHREEQC software is instrumental in directly modeling chemical data, allowing the calculation of saturation indices for minerals present in groundwater (Parkhurst and Appelo 1999).

End member

For the identification of End Members (EMs), A scatter plot was constructed using conservative elements. For this case study, Cl and Sr were used. The EMs correspond to the samples with the highest and lowest concentrations in the system, namely, samples 22 (spring), 1 (sulfurous water spring), and 6 (Valsequillo Dam).

Identification mixture

Through the scatter plot with the EMs, the dynamics of the hydrogeological system are understood, as the identification of the number of EMs indicates whether the mixture is binary or ternary. In this case study, three EMs (F_1, F_2, F_3)

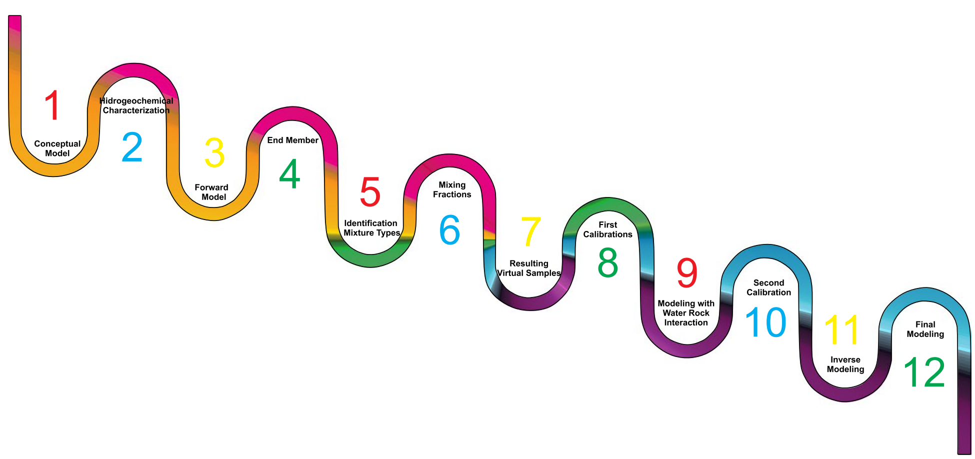

Fig. 2 Sequence of steps used in the VISHMOD methodology, information obtained from Moran-Ramírez and Ramos-Leal (2014)

were identified, suggesting a ternary mixture involving three different types of water. The samples distributed among the EMs are considered as mixing fractions of the end members.

Mixing fractions

To obtain the mixing percentage of the three EM of the system, we use Eq. 1, which is a function of the mass balance equation (Ramos-Leal et al. 2007)

$$F_T = F_1 + F_2 + F_3 = 1 \tag{1}$$

Where F_T is the total sum of the three mixture fractions of the extreme members, F_1 corresponds to the EM with the lowest concentrations of its conservative elements, F_2 is the EM with the highest concentration of Sr and F_3 is the EM with the highest concentration in Cl.

To solve Eq. 1, which has three unknown variables, a system of three equations is required to obtain a unique solution, therefore, for each concentration of conservative elements of an EM ternary mixture model we use Eqs. 2 and 3, in this way it is possible to solve this system of equations

$$F_T * Cl_W = F_1 * Cl_1 + F_2 * Cl_2 + F_3 * Cl_3 \tag{2}$$

$$F_T * Sr_W = F_1 * Sr_1 + F_2 * Sr_2 + F_3 * Sr_3 \tag{3}$$

Solving F_1 of Eq. 2

$$F_1 = \frac{F_T * Cl_W - F_2 * Cl_2 - F_3 * Cl_3}{Cl_1} \tag{4}$$

Substituting F_1 of Eq. 4 in Eq. 1

$$F_T = \frac{F_T * Cl_W - F_2 * Cl_2 - F_3 * Cl_3}{Cl_1} + F_2 + F_3 \tag{5}$$

Solving F_3 of Eq. 5

$$\begin{aligned}
&F_3 - \frac{F_3 * Cl_3}{Cl_1} = F_T - \frac{F_T * Cl_W}{Cl_1} - F_2 + \frac{F_2 * Cl_2}{Cl_1} \\
&Cl_1 * F_3 - \frac{Cl_1 * F_3 * Cl_3}{Cl_1} \\
&\quad = F_T * Cl_1 - \frac{F_T * Cl_W * Cl_1}{Cl_1} - F_2 * Cl_1 \\
&\qquad + \frac{F_2 * Cl_2 * Cl_1}{Cl_1} \\
&F_3(Cl_1 - Cl_3) = F_T * Cl_1 - F_T * Cl_W + F_2 * Cl_2 - F_2 * Cl_1 \\
&F_3 = \frac{F_T(Cl_1 - Cl_W) + F_2(Cl_2 - Cl_1)}{Cl_1 - Cl_3}
\end{aligned} \tag{6}$$

Solving F_3 of Eq. 3

$$F_3 = \frac{F_T * Sr_W - F_1 * Sr_1 - F_2 * Sr_2}{Sr_3} \tag{7}$$

Substituting F_3 of Eq. 7 in Eq. 1

$$F_T = F_1 + F_2 + \frac{F_T * Sr_W - F_1 * Sr_1 - F_2 * Sr_2}{Sr_3} \tag{8}$$

Simplifying Eq. 8

$$\begin{aligned}
&F_T = \frac{F_T * Sr_W}{Sr_3} + F_1 - \frac{F_1 * Sr_1}{Sr_3} + F_2 - \frac{F_2 * Sr_2}{Sr_3} \\
&F_T = \frac{F_T * Sr_W}{Sr_3} + \frac{F_1 * Sr_3 - F_1 * Sr_1}{Sr_3} + \frac{F_2 * Sr_3 - F_2 * Sr_2}{Sr_3} \\
&F_T = \frac{F_T * Sr_W + F_1(Sr_3 - Sr_1) + F_2(Sr_3 - Sr_2)}{Sr_3}
\end{aligned} \tag{9}$$

Solving F_1 of Eq. 9

$$\begin{aligned}
F_1(Sr_3 - Sr_1) &= F_T * Sr_3 - F_T * Sr_W - F_2(Sr_3 - Sr_2) \\
F_1 &= \frac{F_T(Sr_3 - Sr_W) + F_2(Sr_2 - Sr_3)}{(Sr_3 - Sr_1)}
\end{aligned} \tag{10}$$

Solving F_2 of Eq. 1

$$F_2 = 1 - F_1 - F_3 \tag{11}$$

The End Members are calculated using Eq. 6 for F_3 and Eq. 10 for F_1. When $F_T = 1$ we can obtain the solution of F_2, therefore, we substitute F_1 and F_3 in Eq. 1

$$\begin{aligned}
&F_2 = 1 - \left[\frac{F_T(Sr_3 - Sr_W) + F_2(Sr_2 - Sr_3)}{(Sr_3 - Sr_1)}\right] \\
&\quad - \left[\frac{F_T(Cl_1 - Cl_W) + F_2(Cl_2 - Cl_1)}{(Cl_1 - Cl_3)}\right] \\
&\quad \frac{1 - (Cl_1 - Cl_3) * F_T(Sr_3 - Sr_W) - (Cl_1 - Cl_3) * F_2(Sr_2 - Sr_3) - (Sr_3}{(Cl_1 - Cl_3) * (Sr_3 - Sr_1)} \\
&\quad \frac{-Sr_1) * F_T(Cl_1 - Cl_W) - (Cl_2 - Cl_1) * F_2(Sr_3 - Sr_1)}{(Cl_1 - Cl_3) * (Sr_3 - Sr_1)} \\
&\quad 1 - \frac{F_T(Sr_3 - Sr_W)}{Sr_3 - Sr_1} - \frac{F_2(Sr_2 - Sr_3)}{Sr_3 - Sr_1} \\
&\quad - \frac{F_T(Cl_1 - Cl_W)}{Cl_1 - Cl_3} - \frac{F_2(Cl_2 - Cl_1)}{Cl_1 - Cl_3} \\
&\quad 1 - F_T\left[\frac{Sr_3 - Sr_W}{Sr_3 - Sr_1} + \frac{Cl_1 - Cl_W)}{Cl_1 - Cl_3}\right] \\
&\quad - F_2\left[\frac{Sr_2 - Sr_3}{Sr_3 - Sr_1} + \frac{Cl_2 - Cl_1}{Cl_1 - Cl_3}\right] \\
&F_2 = \frac{1 - F_T\left[\frac{Sr_3 - Sr_W}{Sr_3 - Sr_1} + \frac{Cl_1 - Cl_W}{Cl_1 - Cl_3}\right]}{\frac{Li_2 - Sr_3}{Sr_3 - Sr_1} + \frac{Cl_2 - Cl_1}{Cl_1 - Cl_3}}
\end{aligned} \tag{12}$$

we use Eqs. 6, 10, and 12 to obtain the mixing fractions of the EM.

Resulting virtual samples

Following the methodology of virtual samples used in the chemical modeling (Morán-Ramírez et al. 2022), we obtained the virtual chemical composition of each parameter (pH, pe, T, Alk, NO_3^-, SO_4^{2-}, Cl^-, Na^+, Mg^{2+}, Ca^{2+}, K^+), however, these results do not take into account the water–rock interaction.

First calibration

In our calibration process, we employed both qualitative and quantitative analyses. For qualitative analysis, the Piper diagram provided a visual comparison between the theoretical chemical composition and the actual composition of water samples from the PV aquifer. It's important to note that the wide difference observed in the Piper diagram is attributed to the fact that it doesn't account for the intricate interaction processes between water and rock. The diagram serves as a qualitative tool to highlight disparities between theoretical predictions and real-world observations.

Quantitatively, we conducted a rigorous calibration using a method known as 'ionic delta,' which involves determining the difference between the chemical composition of field data and the results derived from the virtual model. In this case study, the ionic deltas exhibited significant disparities.

Modeling with water rock interaction

After determining that mixing was not the dominant process in the groundwater system based on the initial calibration, our focus shifted to exploring the intricate dynamics of water–rock interaction. In this phase, we delved into the saturation indices (SI) of minerals present in the groundwater, a key parameter indicating the saturation level of minerals in water (Mamatha and Rao 2010). These indices play a crucial role in understanding the prevailing hydrogeochemical processes.

Second calibration

The second calibration consists of comparing the results obtained from the virtual mixture modeled with the water–rock interaction. If the obtained ionic deltas are small, then the modeling is concluded.

Results

Conceptual model

At a regional level, the conceptual model suggests that the aquifer is predominantly characterized by volcanic rocks of various compositions, including rhyolites, andesites, basalts, tuffs, and volcanic breccias. Lacustrine sediments and sedimentary breccias are also present, with the Valley area primarily composed of lahars.

Recharge zones, both superficial and underground, for the PV aquifer receive contributions from the Iztaccíhuatl, La Malinche, and Popocatépetl volcanoes. The upper portion of the aquifer consists of unconsolidated alluvial materials, including gravel, sand, and clay, particularly in the valley area. This section has an average thickness of 130 m and exhibits medium to high permeability. The lower portion comprises fractured extrusive igneous rocks, specifically basalts and andesites, with a thickness of several hundred meters. It is demarcated by calcareous rocks at the base, serving as the hydrogeological basement of the basin.

Situated within the Trans-Mexican Volcanic Belt, the aquifer's geology has been profoundly influenced by volcanic activity, contributing to the characteristic profile of the relief, Fig. 1b. Another important component in this aquifer is related to the anthropogenic activities that take place in the Valley of Puebla, where the excessive use of fertilizers and use of wastewater from the Atoyac River, altering the natural quality of groundwater.

Hydrogeochemical characterization

Piper's chart facilitated the identification of three distinct families of water, as depicted in Fig. 3. The dominant hydrogeochemical facie observed in 22 out of 26 samples was of the calcium bicarbonate type (Ca-HCO_3), indicative of waters of recent infiltration and in some other cases, water that has circulated through carbonate rocks. Additionally, three samples out of twenty-six were classified as sodium-calcium-bicarbonate type (Na-Ca-HCO_3), suggesting a mixture of waters originating from basic igneous materials and acidic igneous materials. Notably, a single sample exhibited a calcium chloride–magnesium type facie (Ca–Mg–Cl), where sulfate concentrations were nearly equal to bicarbonate. This composition suggests a mixture of waters with distinct sources.

The Piper diagram provides a visual representation of these hydrogeochemical facies, offering a comprehensive understanding of the composition and origins of the groundwater in the study area.

The hydrogeochemical evolution of groundwater in the PV aquifer is intricately linked to various processes, including rainwater infiltration, CO_2 dilution, dissolution (especially of carbonates), evaporation, and cation exchange, Fig. 3a. These processes initiate in the recharge areas and continue to shape the chemical composition of groundwater as it follows its trajectory through the aquifer.

In Fig. 3a, a strip (green–yellow) of inverse correlation is displayed, where samples with ion exchange processes are

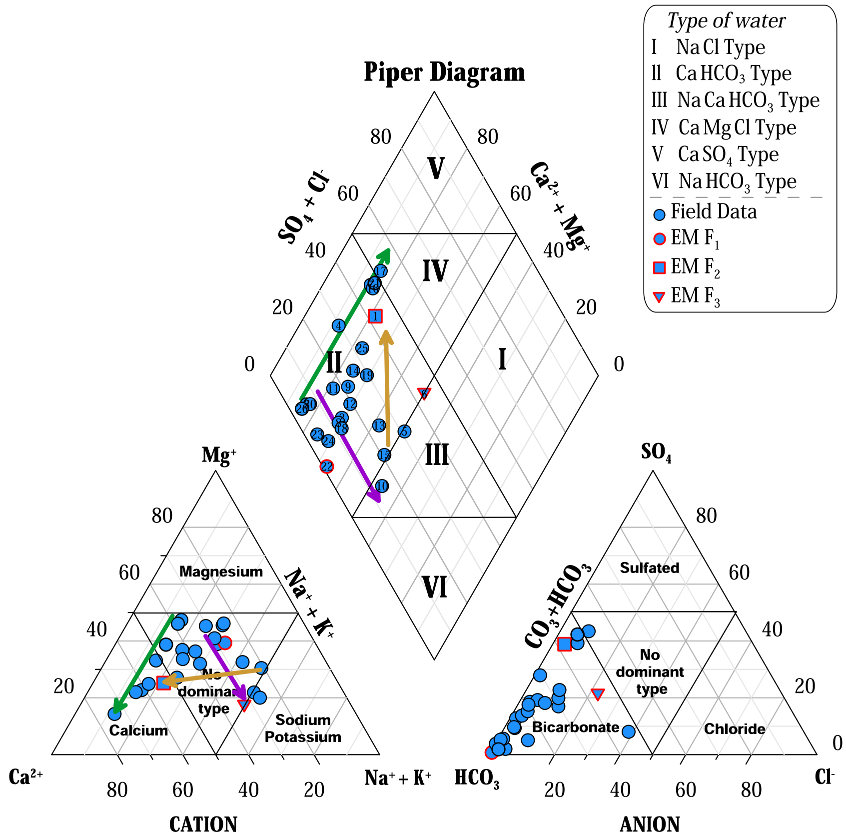

Fig. 3 Piper diagram of water sampled in the PV aquifer

located. Another vertical strip (orange–yellow) groups the samples where the dominant process is mineral dissolution.

The PV aquifer, characterized as a volcano-sedimentary type of fractured rock, exhibits distinct flows within the system. The Mifflin diagram serves as a valuable tool to understand the hydrogeochemical development of groundwater based on the increasing concentration of Na^{+}, K^{+}, Cl^{-}, and SO_4^{2-} ions along the flow, see Fig. 4b. Three types of local discharge, intermediate, and regional can be identified.

The Mifflin diagram reveals the presence of two geological environments: volcanic and carbonate. In the carbonate environment, characterized by regional flow, certain springs such as Sulphurous water and Valsequillo Dam contribute to the groundwater. Conversely, samples taken near the Sierra Nevada fall into the local flow category, suggesting limited circulation and a short water residence time. Samples in the regional flow, with the

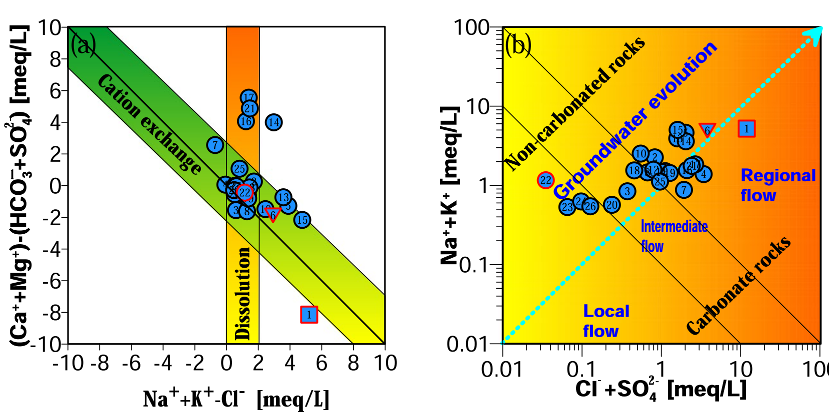

Fig. 4 Distribution of groundwater samples in the PV aquifer. **a** Comparison between Na+K-Cl vs (Ca + Mg)-(HCO_3+SO_4) showing ion exchange and dissolution processes; **b** Mifflin diagram showing the evolution and flow systems

longest residence time, exhibit higher ion concentrations, indicating a more significant evolution through water–rock interaction.

In summary, the PV aquifer exhibits three types of flow: local, regional, and intermediate, each contributing to the complex hydrogeochemical evolution observed in the system.

Foreward model

Calcite, dolomite, gypsum, anhydrite, and sylvite are identified as the most soluble minerals, contributing the majority of ions to the groundwater (Hanshaw and Back 1979; Ford and Williams 2007; Hussien et al. 2021). In contrast, silicates and insoluble rocks give rise to minority ions or trace elements (Chegbeleh et al. 2020).

In the case study of the PV aquifer, saturation indices suggest that the dissolution of minerals, particularly calcite, and ion exchange were the primary processes controlling groundwater chemistry. Groundwater samples predominantly exhibit saturation with calcite and dolomite, while being unsaturated with anhydrite, gypsum, and halite. This interpretation provides crucial insights into the geochemical evolution of the PV aquifer and the dominant controlling factors influencing its chemistry.

End member

In the scatter plot, three distinct End Members (F_1, F_2, and F_3) were identified, each representing specific hydrogeochemical characteristics. F_1 corresponds to sample 22, associated with a spring exhibiting local recharge. Located southwest of the aquifer near the Popocatépetl volcano, this EM features low values of Cl (0.014 meq) and Sr (0.00042 meq) with a temperature of 18.5°C. The water type associated with F_1 is $CaHCO_3$. F_2 is represented by sample 1, a sulfurous water spring in the Puebla Valley area, indicating a regional flow. With a temperature of 28.3°C, F_2 exhibits Cl concentrations of 1.021 meq and Sr concentrations of 0.00750 meq, with the water type identified as $CaHCO_3$. F_3 is associated with sample 6, which is located very close to Valsequillo Dam, and although in the Miffling Diagram, Fig. 4b, this EM is located in a regional flow, we consider it as an intermediate flow because it has passed through rhyolitic rocks that have caused high salt contents. With a temperature of 19.9°C, F_3 has the highest Cl value (1.980 meq) and a low Sr value (0.00130 meq), with the water type identified as $CaNaHCO_3$.

Identification mixture

In the scatter graph (Fig. 5), the brown arrow signifies a linear source influencing water flows, while the green arrow

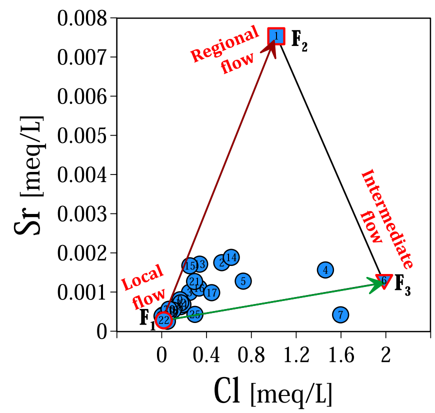

Fig. 5 Ternary mixing model using Cl and Sr concentrations from PV aquifer, where F_1, F_2 and F_3 are end members

represents a diffuse source associated with anthropogenic contamination reaching Valsequillo Dam. This contamination stems from the return of irrigation water and wastewater collected by the Atoyac River along its course.

Sample 4, located approximately 50 ms from the Valsequillo dam, exemplifies the influence of the diffuse source. Additionally, sample 7, a spring in the municipality of Coronango, is contaminated by domestic and industrial activities. Situated in the north-central part of the aquifer, this spring is also influenced by secondary slopes of the Atoyac River.

Understanding these specific examples helps elucidate how human activities alter the natural trajectory of groundwater samples in the hydrogeochemical system. The ternary mixture and its associated sources provide valuable insights into the complex dynamics at play in the study area.

Mixing fractions

Chloride ranges for groundwater from this aquifer were 0.00282−1.980 meq/L and 0.00025−0.00752 meq/L Sr. Quantifying the contribution of each member according to the ternary mix model, it is considered that the greatest contribution comes from Sierra Nevada (F_1) with 74%, and La Malinche to a lesser extent with 9% (F_2), however, End Member F_3 considerably influenced the system with a contribution of 17%, this means that anthropogenic contamination has begun to impact the chemistry of groundwater. The percentages of fraction can of a mixture of each sample are seen in Table 1.

Resulting virtual samples

The Table 2 presents the results obtained from the virtual samples from the chemical composition of EM F1, F2, and F3, that is, a ternary mixture.

Table 1 Mixing fractions for groundwater in the PV aquifer

Sample	F1	F2	F3
1	**0.00**	**1.00**	**0.00**
2	0.65	0.17	0.18
3	0.85	0.07	0.08
4	0.23	0.08	0.70
5	0.60	0.08	0.32
6	**0.00**	**0.00**	**1.00**
7	0.14	0.00	0.86
8	0.91	0.02	0.07
9	0.90	0.05	0.05
10	0.96	0.02	0.02
11	0.90	0.03	0.07
12	0.90	0.04	0.06
13	0.75	0.17	0.08
14	0.60	0.18	0.22
15	0.80	0.17	0.03
16	0.80	0.08	0.12
17	0.75	0.06	0.19
18	0.95	0.01	0.04
19	0.97	0.01	0.02
20	0.97	0.00	0.03
21	0.80	0.11	0.09
22	**1.00**	**0.00**	**0.00**
23	0.99	0.00	0.01
24	0.99	0.00	0.01
25	0.86	0.00	0.14
26	0.97	0.02	0.02

The samples in bold are end members

First calibration

These findings lead us to conclude that mixing is not the dominant process influencing the chemical evolution of groundwater in the PV aquifer.

The Piper diagram and ionic delta analysis collectively contribute to a comprehensive understanding of the calibration results, Fig. 6, shedding light on both qualitative and quantitative aspects of the hydrogeochemical model. It underscores the complex interplay of water–rock interactions and the need for a nuanced approach in modeling groundwater chemistry in the PV aquifer.

Modeling with water rock interaction

Working with a volcano-sedimentary type aquifer in the PV region, characterized by the abundance of volcanic and sedimentary rocks, we assessed the mineral phases present in the groundwater, Table 3. The obtained results offer valuable insights into the processes at play within the aquifer. Notably, the SI analysis reveals a clear influence of water–rock interaction, particularly with alkaline igneous rocks, feldspathic lavas, and carbonate rocks. These findings underscore the significance of geological composition in shaping the hydrogeochemical characteristics of the PV aquifer.

The emphasis on water–rock interaction serves to refine our hydrogeochemical model, aligning it more closely with the geological realities of the PV aquifer. By connecting SI results to the specific geological context, we gain a deeper understanding of the processes driving groundwater chemistry in this complex system.

In the direct modeling of the PV aquifer, it indicates that 100% of the samples are saturated with respect to gypsum and anhydrite. The precipitation of the minerals depends on the contact of the rocks with the water, that is, the unsaturated minerals hardly precipitate and dissolution takes place, however, the saturated ones indicate that there may be precipitation.

The saturation index values for calcite and dolomite in some of the samples exceeded 0, while in other samples, they were below 0. This indicates a gradual transition of carbonate minerals from an unsaturated state to an saturated state. In contrast, the saturation indices for anhydrite and gypsum in all groundwater samples remained below 0, see Table 3, suggesting that anhydrite and gypsum will continuously dissolve in the groundwater.

The saturation index values for calcite and dolomite in some of the samples exceeded 0, while in others, they were below this limit, Table 3. This indicates a gradual transition of carbonate minerals from a saturated to undersaturated state as groundwater flow evolves. In contrast, the saturation indices for gypsum in all groundwater samples remained below 0, suggesting that gypsum remains in a saturated state, indicating that groundwater has not reached its capacity limit to keep the minerals in solution.

The saturation index values for calcite, dolomite, and gypsum ranged from −0.70 to 0.73, −0.65 to 2.54, and −4.09 to −0.76, respectively. Figure 7 (a) showed a weak correlation between the Saturation Index (SI) and Total Dissolved Solids (TDS), with gypsum exhibiting the strongest correlation. Calcite was mostly saturated as flows evolved, while dolomite showed a trend towards saturated.

Concentrations of Ca^{2+} and HCO_3^- with respect to calcite did not show a strong correlation, Fig. 7b. However, a noticeable shift from undersaturated to saturated was observed as flows transitioned from local to regional. For dolomite, see Fig. 7c, Ca^{2+}, Mg^{2+}, and HCO_3^- displayed a higher degree of saturated that may lead to mineral precipitation. On the other hand, concentrations of Ca^{2+} and SO_4^{2-}

Table 2 Theorical chemical composition of rock samples without the water mixing interaction model, ions are in units of meq

Sample	ALK	NO_3^-	SO_4^{2-}	Cl^-	Na^+	Mg^{2+}	Ca^{2+}	K^+	T°C	pH	pe
1 V	**16.176**	**1.016**	**5.465**	**1.021**	**4.891**	**3.047**	**6.437**	**0.319**	**28.2**	**6.1**	**– 5.5**
2 V	4.616	0.117	0.579	0.536	2.142	0.966	1.341	0.237	18.8	7.1	0.0
3 V	3.159	0.026	0.075	0.248	1.431	0.732	0.679	0.202	17.5	7.2	1.1
4 V	4.354	0.004	0.003	1.469	3.601	0.798	1.310	0.335	19.2	7.3	– 1.4
5 V	3.954	0.044	0.191	0.728	2.339	0.818	1.069	0.255	18.4	7.2	0.0
6 V	**4.917**	**0.000**	**0.000**	**1.980**	**4.520**	**0.836**	**1.601**	**0.391**	**19.9**	**7.3**	**–2.5**
7 V	4.549	0.003	0.002	1.646	3.919	0.811	1.410	0.355	19.4	7.3	– 1.8
8 V	2.939	0.015	0.010	0.171	1.272	0.702	0.572	0.194	17.4	7.3	1.3
9 V	3.124	0.032	0.101	0.164	1.289	0.737	0.656	0.193	17.4	7.2	1.2
10 V	2.765	0.012	– 0.012	0.071	1.078	0.682	0.490	0.182	17.1	7.3	1.5
11 V	2.894	0.015	0.010	0.152	1.229	0.695	0.557	0.190	17.2	7.2	1.3
12 V	2.898	0.015	0.010	0.152	1.230	0.696	0.558	0.191	17.2	7.2	1.3
13 V	5.506	0.210	1.071	0.338	1.976	1.156	1.712	0.218	19.4	7.0	0.0
14 V	5.863	0.211	1.090	0.621	2.491	1.186	1.893	0.249	19.9	7.0	– 0.6
15 V	5.748	0.238	1.222	0.251	1.876	1.212	1.811	0.209	19.6	7.0	0.0
16 V	5.193	0.185	0.935	0.333	1.913	1.099	1.575	0.217	19.2	7.1	0.1
17 V	3.921	0.069	0.315	0.446	1.879	0.848	1.029	0.225	18.2	7.2	0.4
18 V	2.845	0.015	0.008	0.102	1.141	0.693	0.528	0.186	17.2	7.3	1.4
19 V	2.756	0.011	– 0.016	0.071	1.076	0.680	0.486	0.182	17.1	7.3	1.5
20 V	2.772	0.016	0.010	0.034	1.019	0.688	0.491	0.178	17.1	7.3	1.6
21 V	3.070	0.014	0.009	0.289	1.485	0.711	0.640	0.207	17.5	7.3	1.1
22 V	**2.753**	**0.016**	**0.010**	**0.014**	**0.985**	**0.687**	**0.480**	**0.176**	**17.1**	**7.3**	**1.6**
23 V	2.797	0.018	0.021	0.016	0.999	0.696	0.495	0.178	17.2	7.3	1.6
24 V	2.802	0.020	0.032	0.014	0.993	0.696	0.502	0.176	17.1	7.3	1.6
25 V	3.067	0.014	0.009	0.289	1.484	0.711	0.639	0.207	17.5	7.3	1.0
26 V	3.070	0.037	0.126	0.065	1.120	0.739	0.623	0.182	17.3	7.2	1.4

The samples in bold are end members

with respect to gypsum exhibited a clear trend from dissolution to equilibrium as flow evolved, Fig. 7d. This suggests that the weathering process of calcite and dolomite is intermittent, meaning only a portion of these minerals will continuously dissolve in the direction of groundwater flow, while gypsum dissolution may result in exponential increases in Na^+, Ca^{2+}, and SO_4^{2-}, indicating that gypsum is one of the main minerals in the flow direction. Additionally, Ca^{2+} release due to gypsum weathering could lead to the saturated of calcite and dolomite, inhibiting the weathering of these minerals.

Second calibration

The Piper diagram, Fig. 8, shows the chemical composition obtained by the virtual mixture modeled with the rock-water interaction, this is adjusted to the real samples, indicating that the main process that occurs in the system is the mixture with the water–rock interaction, where the ionic deltas have been considerably reduced (Table 4).

Discussion of results

The Piper diagram is used to classify water according to the dominant cation and anion, with this information, hydrogeochemical processes such as water mixing, plaster dissolution, and cation exchange are deduced (Karmegam et al. 2011). The samples in the Piper diagram (purple arrow in Fig. 3) suggest the evolution of the water from calcium bicarbonate to calcium sodium bicarbonate, where the TDS are constant, therefore, it can be deduced that there is a cationic exchange between sodium and calcium, that is, sodium passes to solution while calcium is absorbed.

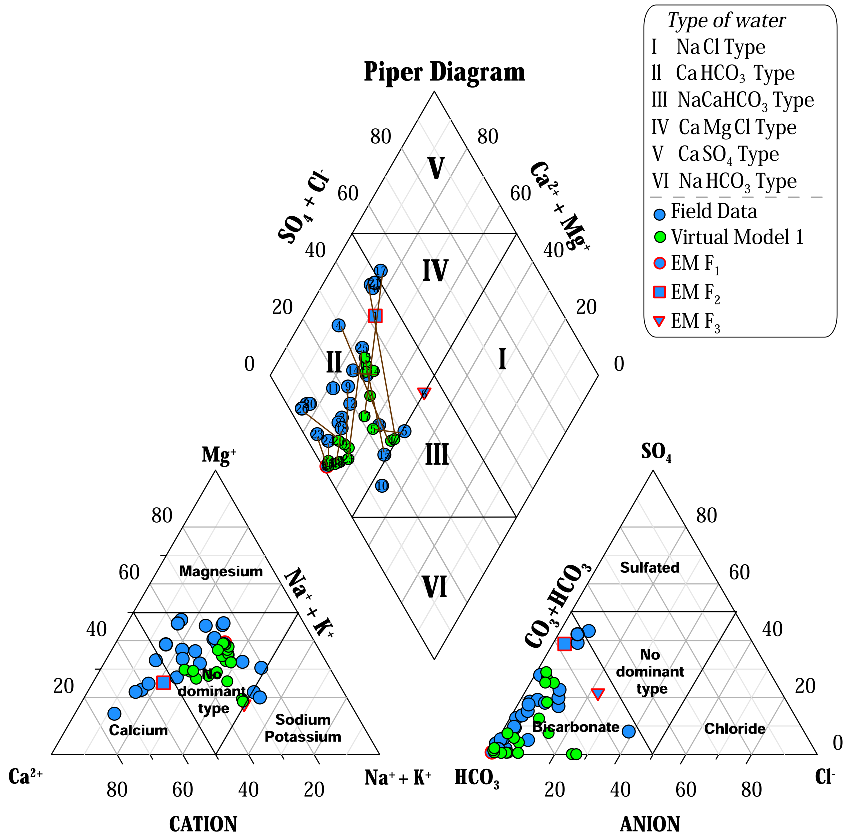

Fig. 6 Piper diagram representing the difference between the real data and the mixing model, the brown lines indicate the ionic deltas

Another trend indicates that the waters also evolve from calcium bicarbonate to calcium magnesium chloride, a product of the dissolution of minerals (green arrow in Fig. 3). While the evolution of calcium sodium bicarbonate waters to calcium magnesium chlorinated waters is the result of mixing processes (Mustard arrow in Fig. 3).

The proposed conceptual model, Fig. 1b; as well as the Mifflin diagram, Fig. 4b, shows us the geological environment where the water interacts with the rock, it is evident that the volcanic rocks are above the carbonate rocks, and through the hydrogeochemical results we have managed to identify the interaction of water with both volcanic rocks and carbonate rocks, this phenomenon is also visible in the Piper diagram. Therefore, it is identified that the flows of Sierra Nevada and La Malinche converge and mix in the Valley area, as suggested by the proposed conceptual model. The flows of a volcanic environment are local, while those of a carbonate environment are only regional.

As can be seen in Table 3, the saturation indices indicated that most of the samples analyzed are in equilibrium with respect to calcite, and only 6 of the samples are in a state of saturation, therefore, it is expected that in these geographical areas there is precipitation of calcite. With respect to gypsum, it can be clearly seen that the values are low in all cases and, therefore, they are completely unsaturated.

The results of the hydrogeochemical modeling suggest that by itself the mixing process that occurs between local flows and those of intermediate and regional hierarchy, does not dominate the system, the adjustment is below 90%, but the mixing with water–rock interaction is the dominant process of the system, it was possible to adjust the model by 94.1%, the remaining percentage that did not adjust is caused by the homogeneity and anisotropy of the aquifer, where the differences of the ionic delta with the real chemical composition were notably reduced. According to the lithology of the study area and the saturation indices, it is visible that the main cation is calcium, where silicates are essential constituents of igneous rocks, specifically the plagioclase group, while in sedimentary rocks it appears in the form of carbonate (calcite and dolomite) and sulfates (gypsum and anhydrite).

The magnesium content suggests that there has been dissolution of carbonate rocks, mainly dolomites, evaporites, and alteration of ferromagnesian silicates; however, the solubility of magnesite is greater than that of calcite, therefore, it is likely that it can be produce saturation of this mineral with respect to the different magnesium carbonates.

Sodium is released by the weathering of silicates, in this case, albite, and the dissolution of sedimentary rocks and evaporitic deposits. The salts are highly soluble and tend

Table 3 Saturation indices of the main mineral phases in the groundwater of the PV aquifer

Sample	Gypsum	Anhydrite	Calcite	Dolomite	Hematite
1	−0.76	−0.91	−0.05	0.74	−14.54
2	−2.6	−2.85	0.73	2.54	9.5
3	−2.9	−3.12	0.31	1.35	6.31
4	−1.44	−1.67	0.54	1.52	4.45
5	−2.04	−2.32	0.24	1.52	−4.35
6	−1.8	−2.04	0.06	0.98	−1.16
7	−2.58	−2.88	−0.68	−0.65	−2.4
8	−2.61	−2.84	−0.38	0.52	5.39
9	−2.18	−2.41	0.02	1.18	6.77
10	−2.65	−2.89	−0.38	0.27	6.32
11	−2.19	−2.43	0.07	1.25	5.66
12	−2.57	−2.78	−0.5	0.42	5.58
13	−2.12	−2.35	−0.34	0.58	5.52
14	−2.03	−2.26	−0.21	0.96	4.18
15	−2.14	−2.37	0	1.32	6.86
16	−1.92	−2.1	−0.7	−0.08	4.63
17	−1.62	−1.88	−0.51	−0.04	4.72
18	−2.74	−2.86	−0.26	0.8	6.65
19	−2.32	−2.55	−0.46	0.52	5.79
20	−2.87	−3.07	0.14	1.1	8.51
21	−1.75	−1.96	−0.09	0.96	6.12
22	−4.09	−4.35	−0.66	−0.02	6.69
23	−3.52	−3.77	−0.35	0.2	9.63
24	−3.61	−3.83	−0.7	−0.11	9.46
25	−2.33	−2.55	−0.23	0.59	7.28
26	−3.5	−3.72	−0.63	−0.01	5.66

to remain in solution because precipitation reactions do not occur (Doneen 1975), however, the predominant soil in the region is Vertisol (Guerrero et al. 2016), which is caused by igneous and sedimentary rocks, and by weathering where they accumulate clays, causing sodium to be adsorbed in the soil and exchanged for Ca^{2+}, causing the hardness of the water to be low in the region (<500 mg/L).

The low K^+ contents come from the weathering of feldspars and tend to be irreversibly fixed in clay formation processes and adsorption on the surfaces of minerals with high ionic exchange capacity, therefore its concentration in the waters of this aquifer is much less than that of Na^{2+}.

On the other hand, it is visible that the contribution of bicarbonates is a function of the dissolution of limestone and dolomites, as well as the hydrolysis of silicates. The evaporites provide a certain proportion of chlorides, however, given the high solubility of their salts, these quickly pass into the aqueous phase and can reach high concentrations (Clark et al. 2005). Rainwater usually contributes Cl^- concentration to the water, but this decreases significantly once it enters the subsoil, as seen in the Mifflin diagram local flow waters have low chloride contents due to the recent infiltration into the system, Fig. 4b.

Sulfates are naturally the product of the oxidation of sulfides that are distributed in igneous and sedimentary rocks. However, the dissolution of gypsum and anhydrite are the main contributors of this ion to the groundwater of the PV aquifer. Additionally, the sulfate content is also associated with anthropogenic activities, as these areas are agricultural, and the return of irrigation influences the chemical composition of the water due to it being a shallow aquifer.

To identify the presence of anthropogenic SO_4, Fig. 9 was used, showing a red polygon where there is a correlation between NO_3 and SO_4, indicative of anthropogenic contamination. In some cases, such as sample 1, there is a high SO_4 content; however, this sample belongs to a spring with sulfur water, justifying its high SO_4 content. It is worth mentioning that this spring is used for recreational purposes and is located a short distance from the Atoyac River, which contributes to NO_3 contamination.

The Fig. 9a shows the relationship between NO_3 and SO_4. In the graph, there are two arrows: the vertical one indicates nitrification processes, while the diagonal arrow of direct correlation indicates mixing processes with poor-quality waters such as wastewater. This latter process is identified in Fig. 9b and c, which are correlation plots between NO_3 vs Cl and TDS. In general, the samples located below the mixing line are samples located near the Valsequillo Dam.

The nitrate content in the rocks is presented only as a minority element. However, the samples suggest that the high contents of this ion are due to pollution associated with agricultural, urban, industrial, and livestock activities, as it is a very shallow aquifer, Fig. 9

In general terms, the VISHMOD methodology was adequate to identify and quantify the hydrogeological processes that occurred in the PV aquifer, where the validation of results defined that the dominant process was the water–rock interaction, the ionic deltas were reduced considerably and the adjustment of the data was 94.1%, therefore, it was not necessary to reach the inverse modeling, as suggested by the last two steps of the VISHMOD methodology. In addition, the sequence of VISHMOD steps proved to evaluate the proposed conceptual model, which corresponds with the results reported in this research.

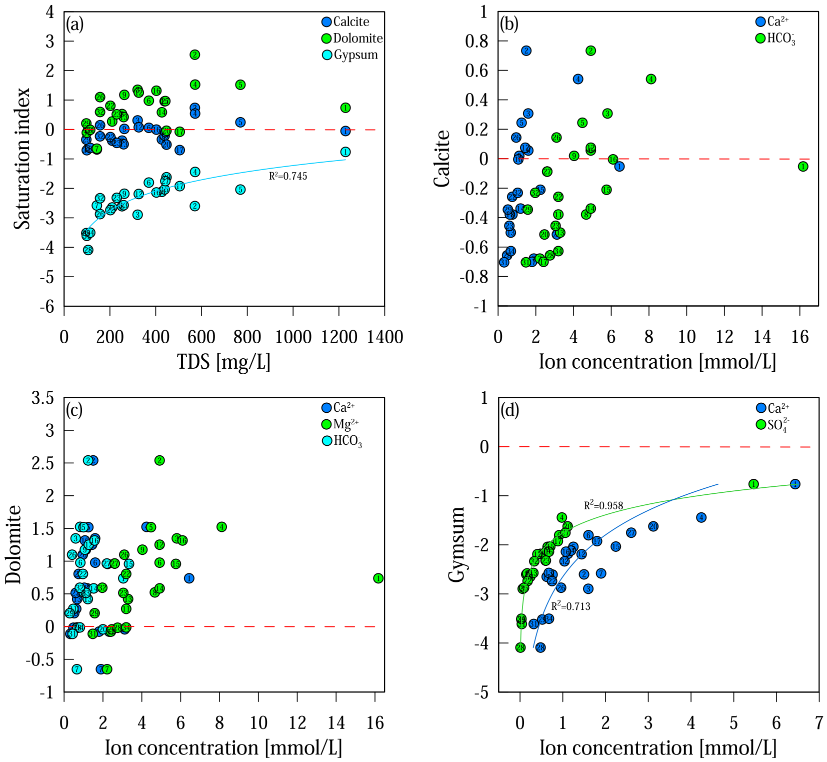

Fig. 7 Saturation indices plots with selected minerals versus TDS or ion concentration. **a** Calcite, Dolomite, Gypsum vs. TDS; **b** Ca^{2+}, HCO_3^- vs. Calcite; **c** Ca^{2+}, Mg^{2+}, HCO_3^- vs. Dolomite; **d** Ca^{2+},SO_4^{2-} vs. Gypsum

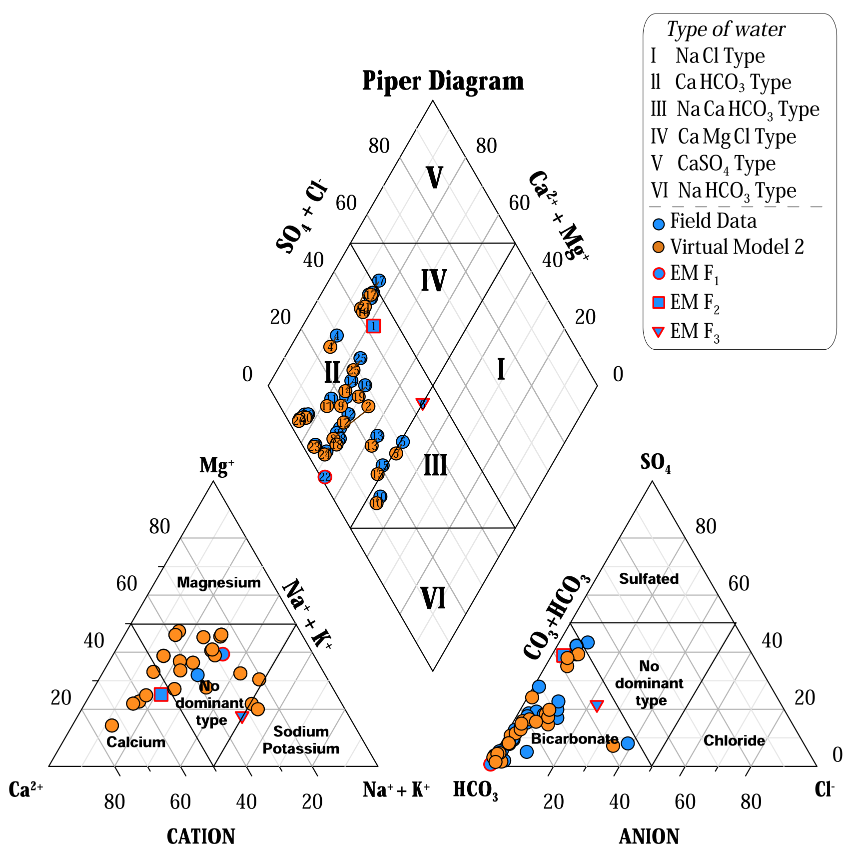

Fig. 8 Piper diagram representing the field samples with Synthetic Model 2, applying the water–rock interaction. The brown lines indicate the ionic deltas

Table 4 Virtual chemical composition 2, of the mixture without water–rock interaction, ions are in units of meq

Sample	ALK	NO_3^-	SO_4^{2-}	Cl^-	Na^+	Mg^{2+}	Ca^{2+}	K^+	T°C	pH	pe
1 V	**16.176**	**1.016**	**5.465**	**1.021**	**4.891**	**3.047**	**6.437**	**0.319**	**28.2**	**6.1**	**− 5.5**
2 V	4.618	0.117	1.158	0.536	2.143	1.932	2.682	0.237	18.7	8.0	0.0
3 V	7.078	0.071	0.125	0.248	0.748	1.187	3.196	0.095	20.94	7.4	1.1
4 V	9.902	0.071	1.959	1.462	1.229	1.650	8.490	0.159	20.06	7.2	− 1.4
5 V	5.456	0.429	1.292	0.728	4.107	1.996	2.496	0.517	15.37	7.7	0.0
6 V	**4.917**	**0.000**	**0.000**	**1.980**	**4.520**	**0.836**	**1.601**	**0.391**	**19.9**	**7.3**	**− 2.5**
7 V	2.700	33.650	0.333	1.598	0.656	1.318	3.796	0.222	12.8	7.0	−1.8
8 V	5.698	0.929	0.500	0.169	1.269	2.032	1.521	0.190	19.8	7.1	1.3
9 V	4.919	1.357	0.958	0.164	1.319	2.142	2.242	0.194	20.5	7.4	1.2
10 V	3.898	0.429	0.479	0.071	2.331	0.945	1.248	0.190	19.4	7.4	1.5
11 V	5.999	3.357	0.813	0.189	1.310	2.544	2.884	0.170	19.4	7.3	1.3
12 V	4.019	2.428	0.625	0.169	1.339	2.442	1.348	0.237	22.0	7.2	1.3
13 V	5.999	4.072	1.250	0.339	3.613	3.048	2.386	0.311	19.3	7.0	0.0
14 V	7.024	38.320	1.418	0.621	2.832	6.690	4.488	0.772	20.1	6.9	−0.6
15 V	7.440	3.001	1.355	0.251	4.617	3.144	2.148	0.409	20.4	7.3	0.0
16 V	2.940	25.360	1.771	0.333	1.389	4.644	3.604	0.168	25.8	6.8	0.1
17 V	3.000	30.010	2.230	0.446	1.655	4.004	6.244	0.189	17.8	6.9	0.4
18 V	3.898	0.714	0.354	0.102	1.372	1.937	1.497	0.174	31.4	7.2	1.4
19 V	3.718	0.857	1.208	0.071	1.270	2.252	1.195	0.164	20.5	7.3	1.5
20 V	3.778	2.142	0.187	0.051	0.505	0.825	1.922	0.063	23.5	7.6	1.6
21 V	3.180	38.810	2.126	0.294	1.422	4.404	5.208	0.344	21.9	7.3	1.1
22 V	**2.753**	**0.016**	**0.010**	**0.014**	**0.985**	**0.687**	**0.480**	**0.176**	**17.1**	**7.3**	**1.6**
23 V	1.919	0.357	0.062	0.003	0.448	0.584	1.041	0.084	18.52	7.7	1.6
24 V	1.799	0.857	0.083	0.014	0.489	0.878	0.640	0.138	20.8	7.6	1.6
25 V	2.399	3.285	0.666	0.296	1.022	1.620	2.082	0.094	21.89	7.5	1.0
26 V	3.898	1.285	0.062	0.065	0.444	1.620	1.353	0.100	21.26	7.0	1.4

The samples in bold are end members

Conclusions

In the center of the Puebla Valley aquifer, three families of water have been identified: (1) Calcium Bicarbonate Ca–HCO_3, (2) Calcium, Sodium and Bicarbonate Na–Ca–HCO_3 and (3) Calcium Chloride–Magnesium Ca–Mg–Cl. This is due to the interaction of water with carbonate rocks and mixture of waters that have circulated by mafic and felsic rocks. Three flow systems were identified, the local, intermediate and regional, which are mixed in the valley area. The local flow is associated with the Sierra Nevada and La Malinche area, the intermediate flow

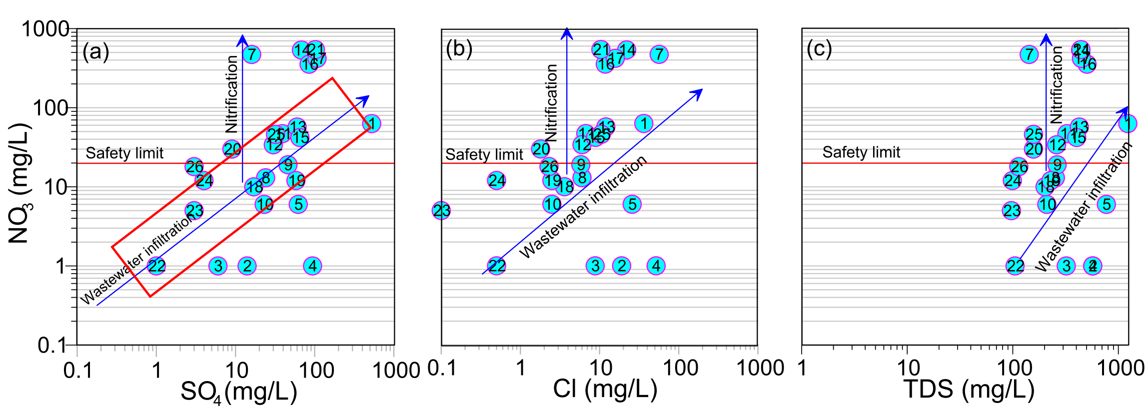

Fig. 9 Diagrams showing nitrification processes in the VP aquifer. **a** SO_4 vs NO_3; **b** Cl vs NO_3; **c** TDS vs NO_3

comes from the center-west and south-east of the valley, the regional flow has been associated with the presence of geological faulting as a result of tectonic activity in the area.

Water from PV aquifer represents the ternary mixture of three End Members, a contribution of 74% of F_1 is received (local flow), a 9% contribution from F_2 (regional flow), and 17% from the contribution from F_3 (intermediate flow). According to the results obtained through the VISHMOD, it was identified that the dominant process is modeling of the chemical composition with water–rock interactions because notably reduced the chemical differences. The mixing model was only used as the first approach to analyze the virtual chemical compositions of groundwater, in this first calibration large chemical differences were obtained between the virtual composition and the real data.

The VISHMOD methodology gave us an effective result to identify and model the mixing and water–rock interaction processes. According to the saturation indices, the possible mineral phases that can be formed due to the chemical composition of the PV aquifer water were calcite, dolomite, these showed high variability for to precipitate. The totally saturated phases are gypsum and anhydrite, therefore, these minerals can weather.

Acknowledgements The authors wish to thank the Instituto Potosino de Investigación Científica y Tecnológica A.C. (IPICYT) and to CONAHCYT. To the reviewers for their valuable time and comments on this manuscript. They also thank CONAGUA (Puebla) for their support and facilities granted in data acquisition.

Author contributions All authors have equally contributed to the research and manuscript preparation. All authors have read and agreed to the published version of the manuscript.

Data availability All data that was used in this study are in the manuscript. Any other data that may be required from the author's will be available on request.

Declarations

Conflict of interest I declare that the authors have no Conflict of interest.

References

Chegbeleh LP, Akurugu BA, Yidana SM (2020) Assessment of groundwater quality in the talensi district, northern ghana. The scientific world Journal. https://doi.org/10.1155/2020/8450860

Che Q, Su X, Wang S, Zheng S, Li Y (2021) Hydrochemical characteristics and evolution of groundwater in the alluvial plain (anqing section) of the lower yangtze river basin: Multivariate statistical and inversion model analyses. Water 13(17). https://doi.org/10.3390/w13172403

Clark BC, Morris RV, McLennan SM, Gellert R, Jolliff B, Knolland AH, Rieder R (2005) Chemistry and mineralogy of outcrops at meridiani planum. Earth Planet Sci Lett 240(1):73–94. https://doi.org/10.1016/j.epsl.2005.09.040

CLICOM (2000) Base de datos climatológica nacional (sistema clicom): Datos climáticos diarios del clicom del smn a través de su plataforma web del cicese. http://clicom-mex.cicese.mx/mapa.html

CONAGUA (2020) Actualización de la disponibilidad media anual de agua en el acuífero valle de puebla, estado de puebla, conagua, mexico city. https://sigagis.conagua.gob.mx/gas1/Edos_Acuiferos_18/puebla/DR_2104.pdf

CONAGUA (2022) Comisión nacional del agua: Subdirección general técnica. http://sina.conagua.gob.mx/sina/tema.php?tema=acuiferos# &ui-state=dialog

Cook PG (2003) A guide to regional groundwater flow in fractured rock aquifers. Seaview Press, Henley Beach, South Australia

Cserna ZD (1989) An outline of the geology of mexico. the geology of north america–an overview. The Geological Society of America A: Boulder:233–264. https://doi.org/10.1130/DNAG-GNA-A.233

Doneen LD (1975) Water quality for irrigated agriculture. Plants in saline environments pp 56–76. https://doi.org/10.1007/978-3-642-80929-3_5

Epting J, Michel A, Affolter A, Huggenberger P (2021) Climate change effects on groundwater recharge and temperatures in swiss alluvial aquifers. Journal of Hydrology X 11(100071).https://doi.org/10.1016/j.hydroa.2020.100071

Esteller M, Kondratenko N, Expósito J, Medina M, del Campo MM (2017) Hydrogeochemical characteristics of a volcanic-sedimentary aquifer with special emphasis on fe and mn content: A case study in mexico. J Geochem Explor 180:113–126. https://doi.org/10.1016/j.gexplo.2017.06.002

Flores-Márquez EL, Jiménez-Suárez G, Martínez-Serrano R, Chávez R, Pérez DS (2006) Study of geothermal water intrusion due to groundwater exploitation in the puebla valley aquifer system, mexico. Hydrogeol J 14:1216–1230. https://doi.org/10.1007/s10040-006-0029-0

Fonseca-Montes RMG, Ramos-Leal JA, Morán-Ramírez J, Esquivel-Martínez JM, Álvarez Bastida C, Fuentes-Rivas RM (2020) Hydrogeochemical characterization and assessment of contamination by inorganic and organic matter in the groundwater of a volcano-sedimentary aquifer. Bull Environ Contam Toxicol 104:520–531. https://doi.org/10.1007/s00128-020-02819-8

Ford D, Williams PD (2007) Karst hydrogeology and geomorphology. John Wiley & Sons, The Atrium, Southern Gate, Chichester, West Sussex PO19 8SQ, England

Guerrero CAT, Castorena MG, Carmen D, Solorio CAO, Castorena EVG (2016) Manejo agronómico de los vertisoles en méxico: una revisión. Terra Latinoamericana 34(4):457–466. https://doi.org/10.1306/eg.0820303011

Hanshaw BB, Back W (1979) Major geochemical processes in the evolution of carbonate—aquifer systems. Journal of Hydrology pp 287–312. https://doi.org/10.21123/bsj.2021.18.1(Suppl.).0670

Hussien BM, Rabeea MA, Mekhlef HN (2021) Characterization of the groundwater within regional aquifers and suitability assessment for various uses and purposes-western iraq. Baghdad Science Journal p. 0670. https://doi.org/10.21123/bsj.2021.18.1(Suppl.).0670

Jakeman AJ, Barreteau RJO, Hunt RJD, Ross A (2016) Integrated groundwater management, Concepts. Approaches and Challenges. Springer, Heidelberg, Germany

Karmegam U, Chidambaram S, Prasanna MV, Sasidhar P, Manikandan S, Johnsonbabu G, Anandhan P (2011) A study on the mixing proportion in groundwater samples by using piper diagram and phreeqc model. Chin J Geochem 30:490–495. https://doi.org/10.1007/s11631-011-0533-3

Laaksoharju M, Smellie J, Tullborg E, Gimeno M, Molinero J, Gurban I, Hallbeck L (2008) Hydrogeochemical evaluation and modelling performed within the swedish site investigation programme. Appl

Geochem 23(7):1761–1795. https://doi.org/10.1016/j.apgeochem.2008.02.015

Lakshmanan E, Kannan R, Kumar MS (2003) Major ion chemistry and identification of hydrogeochemical processes of ground water in a part of kancheepuram district, tamil nadu, india. Environ Geosci 10(4):157–166. https://doi.org/10.1306/eg.0820303011

Mamatha P, Rao SM (2010) Geochemistry of fluoride rich groundwater in kolar and tumkur districts of karnataka. Environmental Earth Sciences 61:131–142. https://doi.org/10.1007/s12665-009-0331-y

Manciati C, Taupin JD, Patris N, Leduc C, Casiot C (2021) Diverging water ages inferred from hydrodynamics, hydrochemical and isotopic tracers in a tropical andean volcano-sedimentary confined aquifer system. Frontiers in Water 3:1–20. https://doi.org/10.3389/frwa.2021.597641

Mora A, Mahlknecht J, Rosales-Lagarde L, Hernández-Antonio A (2017) Assessment of major ions and trace elements in groundwater supplied to the monterrey metropolitan area, nuevo león, mexico. Environmental Monitoring and Assessment pp 1–15. https://doi.org/10.1007/s10661-017-6096-y

Moran-Ramírez J (2016) Modelación hidrogeoquímica en tres ambientes naturales en méxico: cárstico, volcánico y cuenca sedimentaria https://repositorio.ipicyt.edu.mx/handle/11627/3042

Moran-Ramírez J, Ramos-Leal JA (2014) The vishmod methodology with hydrochemical modeling in intermountain (karstic) aquifers: case of the sierra madre oriental, mexico. Journal of Geography and Geology 6(2):132–144. https://doi.org/10.5539/jgg.v6n2p132

Moran-Ramírez J, Ramos-Leal JA, Mahlknecht J, Santacruz-DeLeón G, Martín-Romero AMR, Rivas F (2018) Modeling of groundwater processes in a karstic aquifer of sierra madre oriental, mexico. Appl Geochem 95:97–109. https://doi.org/10.1016/j.apgeochem.2018.05.011

Morán-Ramírez J, Morales-Arredondo J, Armienta-Hernández MA, Ramos-Leal JA (2020) Quantification of the mixture of hydrothermal and fresh water in tectonic valleys. Journal of Earth Science 31(5):1007–1015. https://doi.org/10.1007/s12583-020-1294-x

Morán-Ramírez J, Leal JAR, Fuentes-Rivas R, Arango-Galvan C, R. Fonseca-Montes de Oca AMC, Sandoval-Montes I, (2022) Hydrogeochemical processes in aquifers of volcano-sedimentary origin using inverse modeling. J S Am Earth Sci 117:1–16. https://doi.org/10.1016/j.jsames.2022.103888

Parkhurst DL, Appelo CAJ (1999) User's guide to phreeqc (version 2): A computer program for speciation, batch-reaction, one-dimensional transport, and inverse geochemical calculations. Water-resources investigations report 99(4259). https://doi.org/10.3133/wri994259

Peel HR, Balogun FO, Bowers CA, Miller CT, Obeidy CS, M. L. Polizzotto PMLC. S., Duckworth OW (2022) Towards understanding factors affecting arsenic, chromium, and vanadium mobility in the subsurface. Environmental Monitoring and Assessment 14(22). https://doi.org/10.3390/w14223687

Ramos-Leal JA, Martínez-Ruiz VJ, Rangel-Mendez JR, Torre MCADL (2007) Hydrogeological and mixing process of waters in aquifers in arid regions: a case study in san luis potosi valley, mexico. Environ Geol 53:325–337. https://doi.org/10.1007/s00254-007-0648-3

Siebe C, Abrams M, Macías JL, Obenholzner J (1996) Repeated volcanic disasters in prehispanic time at popocatépetl, central mexico: Past key to the future? Geology 24(5):399–402. https://doi.org/10.1130/0091-7613(1996)024<0399:RVDIPT>2.3.CO;2

Spring UO (2014) Water security and national water law in mexico. Earth Perspectives 1(1):1–15. https://doi.org/10.1186/2194-6434-1-7

Tay CK (2021) Hydrogeochemical framework of groundwater within the asutifi-north district of the brong-ahafo region, ghana. Applied Water Science 11(4). https://doi.org/10.1007/s13201-021-01398-1

Tikhomirov VV (2016) Hydrogeochemistry Fundamentals and Advances. Groundwater Composition and Chemistry. Wiley-Scrivener, New Jersey

Varol S, Sekerci M (2018) Hydrogeochemistry, water quality and health risk assessment of water resources contaminated by agricultural activities in korkuteli (antalya, turkey) district center. J Water Health 16(4):574–599. https://doi.org/10.2166/wh.2018.003

Xiao Y, Shao J, Cui Y, Zhang G, Zhang Q (2017) Groundwater circulation and hydrogeochemical evolution in nomhon of qaidam basin, northwest china. J Earth Syst Sci 126(2):1–16. https://doi.org/10.1007/s12040-017-0800-8

Chapter 6

Numerical modeling of groundwater flow

This article corresponds to a draft expected to be published in the journal *Journal of Hydrology* under the title *"Hydrogeological study of the Puebla Valley aquifer through numerical groundwater flow modeling"*.

The study objective was to develop a conceptual hydrogeological model serving as the basis for constructing a numerical model capable of simulating groundwater flow dynamics in the Valle de Puebla aquifer. This enabled understanding its hydrodynamic functioning, assessing current availability, and projecting its behavior under scenarios of intensive extraction and climate change. Based on geological, geophysical and hydrogeological characterization, a multilayer aquifer system was identified consisting of: (1) a shallow granular aquifer, (2) an intermediate confined aquifer with sulfurous waters, and (3) a deep fractured aquifer. This structural configuration, determined by grabens, tectonic horsts and fault zones, controls flow directions and recharge dynamics.

The model was implemented in MODFLOW and calibrated under steady-state and transient conditions, reproducing observed piezometric levels from 2010 to 2021. It showed a positive water balance, suggesting overall groundwater availability, though a growing cone of depression was detected in the south-central zone due to local overexploitation.

Projections to 2050 warn of potential deficits from increased demand and reduced recharge due to climate change, highlighting the urgency to implement sustainable management strategies based on this numerical model.

Hydrogeological study of the Puebla Valley aquifer through numerical groundwater flow modeling

Ana Beatriz Rubio-Arellano †[a], José Alfredo Ramos-Leal*†[a], Claudia Arango Galván†[b], Berenice Zapata Norberto †[a]

[a] *División de Geociencias Aplicadas, Instituto Potosino de Investigación Científica y Tecnológica (IPICYT), Camino a la Presa de San José 2055, Lomas 4ta Secc., 78216, San Luis Potosí, México.*

[b] *Instituto de Geofísica, Universidad Nacional Autónoma de México, Circuito de la, Investigación Científica s/n, C.U., Coyoacán, 04150 CDMX.*

Abstract

The present study aimed to evaluate changes in water tables and analyze the hydrological response of the system to natural and anthropogenic stressors in the Puebla Valley aquifer. This made it possible to understand its hydrodynamic functioning, assess its current availability, and project its behavior under scenarios of intensive extraction and climate change. Based on geological, geophysical, and hydrogeological characterization, a multilayer aquifer system was identified, consisting of a shallow granular aquifer, an intermediate confined aquifer with the presence of sulfidic waters, and a deep fractured aquifer. This structural configuration, determined by grabens, tectonic horsts, and fault zones, conditions flow directions and recharge dynamics. Numerical modeling was implemented in MODFLOW and calibrated under steady-state and transient conditions, accurately reproducing the observed piezometric levels during the 2010–2021 period. The model yielded a positive water balance since 2010, indicating general groundwater availability. However, a cone of depression was identified in the south-central part of the valley, which has progressively increased due to local overexploitation. The simulated scenarios for the year 2050 warn of a potential deficit, driven both by increased extraction demand and the projected decrease in recharge associated with adverse climate conditions. These results highlight the need to implement sustainable management strategies, supported by the numerical model as a tool for decision-making in water planning for the Puebla Valley aquifer.

Keywords: Numerical simulation, MODFLOW, Volcano-sedimentary aquifer, Conceptual hydrogeological model , Puebla valley

1. Introduction

In recent decades, an increase in groundwater use has been documented, extending even to regions traditionally less dependent on this resource, such as sub-humid and humid zones (Bourmada et al., 2024; Guevara-Ochoa et al., 2024; Márquez Molina et al., 2021). This growth has been driven by rising water demand in sectors like agriculture, industry, and urban supply. The pressure on groundwater resources has motivated the development and application of advanced tools. For example, Omar et al. (2021) used numerical models coupled with Geographic Information Systems (GIS) to assess recharge areas; Adombi et al. (2022) applied innovative techniques like machine learning for

*Corresponding author.

Email addresses: ana.rubio@ipicyt.edu.mx (Ana Beatriz Rubio-Arellano †), jalfredo@ipicyt.edu.mx (José Alfredo Ramos-Leal*†), claudiar@igeofisica.unam.mx (Claudia Arango Galván†), berenice.zapata@ipicyt.edu.mx (Berenice Zapata Norberto †)

[1] These authors contributed equally to this work.

groundwater monitoring; and Ghazi et al. (2021) studied coastal aquifers with saltwater intrusion under climate change conditions, using artificial intelligence models to predict declines in water tables. In this context, numerical modeling has emerged as an effective methodology to analyze groundwater flow dynamics (Gan et al., 2025), as it integrates the system's key hydrogeological features and evaluates future behavior under different use and recharge scenarios (Fiorese et al., 2025).

Once properly calibrated, a numerical model can be used to explore the possible responses of the aquifer to modifications in extraction or recharge conditions, thereby facilitating informed decision-making (Vianney et al., 2025; Tiwari et al., 2024). However, the development of these models depends on rigorous hydrogeological characterization, integrating geological, hydraulic, and geophysical data, in order to reduce uncertainties associated with the system's behavior (Pleasants et al., 2025; Hernández-Espriú et al., 2017).

The conceptual hydrogeological model constitutes a key stage in this process, as it synthesizes the available knowledge about the aquifer system's structure, functioning, and dominant processes (Fiorese et al., 2025; Kinoti et al., 2024; Giglou et al., 2023); therefore, conceptual models are based on a set of hypotheses supported by the interpretation of geological-geophysical data (Pleasants et al., 2025; Enemark et al., 2019; Hernández-Espriú et al., 2017), and incorporate elements such as the hydraulic properties of materials, structural constraints, recharge and discharge sources, as well as boundary conditions (Enemark et al., 2019; Mustafa et al., 2020). The conceptual model not only guides the construction of the numerical model but also represents an essential tool for the comprehensive planning and management of groundwater resources.

The increasing pressure on aquifers in Mexico demands sustainable management strategies, based on a detailed understanding of their dynamics (Hernández-Cruz et al., 2022; Martinez et al., 2015). To achieve this, it is essential to thoroughly understand hydrogeological systems, including the development and evolution of water tables. An effective tool for gaining such understanding is the combined application of hydrological and numerical models, capable of reproducing geological heterogeneity and complex hydrogeological conditions (Hermans et al., 2023; Tanachaichoksirikun et al., 2020).

Despite methodological advances, significant challenges persist regarding data availability, resolution, and consistency, which may limit the accuracy of numerical models and compromise the effectiveness of resource management strategies (Lévesque et al., 2023; Barthel et al., 2021). This is the case for the Puebla Valley (PV) aquifer system, where no updated conceptual hydrogeological model exists to support decision-making for sustainable management. Therefore, this research proposes the development of a regional hydrogeological model of this system, located in a volcanosedimentary geological context, to serve as the basis for numerical groundwater flow simulation. The primary objective is to evaluate changes in groundwater levels and analyze the system's hydrological response to both natural and anthropogenic stressors.

This approach not only allows evaluating water availability in the aquifer, but also provides an understanding of flow patterns, changes in hydraulic gradients, and modifications to surface hydrology. This information is key for decision-making aimed at conservation and efficient use of groundwater resources.

2. Study area and conceptual hydrogeological model

2.1. Study area

The PV aquifer is located in a subhumid region in central Mexico (Fig. 1). The mean annual precipitation ranges between 690 and 1350 mm/year, while actual evapotranspiration varies between 250 and 558 mm/year in the valley. The most significant topographic elevations in the region include the Popocatepetl volcano, Iztaccíhuatl, Telapón, and La Malinche.

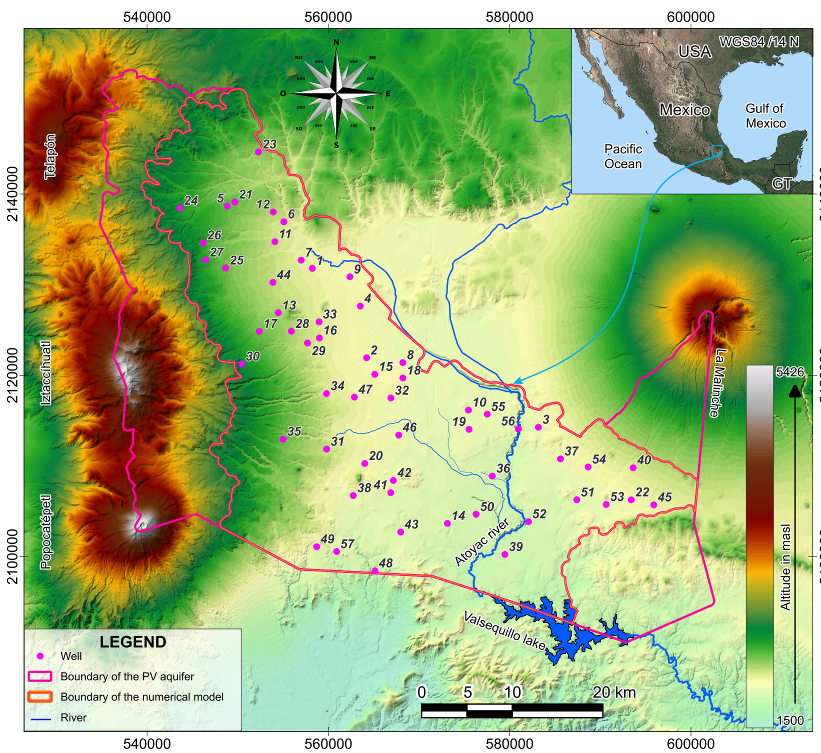

Fig. 1: Study area, boundary of the numerical groundwater flow model, and location of observation wells.

In the west-central part of the valley are located the Zapotecas hills, El Tecajete and Teotón of volcanic origin (Fig. 2a), belonging to the Trans-Mexican Volcanic Belt. Hydrologically, the region is characterized by the presence of the Atoyac River, which originates in Sierra Nevada (Iztaccíhuatl) and extends along the valley, passing through the State of Tlaxcala before returning and crossing the city of Puebla and continuing its course to Valsequillo Lake.

The Puebla valley is composed of a variety of geological materials; continental sedimentary rocks and volcanic products predominate, with a lesser presence of marine sedimentary rocks.

The continental sedimentary rocks include sands, clays, gravels, and boulders, interbedded with volcanic products and lacustrine calcareous materials. These deposits belong to the Cretaceous-Quaternary period. Meanwhile, the marine sedimentary rocks are represented by limestones, with a smaller proportion of shales that correlate with the Upper Cretaceous Maltrata formation (Fig. 2a).

The tectonic structure of the Puebla valley is influenced by various faults. Tectonic faults with NW-SE orientation are inferred, associated with the origin of La Malinche. Additionally, normal faults with east-west orientation are observed, forming two topographic steps in the northern part of the valley, as shown in Fig. 2a.

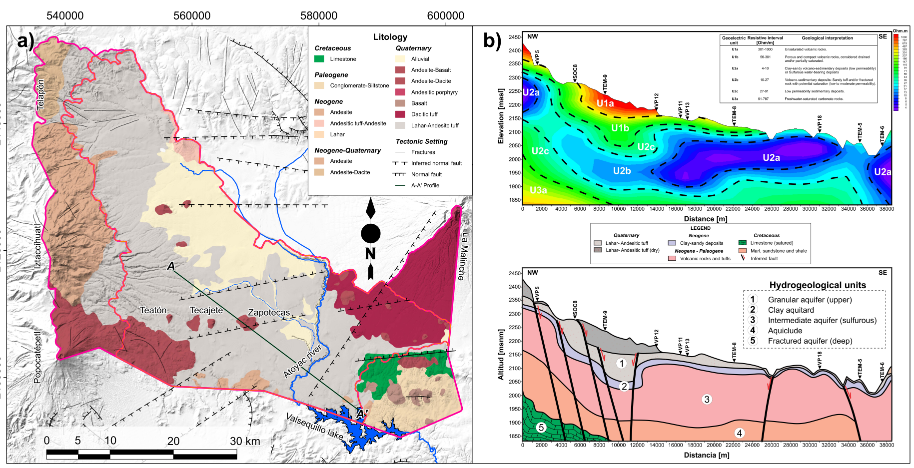

Fig. 2: Surface and structural geology of the PV aquifer. a) Geological map; b) Geophysical-geological section obtained from transient electromagnetic soundings (TEM).

2.2. Conceptual hydrogeological model

The conceptual model represents the structural basis of the numerical modeling process, as its fidelity largely determines the accuracy and reliability of subsequent simulations (Samani, 2025). Therefore, this work proposes a conceptual hydrogeological model of the PV aquifer (Fig. 3).

Recharge of the PV aquifer system comes mainly from rainfall, which infiltrates through permeable subsurface materials. The main recharge zones are located in Sierra Nevada and La Malinche. Surface runoff from high topographic areas flows down to the valley, where part of this water infiltrates into the aquifer

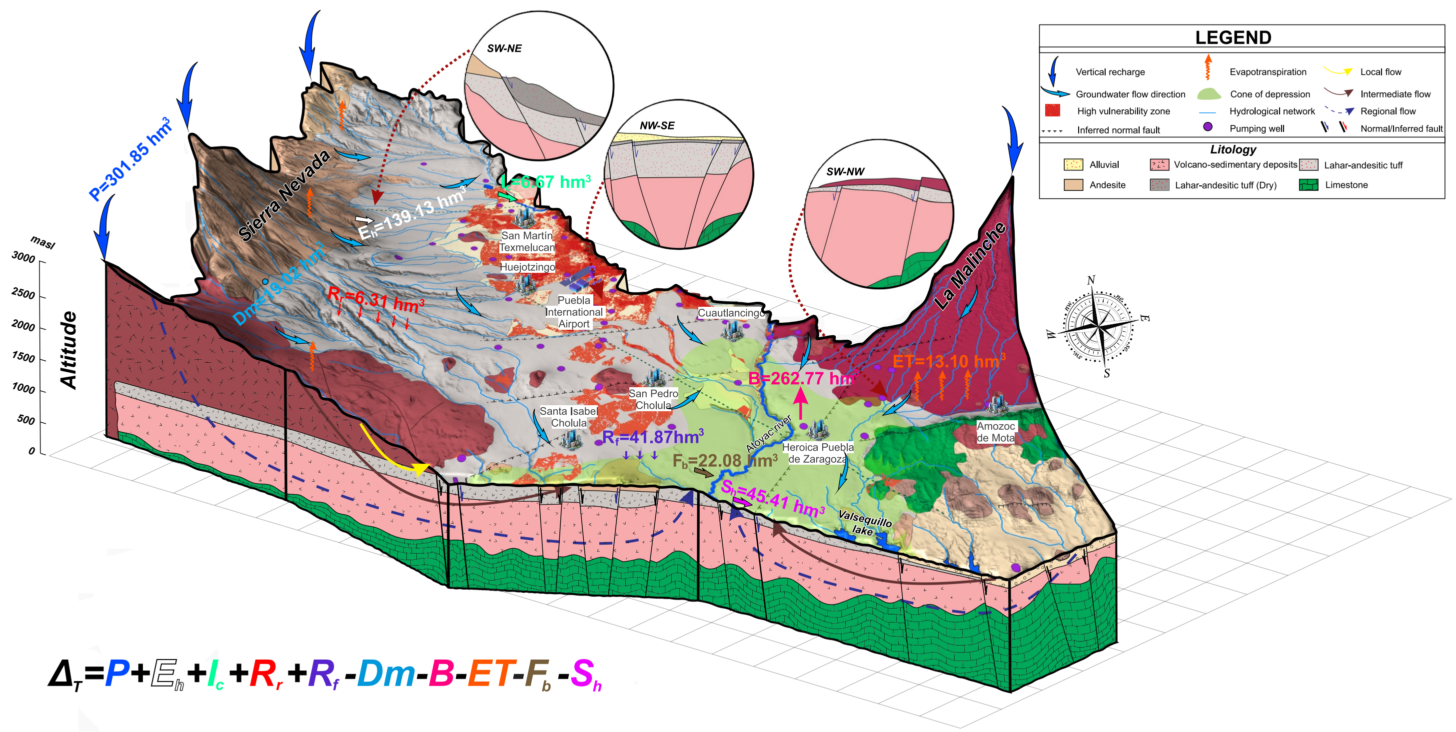

Fig. 3: Three-dimensional conceptual hydrogeological model of the functioning of the PV aquifer. **Inputs to the system:** Vertical recharge (P), horizontal inflows (E_h), streambed infiltration (I_c), irrigation return flow (R_r), and infiltration from urban pipeline leakage (R_f). **Outputs from the system:** Spring discharge (D_m), pumping (B), evapotranspiration (ET), baseflow (F_b), and horizontal outflows (S_h).

system and another part flows to the Atoyac River, following its course south of Puebla city and eventually reaching Valsequillo Lake.

The aquifer discharge occurs both through regional groundwater flow towards the south and direct extraction via deep wells located in the valley and the Puebla metropolitan area. Overexploitation has generated significant cones of depression, particularly in the south-central part of the aquifer.

The Fig. 2b shows the distribution of hydrogeological units in this system.

i) Unconfined upper aquifer of granular type, formed by alluvial deposits, gravels, sands and clays. It has an approximate thickness of 150 m and presents good water quality suitable for agricultural, public and urban use. The static water level is shallow, reaching values of up to 5 m in the northwest of the valley.

ii) Confined intermediate aquifer, separated from the upper one by a clayey aquitard of low permeability. This aquifer has an average thickness of 200 m and is characterized by the presence of sulfurous waters. In the western part of Puebla city, geological faults allow hydraulic mixing between both aquifers due to confinement rupture.

iii) Fractured lower aquifer, separated by an aquiclude composed of limestones and marls of very low permeability. This aquifer is not currently exploited; there are no well records, so its water quality and actual thickness are unknown. The geological basement is inferred to be composed of metamorphic schists from the Acatlán Complex.

Regarding hydraulic behavior, the deepest static levels (125 m) are located near the sierras and in the south-central area of Puebla city, while the shallowest levels (5-8 m) are recorded in the north-central part of the valley.

Groundwater flow in the PV aquifer follows the hydraulic gradient, from higher elevation zones (Sierra Nevada and La Malinche) toward the south and southwest of the valley, where the lowest piezometric levels are found. This pattern reflects a general downward and radial flow, with convergence toward areas of intensive extraction, particularly in southern Puebla City, where a large cone of depression has developed, extending approximately 33.2 km. Flow directions indicate active recharge from peripheral mountainous areas, while the south-central valley acts as a pumping-induced discharge zone, which may be affecting aquifer connectivity and promoting vertical water mixing in areas with structural faulting.

The system exhibits anthropogenic modifications both at the surface and subsurface. At the surface, the course of the Atoyac River has been altered, and the Manuel Ávila Camacho dam has been constructed. Subsurface overexploitation has modified aquifer behavior. Although natural water inputs currently exceed extractions, the system requires improved resource management. Otherwise, water tables may progressively decline, returning to critical conditions similar to those observed in 2010, when severe overexploitation problems were documented.

3. Materials and Methods

3.1. Aquifer system characteristics

3.1.1. Piezometry and hydraulic parameters

The data used to develop piezometric configurations and determine groundwater flow direction, as well as hydraulic parameters, were obtained through the National Water Commission - Puebla (CONAGUA-Puebla, by its acronym in Spanish). This institution provided historical records of static level depth and elevation corresponding to the 2010-2021 period, as well as pumping test data from 1990, 2010 and 2021. Fig. 1 shows the spatial distribution of observation wells.

Using the hydraulic head from each well, interpolation was performed using the Kriging method to generate isolines and infer groundwater flow direction, considering the principle that flow occurs from zones of higher hydraulic head to zones of lower hydraulic head. This operation was performed for each year with available data.

The pumping test database includes information from both drawdown and recovery phases. The applied methodology consisted of analyzing these tests using AquiferTest software, which allowed generating graphs for both stages. From these analyses, parameters such as hydraulic conductivity (K), the type of evaluation method used (Theis, Theis and Jacob, Hantush), the aquifer type where the well is located, the considered aquifer thickness, and transmissivity (T) were obtained.

3.1.2. Lithological subsurface arrangement

Information was compiled from the Mexican Geological Survey to define the surface geology of the area. For subsurface characterization, 10 geophysical profiles composed of 42 transient electromagnetic soundings (TEM) were hydrogeologically interpreted. Fig. 2b shows an example of a NW-SE oriented geophysical-geological profile, where hydrogeological units were delineated based on the correlation between electrical resistivity values of lithological materials and the geostructural context.

From the geological interpretation of geophysical profiles, the thickness of each aquifer unit was determined by measuring the elevations of their upper and lower boundaries. For the shallow aquifer, topography was used; for the intermediate aquifer, the upper boundary was established at the contact between alluvial deposits and Pliocene volcanic rocks; and for the fractured aquifer, the upper boundary was defined at the contact between volcano-sedimentary materials and limestones. Elevations were measured along the profiles at points spaced two kilometers apart.

Based on these measurements, three surfaces were interpolated: i) the upper boundary of the granular aquifer, ii) the contact between the granular and intermediate aquifers, and iii) the lower boundary of the intermediate aquifer in contact with the fractured aquifer. These surfaces define the layers of the conceptual model, structured as follows: i) granular aquifer, from the topographic surface to the middle interface (Top-Middle), ii) intermediate aquifer, between the middle and bottom interfaces (Middle-Bottom), and iii) fractured aquifer, below the bottom layer (Bottom).

3.2. Mathematical model

3.2.1. Numerical Code

The numerical modeling aims to replicate the piezometric levels of the system to understand the general behavior of current groundwater flow and predict potential future variations. The analysis period spans from 2010 to 2021, subdivided into two stages: a steady-state flow condition and a transient regime. Simulations were developed using the MODFLOW-6 numerical code.

The model structure evaluated the spatial and temporal distribution of hydrogeological parameters such as hydraulic conductivity and specific storage. These parameters were defined for the three identified aquifer units: upper, intermediate, and deep.

3.2.2. Spatial Discretization

The VP aquifer is surrounded by significant topographic elevations, such as the Sierra Nevada (5,393 masl) and La Malinche (4,461 masl). The valley area, composed mainly of volcano-sedimentary materials, was delineated by the 2,650 masl contour. Consequently, the surface area considered for the simulation covers 1,478 km^2, as shown in Fig. 1. This area was discretized into a grid of 133 cells in the X-direction and 124 in the Y-direction, resulting in a total of 16,492 square cells of 500 $\times$ 500 m. Of these, only 5,940 were considered active in the numerical modeling.

The grid was locally refined along the Atoyac River, where a steeper horizontal hydraulic gradient was anticipated, achieving a cell size of 125 m in this area of interest.

The conceptual model layers (Top, Middle, and Bottom) were incorporated as GRD files. The final model structure consists of three hydrogeological units represented by six modeled layers: i) Zone 1 (Top-Middle): Granular aquifer; ii) Zone 2 (Middle-Bottom): Intermediate aquifer; and iii) Zone 3 (Bottom): Fractured aquifer.

To enhance the model's vertical resolution, it was doubled, allowing more precise delineation of six specific zones. The distribution of active cells was maintained from the first to the last layer, ensuring hydraulic connectivity between the different aquifer units. This vertical connection is maintained through spatial variation of hydrogeological parameters.

3.2.3. Temporal discretization

The model was configured with an initial steady state using ground topography as hydraulic head, simulated over a nominal 1-day period for numerical stabilization. For the transient state (2011-2021), five stress periods were defined based on piezometric data availability. The time unit was days; Table 1 presents the schedule of stress periods used in the numerical model.

Table 1: Distribution of stress periods in the numerical model.

Stress period	Time [days]	Years	Cumulative days
0	Steady-state	2010	Not applicable
1	1096	2011–2013	0–1096
2	1461	2014–2017	1097–2558
3	365	2018	2559–2923
4	365	2019	2924–3288
5	731	2020–2021	3289–4019

The total simulated time was equivalent to 11 years (4,019 days), covering the period from January 1, 2011, to December 31, 2021. This discretization aligns the stress periods with the observed data available for model calibration.

3.3. Hydrogeological Parameters

For the numerical modeling of the VP aquifer, hydraulic conductivity, specific storage, recharge, rivers, evapotranspiration, and springs were incorporated. MODFLOW 6 incorporates these parameters through modules, where values for flow rates per unit time, conductances, and stress periods are entered.

3.3.1. Constant Head

The constant head represents an infinite water source to maintain constant water table elevation. It is referred to as a polyline and for this case was defined in the horizontal inflow and outflow zones according to the configuration based on static water level elevations and their evolution during the 2010-2021 period. For the transient state, these were input using the CHD package.

Constant head (CHD) boundary conditions were defined as polylines in the model's inflow and outflow zones, with values based on the initial static water level and its temporal evolution (2010-2021). For Valsequillo Lake, whose interaction with the aquifer is dynamic, it was considered as GHB.

3.3.2. Recharge

To incorporate recharge into the numerical model, the RCH package was used, through a GRD file that spatially distributes recharge. The discretization and units of the GRD were consistent with the model grid.

3.3.3. Pumping

Pumping extractions during the modeling period (2010-2021) were estimated using data from the Public Registry of Water Rights (REPDA, by its acronym in Spanish), considering active wells and authorized volumes. These are integrated into the model using the MODFLOW WEL package, assigning flow rates per cell according to well locations.

Table 2 shows the total number of wells per year and the extraction volume in cubic hectometers per year, which are distributed throughout the valley.

Table 2: Total extraction well volume per year.

Year	**Total wells**	**Total extraction volume (hm^3 $year^{-1}$)**
2010	1003	227.5
2011	1024	231.0
2012	1045	232.3
2013	1080	235.6
2014	1089	236.0
2015	1107	236.7
2016	1138	239.2
2017	1154	242.2
2018	1216	248.7
2019	1241	254.3
2020	1276	258.6
2021	1299	262.8

3.3.4. Spring Discharge

The discharge from 102 springs was modeled using the MODFLOW DRN package, assigning each spring its topographic elevation and adjusting conductance through validation with observed data.

3.3.5. Evapotranspiration

To incorporate evapotranspiration rates into the numerical model, the ETS package was used through a GRD file that spatially distributes actual evapotranspiration (ETR). The discretization and units of the GRD were consistent with the model grid.

3.3.6. Rivers

The interaction of the Atoyac River with the aquifer was simulated through the RIV package. The river was assigned using polylines, where each cell intersected by the river received individual parameters (elevation, conductance, water level). Primarily in the northwest valley, the Atoyac River infiltrates water into the aquifer, especially where it crosses permeable alluvial deposits, therefore a high conductance and river level above the water table were assigned. Near Puebla city, the aquifer feeds the river, contributing to its base flow, so a river level below the water table was assigned.

3.3.7. Hydraulic conductivity

Horizontal hydraulic conductivity K_h was assigned based on tests conducted in 39 wells by CONAGUA. A Kriging interpolation was performed to obtain a grid of hydraulic conductivity values for the granular aquifer. It should be noted that the method applied for pumping tests (Theis and Jacob) yields average values of lithology, so the best definition was achieved in the SW and NW of the aquifer where more data were available.

For the sulfurous aquifer, the granular aquifer conductivity was reduced by half an order of magnitude, while for the fractured aquifer, the granular aquifer conductivity was reduced by one order of magnitude.

3.3.8. Specific Storage

The S_s was obtained from the same 39 pumping tests used for hydraulic conductivity. For each well, the storage coefficient (S) was calculated and, by dividing by the local saturated thickness, S_s was derived. Point values were interpolated with Kriging to generate the continuous map of the granular aquifer. For the sulfurous aquifer, S_s was reduced by half an order of magnitude, and for the fractured aquifer, by a full order, consistent with its greater confinement and lower compressibility.

3.4. Calibration

Calibration is a fundamental stage in numerical modeling, whose objective is to adjust model parameters through iterative comparison between calculated results and observed historical data, so that the response of the real system is adequately reproduced (Barnett et al., 2012). According to Jimenez et al. (2025), calibration and validation are key processes to ensure model accuracy in predictive simulations.

In this study, the principle of parsimony was initially applied (Poeter and Hill, 1997; Hill and Tiedeman, 2007), keeping the model as simple as possible without omitting the key elements that control the aquifer's hydrodynamic behavior. This strategy aimed to avoid overparameterization and ensure that each parameter had a physical justification. Subsequently, an automatic optimization was carried out using PEST to refine global parameters and improve the match between calculated and observed groundwater levels. This hybrid strategy, based on initial simplicity followed by automated adjustment, enhanced model efficiency and reduced systematic biases.

Following Anderson and Woessner (2015), a common way to evaluate calibration quality is by comparing calculated (H_{cal}) and observed (H_{obs}) hydraulic heads. Three fundamental statistical metrics were used to quantify the fit: root mean square error (RMSE), mean error (ME), and mean absolute error (MAE) (Kaur et al., 2023; Nejatian et al., 2024).

The RMSE measures the average of squared errors or deviations, that is, the differences between H_{calc} and H_{obs} (Chai and Draxler, 2014). It is defined as the square root of the sum of squared residuals divided by the total number of wells (Eq. 1), and is expressed in meters:

$$RMSE = \sqrt{\frac{1}{n}\sum_{i=1}^{n} R_i^2} \tag{1}$$

The RMSE is always positive and reflects the degree of fit between H_{calc} and the trend represented by H_{obs}. High values indicate greater discrepancy between calculated and observed values, while low values reflect better fit. Therefore, the calibration objective is to minimize this value.

The ME helps identify whether the model exhibits systematic bias, assessing whether it tends to overestimate (positive ME) or underestimate (negative ME) hydraulic heads (Gebru et al., 2025). However, a value near zero does not necessarily indicate high precision, as positive and negative errors may offset each other. Thus, this metric should be interpreted together with RMSE. It is defined as the mean difference of residual errors (Eq. 2) and its unit is meters.

$$\mathrm{ME} = \frac{1}{n}\sum_{i=1}^{n} (h_{obs,i} - h_{cal,i}) \tag{2}$$

Finally, the MAE calculates the absolute difference between H_{obs} and H_{calc} (Igwebuike et al., 2025). It is used as a complementary measure since it reflects the average magnitude of absolute errors (Eq. 3). Unlike the ME, it does not allow compensation between opposite errors, making it useful for evaluating the overall robustness of the model. It is expressed in meters.

$$\mathrm{MAE} = \frac{1}{n}\sum_{i=1}^{n} |h_{obs,i} - h_{cal,i}| \tag{3}$$

3.5. MODFLOW Projections

The PV aquifer is the main water source for the region, with public-urban use being the most demanding, followed by agricultural use. Therefore, a baseline scenario was developed to evaluate the system's sustainability under current conditions, corresponding to the year 2025. In this scenario, the system's input and output data were updated through January 2025 to more accurately represent the current state of the aquifer.

Subsequently, two additional projection scenarios were developed for the years 2035 and 2050, incorporating three key factors: climate change, population growth, and increased agricultural demand. These projections make it possible to anticipate the system's behavior under different future pressures, providing key elements for decision-making regarding the region's water management.

The aquifer's natural recharge depends heavily on seasonal rainfall, meaning any climate variation directly impacts its water balance. Likewise, anthropogenic pressure resulting from population growth and agricultural expansion could compromise the system's sustainability if not properly managed.

3.5.1. Climate Change

To incorporate climate change effects, short-term precipitation and temperature projections (2021-2040) from the National Institute of Ecology and Climate Change (INECC) database for Puebla state were used. According to this data, a 1.4% increase in precipitation and a 1.1°C rise in mean annual temperature are expected. Based on these projections, the model's climate parameters were adjusted, allowing recalculation of the estimated recharge volume to the aquifer.

3.5.2. Population Growth

Population growth projections were developed using census data from the National Institute of Statistics and Geography (INEGI) for 2000-2020, supplemented with demographic projections from the National Population Council (CONAPO) until 2040. A polynomial trend model (degree 1) was fitted to extrapolate population to 2050, validated through the coefficient of determination (R^2=0.99). Annual drinking water demand was then estimated by multiplying projected population by a per capita consumption of 72 m^3/inhabitant/year (equivalent to 200 L/inhab/day), based on local water consumption reports (Villegas, 2024).

3.5.3. Increased Pumping in Agricultural Areas

Since the majority of groundwater consumption in the PV aquifer corresponds to the agricultural sector (REPDA, 2021), the reported extraction volumes for this sector between 2010 and 2021 were analyzed. From this time series, a polynomial trend adjustment was performed to project agricultural extraction volumes between 2022 and 2050.

4. Results and Discussion

4.1. Calibration of the Hydrogeological Numerical Model

The numerical model calibration in MODFLOW was performed by adjusting the hydrogeological parameters of horizontal hydraulic conductivity (K_h) and specific storage (S_s), as shown in Fig. 4.

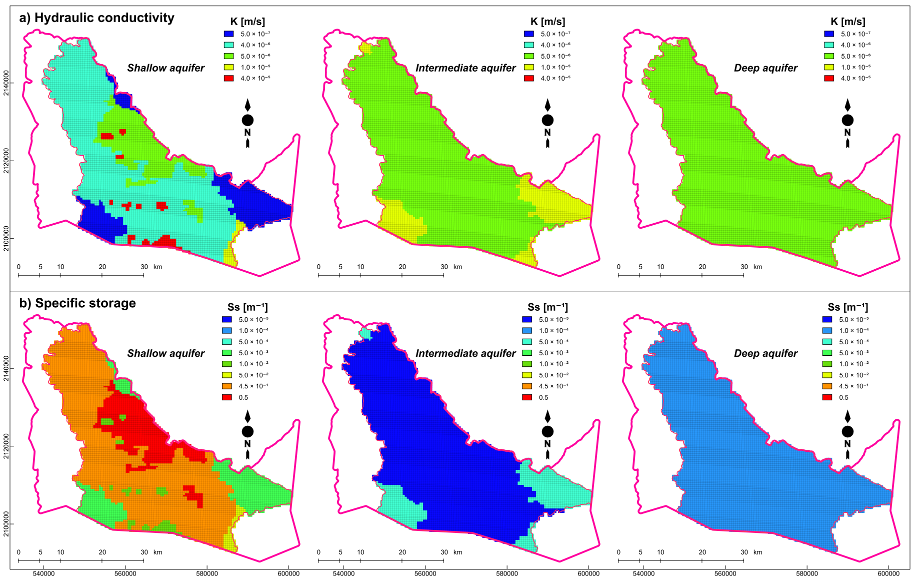

Fig. 4: Calibration results. a) Hydraulic conductivity; b) Storage coefficient.

The upper aquifer shows K_h variations between 5.0×10^{-7} and 4.0×10^{-5} m/s; the intermediate aquifer presents values between 1.0×10^{-5} and 5.0×10^{-6} m/s; while the lower aquifer shows homogeneous K_h with a constant value of 5.0×10^{-6} m/s, as shown in Fig. 4a.

Specific storage (S_s) values ranged from 5.0×10^{-5} to 0.5, with the highest values located in the north-central zone of the upper aquifer (Fig. 4b). The calibrated values fall within ranges reported by previous studies in the area (Flores-Márquez et al., 2006; Salcedo-Sánchez et al., 2013) and align with reference values from specialized literature, considering adjustments for structural geology (Freeze and Cherry, 1979; Chen et al., 2018; Shahbazi et al., 2020).

MODFLOW calculations through ModelMuse for steady-state conditions showed excellent agreement with CONAGUA-Puebla observations, evidenced by a positive linear correlation (r = 0.99) between H_{obs} and H_{calc}. Fig. 5a presents the calibration scatter plot, where most points cluster near the 1:1 line within prediction intervals (2σ). Calculated RMSE, MAE and ME values were 6.61, 6.01 and 1.74 m, respectively.

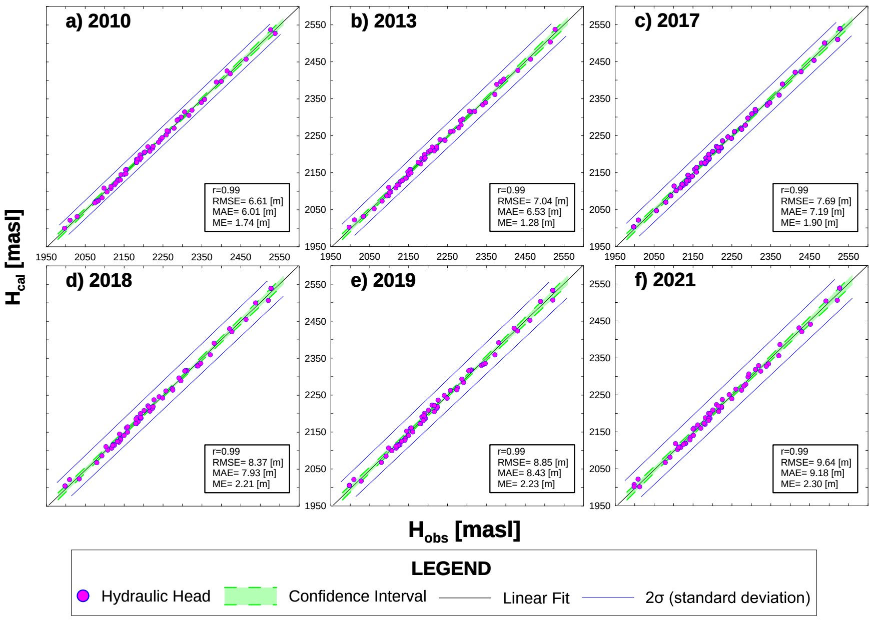

Fig. 5: Water table calibration results for monitored wells in the numerical model. a) 2010 steady-state regime; b) 2013 transient regime; c) 2017 transient regime; d) 2018 transient regime; e) 2019 transient regime; f) 2021 transient regime.

The calibration process fully satisfied the evaluation criteria proposed by Anderson and Woessner (2015). In particular, the maximum absolute residual of 11.8 m was below 10% of the total head variation range (Δh = 541 m), equivalent to 54.1 m; the MAE (6.61 m) was less than 2% of Δh (10.8 m); and the RMSE/Δh ratio was only 1.22%, well below the 10% limit.

These results confirm that the calibrated model faithfully reproduces the system's behavior, with minimal discrepancies between calculated and observed values. The high correlation obtained, together with strict compliance with all evaluated error criteria, demonstrate that the steady-state model achieved robust and reliable calibration for its intended application.

During transient regime calibration, the years 2013, 2017, 2018, 2019, and 2021 were adjusted. Overall, all years showed positive correlation between observed and calculated hydraulic heads, with a coefficient of determination of 0.9. The RMSE/Δh ratio ranged between 1.22 and 1.82, which according to Anderson and Woessner (2015) indicates good model performance. Additionally, the maximum absolute residuals were below 10% of the total head variation range, while the MAE remained under 2% of Δh for all studied years, as shown in Fig. 5.

It should be noted that year after year there is an increase in RMSE, suggesting a deterioration in the predictive model's accuracy over time. This may be primarily related to data quality (incomplete in recent years), highlighting the importance of working on continuous updating and monitoring of piezometric measurements since they constitute the model's input data, thereby improving the accuracy of obtained results.

4.2. Flow Directions

The static water level elevation configuration, or hydraulic heads, calculated by MODFLOW through ModelMuse shows notable spatial correspondence with field-observed data. The Fig. 6 presents the spatial distribution of static water levels for years 2010, 2017, and 2021.

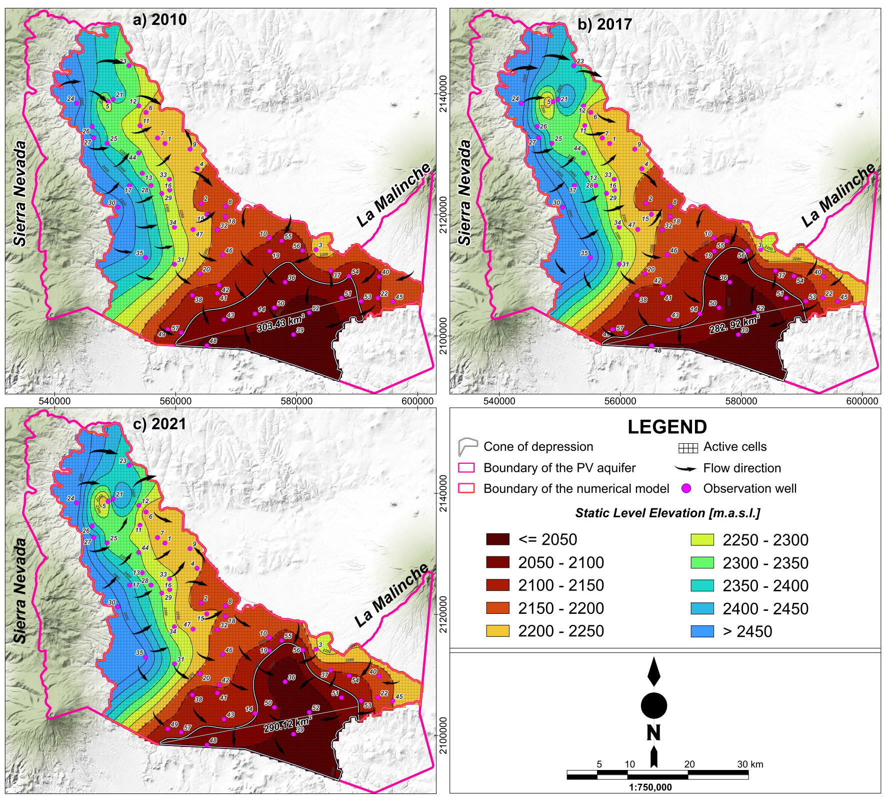

Fig. 6: Spatial distribution maps of hydraulic head. a) Steady-state regime simulation for year 2010; b) Transient regime simulation for year 2017; c) Transient regime simulation for year 2021.

In 2010, a well-defined cone of depression was identified in the south-central valley, with static groundwater levels ranging between 2050 and 2100 masl (represented by dark wine to red tones). This depression cone extends in a southwest-northeast (SW-NE) direction, reaching nearly the center of Puebla City (Fig. 6a). The presence of this depression reflects intensive groundwater extraction in the region, likely associated with urban growth and industrial activities. The area affected by this cone covered approximately 303 km^2.

4.3. Evolution of the Cone of Depression

In 2017, the cone of depression covered an area of 290 km^2, indicating a slight decrease compared to 2010. However, a lateral expansion and mild intensification toward the northwest was observed (Fig. 6b). While maintaining the general pattern identified in 2010, the area affected by drawdown has expanded, suggesting increased local aquifer exploitation in this region during the period.

As evidenced by the hydraulic heads obtained from the transient simulation through 2021, the cone of depression did not expand in the east-west direction, suggesting a near-equilibrium state in this orientation. This behavior underscores the importance of recharge from both the Sierra Nevada and La Malinche. However, in the northwest-southeast direction, the cone of depression exhibited expansion between 2010 and 2021, likely associated with increased groundwater extraction in agricultural areas. The area of the depression cone during this period reached 290 km^2 (Fig. 6c).

Collectively, the maps reveal the temporal evolution of drawdown, highlighting the persistence of the most overexploited zones, the maintenance of the general direction of groundwater flow, continuous flow from recharge areas (primarily Sierra Nevada and La Malinche) and the presence of a natural hydraulic gradient directing flow toward the center of the valley.

The Fig. 7 shows the superposition of observed and calculated hydraulic head contour lines, aimed at identifying zones with the highest similarity and differences between both datasets. Overall, the analyzed years show good correspondence between calculated and observed hydraulic heads. However, some notable discrepancies were identified, particularly in the southwest and northwest sectors of the model - areas where there is insufficient observational well data or geophysical information to more precisely characterize hydrogeological units.

These differences, nevertheless, do not occur in areas with good data density, and therefore do not represent a significant problem for the overall model evaluation nor compromise the quality and reliability of the obtained results.

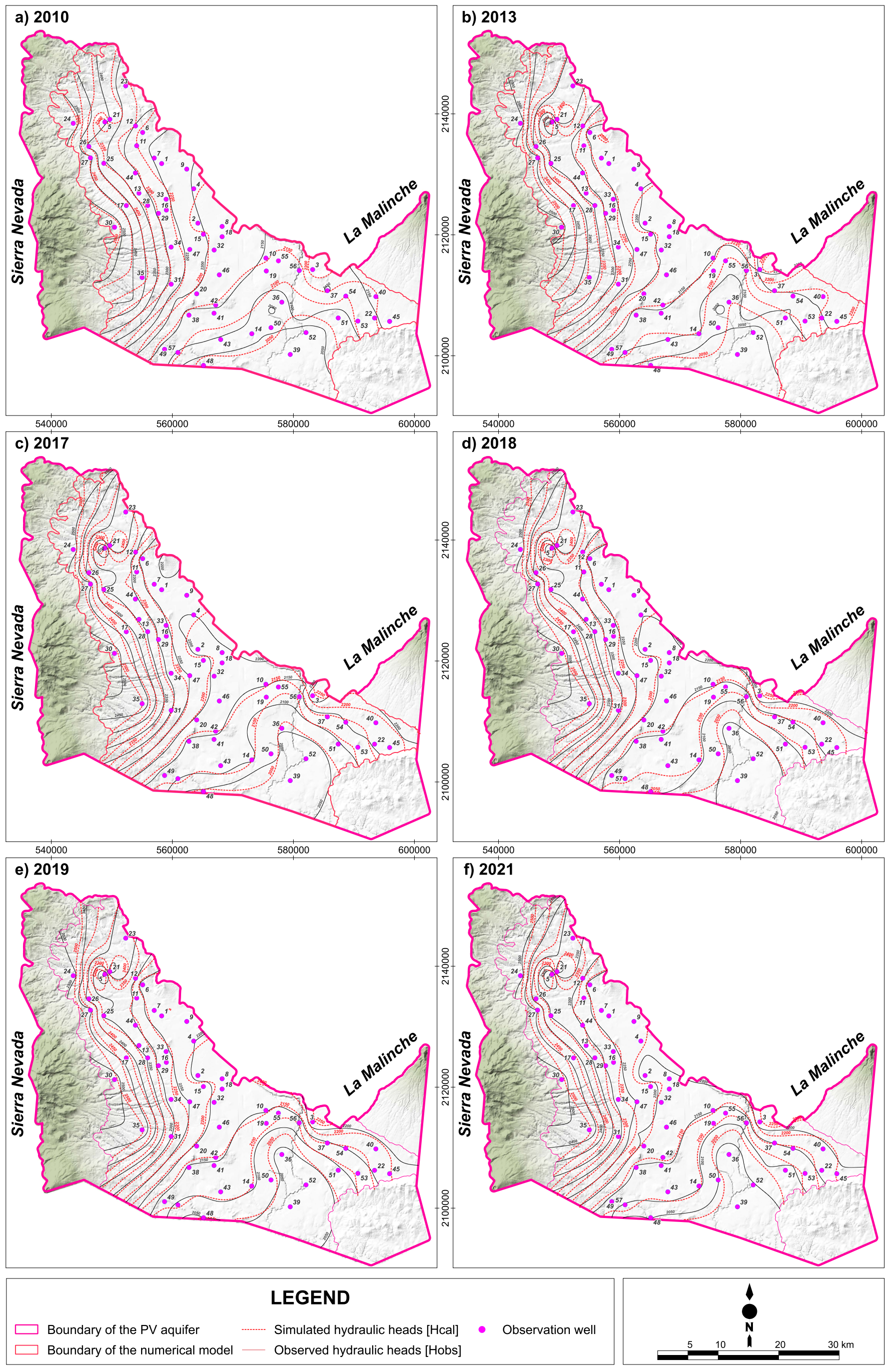

Fig. 7: Comparison of observed and calculated hydraulic head. a) 2010; b) 2013; c) 2017; d) 2018; e) 2019; f) 2021.

4.4. Mass balance

The change in storage (ΔS) within the PV aquifer system has remained positive throughout the period from 2010 to 2021, indicating that recharge consistently exceeded discharge (Fig. 8). In 2010, total inflows amounted to 356.07 hm^3, while outflows reached 349.26 hm^3, resulting in a marginal storage increase of 6.81 hm^3, reflecting limited water availability. By 2017, the system exhibited a marked improvement, with an estimated storage gain of 76.15 hm^3. This trend continued through 2021, when storage availability rose to 126 hm^3, driven by a significant increase in recharge despite the concurrent rise in groundwater extraction.

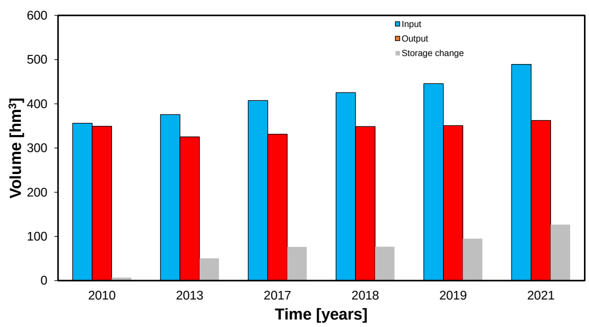

Fig. 8: Mass balance in the PV aquifer from 2010 to 2021.

4.5. Model Sensitivity Analysis

To assess the reliability of the model results, a manual sensitivity analysis was performed to identify the input parameters that exert the greatest influence on the calculated hydraulic heads. The analysis focused on three key parameters: hydraulic conductivity, recharge, and specific storage; each of these parameters was modified by $\pm 10\%$, $\pm 20\%$, and $\pm 30\%$ from their calibrated values.

Fig. 9 shows that the model is highly sensitive to variations in hydraulic conductivity and specific storage, as small modifications ($\pm 10\%$) result in a significant increase in the RMS value, indicating a strong influence of these parameters on the calculated results. In contrast, the recharge parameter exhibits a gentler slope curve, suggesting lower model sensitivity to changes in this input. A slight asymmetry is also observed in the curves, with RMS values tending to increase more with positive deviations than with reductions, which could be associated with a non-linear behavior of the aquifer system. These results underscore the importance of improving the estimation of hydraulic conductivity and specific storage in future model calibration stages.

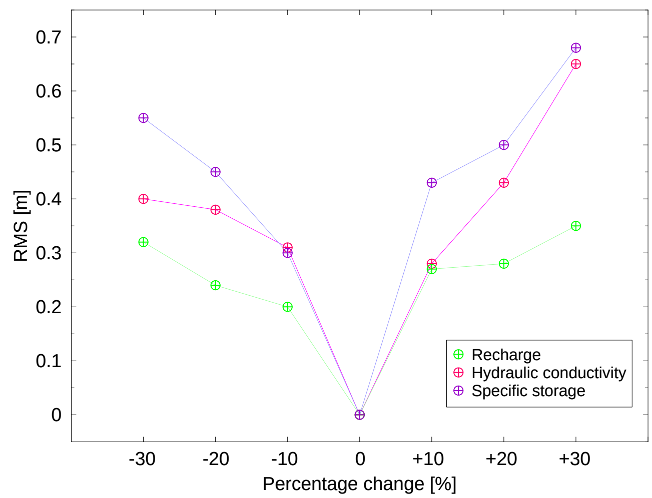

Fig. 9: Model sensitivity analysis results.

4.6. Model Projection

Projected climate change scenarios indicate a reduction in aquifer recharge for the years 2025, 2035, and 2050, which translates into a sustained decline in groundwater levels. This phenomenon could exacerbate pressure on the system, particularly when contrasted with the simultaneous growth in water demand.

The population growth for the year 2025 is estimated at 3,133,556 inhabitants, with a projected water demand of 225 hm^3 per year. By 2035, the population is expected to reach 3,561,021, with an estimated annual demand of 256 hm^3, and by 2050, the population could increase to 4,217,100 inhabitants, requiring 303 hm^3 of water annually (Fig. 10a).

In parallel, agricultural water withdrawals show an upward trend, increasing from 80.33 hm^3 in 2025 to 94.65 hm^3 in 2035 (a 17.8% increase), and reaching 116.13 hm^3 by 2050 (44.5% more than in 2025). This trend reflects an average annual increase of 1.43 hm^3 (Fig. 10b), which could strain available water resources if efficiency strategies are not implemented, such as irrigation modernization or crop adjustments. The results highlight the need to align agricultural policies with aquifer sustainability, particularly in contexts where natural recharge falls short of projected demand.

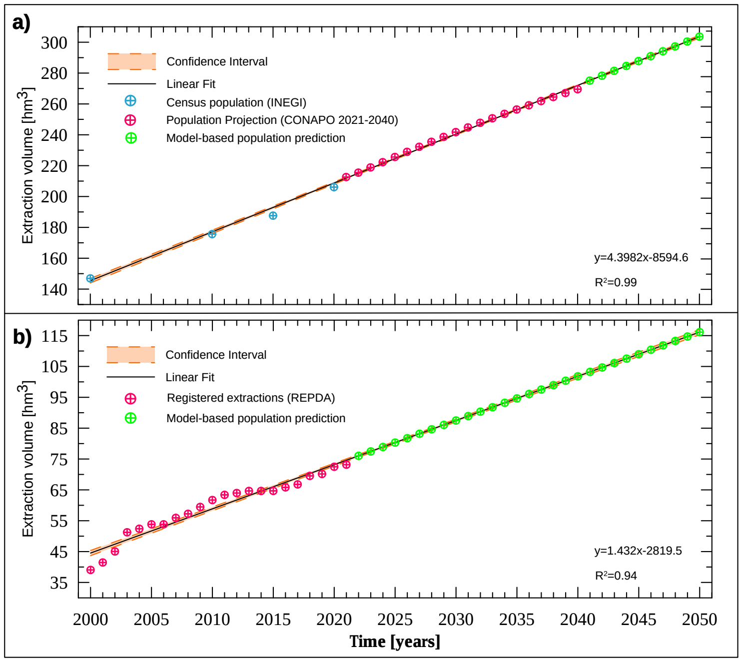

Fig. 10: Hydraulic head elevation by zones for the year 2021. a) Zone 1; b) Zone 2; c) Zone 3; d) Zone 4; e) Zone 5

In general terms, the depth of the static water level shows a progressive increase over time. For the year 2025 (Fig. 11a), an increase ranging from 1 to 20 m is observed, which intensifies in 2035 (Fig. 11b), reaching a range of 4 to 29 m. By 2050, increases exceed 50 m in some areas (Fig. 11c).

The Fig. 11 shows the presence of a drawdown cone in the south-central region of the valley, identified since 2010. Between 2025 and 2035, this cone does not exhibit significant expansion; however, by 2050 its extent reaches 34.46 km in the WSW-ENE direction and 23.88 km in the NNW-SSE direction. Significant changes occur at wells 36, 39, 48, and 52, located within the area affected by the drawdown.

The recharge zones, particularly Sierra Nevada, do not show substantial changes in the static water level elevation. In contrast, the La Malinche region records a slight increase in static level depth, attributable to the elongation of the drawdown cone in the WSW-ENE direction.

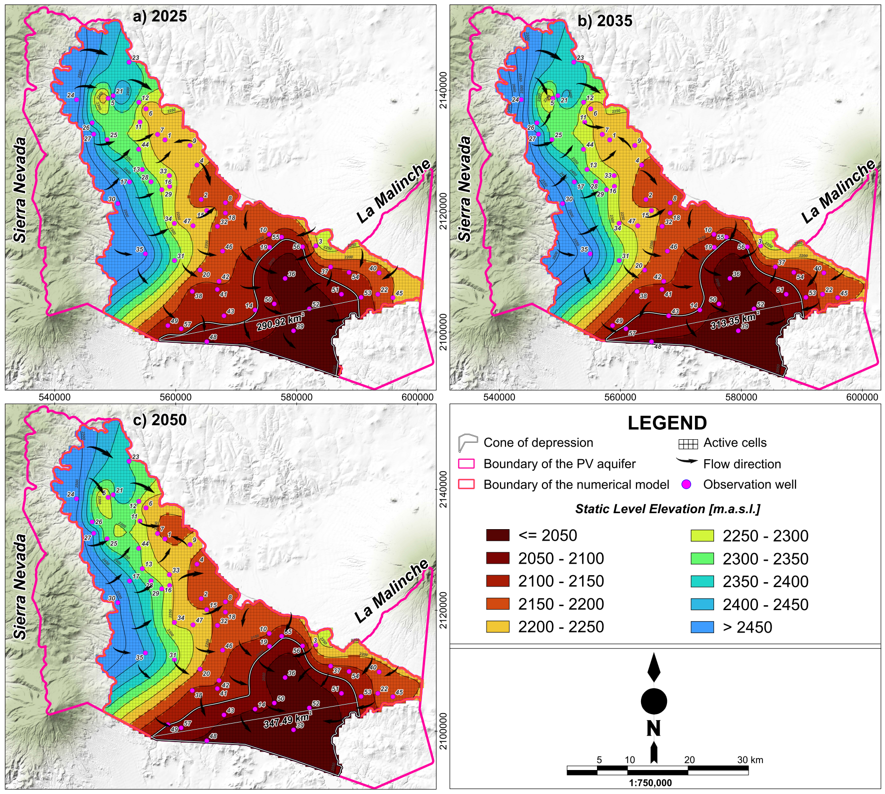

Fig. 11: Static water level elevation of the PV aquifer resulting from the projection scenario in MODFLOW. a) Projected static level for 2025; b) Projected static level for 2035; c) Projected static level for 2050.

To evaluate the spatial performance of the model, data corresponding to the year 2021 was analyzed, dividing the study area into five distinct zones.

In Zone 1 (Fig. 12a), which includes wells located in the northern sector of the study area, an RMSE of 10.92 m was obtained, indicating poor fit. This low accuracy is mainly attributed to the lack of reliable geological and piezometric data, especially in the border region between Puebla and Tlaxcala, where there is insufficient information about subsurface conditions.

Zone 2 (Fig. 12b) presents similar characteristics to the previous one. Although adequate information was available for geological characterization, it was not possible to reduce the RMSE, suggesting that pumping extractions could be affecting the aquifer's behavior. This region is distinguished by its high population density and industrial activity, notably the presence of textile companies that demand large volumes of groundwater.

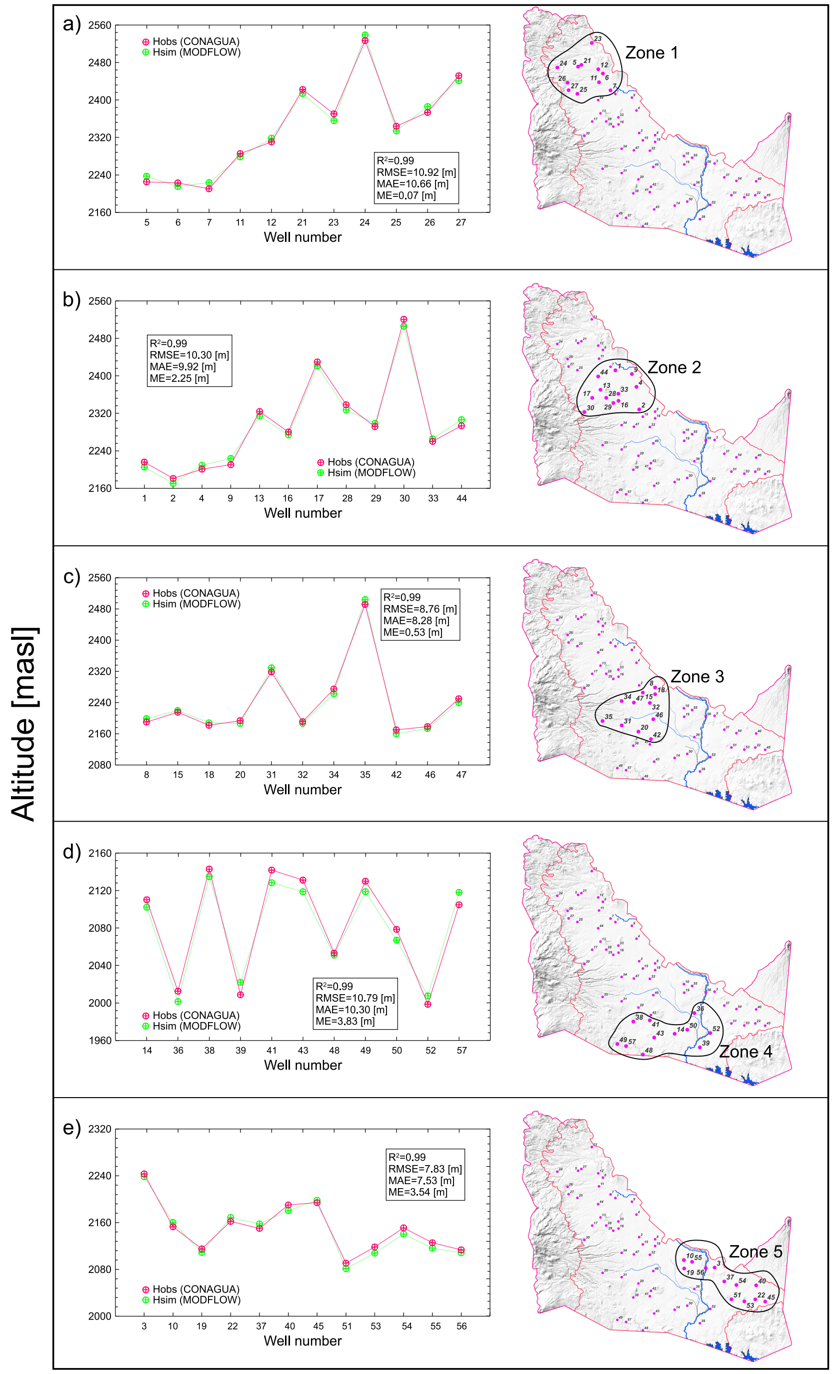

Fig. 12: Spatial division of the study area into five zones to evaluate model performance in 2021.

In Zone 3 (Fig. 12c), a significant improvement in model performance was observed, with an RMSE of 8.76 m. This area was geophysically characterized, allowing better identification of hydrogeological units. Furthermore, the homogeneous distribution of monitoring wells contributed to greater reliability in simulating the hydraulic heads.

Zone 4 (Fig. 12d) has documented history of severe drawdown of piezometric levels, which has notably impacted the model results. Additionally, the scarce information available on the subsurface limits the ability to accurately represent the hydrogeological system in this zone.

Finally, in Zone 5 (Fig. 12e), a good fit between observed and calculated hydraulic heads was achieved, with an RMSE of 7.83 m. This improvement is related to an adequate distribution of observation wells and the availability of detailed information on subsurface characteristics, which facilitated a better representation of the system in the numerical model.

5. Limitations and model perspectives

The primary source of uncertainty in numerical groundwater flow models stems from the three-dimensional geological conceptualization, largely due to limited lithological information from well logs and, in some cases, incomplete stratigraphic interpretations. The Puebla Valley is no exception to this challenge. In this study, we delineated hydrogeological units using transient electromagnetic soundings (TEM), enabling more accurate subsurface characterization. This improvement is evidenced by reduced discrepancies between calculated and observed hydraulic heads. In contrast, areas lacking geophysical coverage show greater mismatches, demonstrating that TEM are well-suited for large-scale aquifer system characterization and conceptual model refinement.

Despite the advantages of TEM, the thickness of the deep aquifer could not be precisely defined because the method failed to fully penetrate it. In this regard, integrating additional geophysical techniques, such as magnetotelluric surveys, could significantly improve the delineation of deeper hydrogeological units. This multi-method approach would yield a more comprehensive aquifer system conceptualization, ultimately enhancing the accuracy and reliability of numerical model results.

Similarly, it is critical to collect lithological logs in the northern and southeastern zones of the aquifer, where the numerical model currently exhibits the highest uncertainty. Improved characterization of the geological framework in these areas would enhance understanding of aquifer geometry and associated aquitard distribution.

Another identified limitation was the low density of well records with continuously available data over time, especially in the cone of depression area, located in the most urbanized zone of the study area. This scarcity of information hinders the accurate temporal representation of the system. Therefore, the implementation of piezometers with systematic monitoring, at least on an annual basis, is recommended to improve the transient calibration of the numerical model and strengthen its predictive capacity. Likewise, in areas where no piezometric monitoring currently exists, it is suggested to establish an adequate observation network to more faithfully represent the behavior of groundwater flow and to enable continuous tracking of its evolution over time.

In areas where pumping tests or specific records were not available, regional average values were assigned for hydraulic conductivity and storage, which may introduce errors in the flow simulation. Nevertheless, these values were verified to fall within the ranges reported by Flores-Márquez et al. (2006) and Salcedo-Sánchez et al. (2013) for the study area.

Finally, the development of a coupled flow and contaminant transport model is proposed as a future line of research, due to the presence of sulfurous water in deep wells within the urban area of Puebla. Likewise, it is recommended to continue the systematic monitoring and collection of hydrogeological data in order to feed and update the proposed model. A recalibration of the model will be necessary as the projected years (2025 and 2050) are reached, which will improve its predictive capacity and its usefulness as a decision-support tool for the sustainable management of water resources.

6. Conclusions

6.1. Conceptual hydrogeological model

The conceptual hydrogeological model of the PV aquifer establishes a robust framework for developing the system's numerical model. This integrated geophysical and geological characterization enabled the delineation of hydrogeological units and thickness estimations, revealing a multilayer system comprising: 1) an upper unconfined granular aquifer with thicknesses reaching 150 m in the valley's central sector; 2) a middle confined aquifer averaging 200 m thickness, containing sulfurous waters; and 3) a lower fractured aquifer of undefined thickness, as TEM soundings did not penetrate to bedrock. Geological faults induce vertical mixing zones, particularly west of Puebla city where they disrupt the middle aquifer's confinement.

Groundwater flow is primarily driven by recharge from the Sierra Nevada and La Malinche highlands, generating downward flow paths from the mountain ranges toward the valley. However, intensive groundwater extraction in the urban area (central-south zone) has formed a cone of depression, which by 2021 had expanded to 33.2 km in diameter with observed static water levels as deep as 125 m. In contrast, the central-northern sector of the aquifer maintains shallow water tables between 5-8 m depth.

Anthropogenic alterations - including groundwater withdrawals for urban-public and agricultural uses, channelization of the Atoyac River, land-use changes, and vegetation loss - have significantly impacted the system's water balance. Although current recharge rates exceed total extractions, risks remain of returning to critical conditions like those recorded in 2010. Furthermore, despite overall water availability, the persistent annual expansion of the cone of depression in the southern aquifer sector demonstrates localized overexploitation, directly attributable to human activities in the valley's central-south region.

The numerical modeling of the Puebla Valley aquifer, developed in MODFLOW and calibrated under both steady-state and transient conditions, successfully reproduced observed piezometric levels during the 2010-2021 period with reliable statistical fit (r, RMSE, MAE, ME). The numerical model thus confirms the hydraulic plausibility of the PV aquifer's conceptual model.

While certain zones exhibited slower model response compared to the real system, this discrepancy may be attributed to differences in calculated drawdown rates, potentially related to either insufficient spatial detail in pumping distribution or subsurface heterogeneity.

The 2013-2021 water balance shows greater water inflow than outflow, reflecting overall availability conditions. However, projected scenarios for 2050 anticipate a deficit, driven by both increasing withdrawals and expected climate change impacts. This outlook highlights the need for preventive and adaptive management strategies supported by simulation tools like the developed numerical model.

Author contributions

All authors contributed equally to the development of this research. Ana Beatriz Rubio Arellano and José Alfredo Ramos Leal led the study's conceptualization and the formal data analysis. Funding acquisition was managed by José Alfredo Ramos Leal. Claudia Arango Galván and Berenice Zapata Norberto actively participated in the critical review and methodological supervision of the work. In the manuscript preparation, Ana Beatriz Rubio Arellano drafted the initial version, while José Alfredo Ramos Leal carried out the first substantive revision. All authors provided comments and suggestions during the editing stages and approved the final version of the manuscript for publication.

References

Adombi, A.V.D.P., Chesnaux, R., Boucher, M.A., 2022. Comparing numerical modelling, traditional machine learning and theory-guided machine learning in inverse modeling of groundwater dynamics: A first study case application. Journal of Hydrology. 615, 128600. doi:10.1016/j.jhydrol.2022.128600.

Anderson, M.P., Woessner, W.W., 2015. Applied Groundwater Modeling: Simulation of Flow and Advective Transport. 2 ed., Academic Press, San Diego.

Barnett, B., Townley, L., Post, V., Evans, R., Hunt, R., Peeters, L., Richardson, S., Werner, A., Knapton, A., Boronkay, A., 2012. Australian Groundwater Modelling Guidelines. Waterlines Report, National Water Commission, Canberra.

Barthel, R., Haaf, E., Giese, M., Nygren, M., Heudorfer, B., Stahl, K., 2021. Similarity-based approaches in hydrogeology: proposal of a new concept for data-scarce groundwater resource characterization and prediction. Hydrogeology Journal. 29, 1693–1709. doi:10.1007/s10040-021-02358-4.

Bourmada, A., Khammar, H., Ramzi, H., Chaffai, A., Bouchema, N., Hamida, B., 2024. Integrated assessment of groundwater quality in algeria's souk ahras region: Implications for sustainable and management water for drinking and irrigation purpose. Desalination and Water Treatment- 320, 100827. doi:10.1016/j.dwt.2024.100827.

Chai, T., Draxler, R.R., 2014. Root mean square error (rmse) or mean absolute error (mae)? Geoscientific Model Development Discussions. 7, 1525–1534.

Chen, Y., Ling, X., Liu, M., Hu, R., Yang, Z., 2018. Statistical distribution of hydraulic conductivity of rocks in deep-incised valleys, southwest china. Journal of Hydrology. 566, 216–226. doi:10.1016/j.jhydrol.2018.09.016.

Enemark, T., Peeters, L.J., Mallants, D., Batelaan, O., 2019. Hydrogeological conceptual model building and testing: A review. Journal of Hydrology. 569, 310–329. doi:10.1016/j.jhydrol.2018.12.007.

Fiorese, G.D., Balacco, G., Bruno, G., Nikolaidis, N., 2025. Hydrogeological modelling of a coastal karst aquifer using an integrated swat-modflow approach. Environmental Modelling & Software. 183, 106249. doi:10.1016/j.envsoft.2024.106249.

Flores-Márquez, E., Jiménez-Suárez, G., Martínez-Serrano, R., Chávez, R., Pérez, D., 2006. Study of geothermal water intrusion due to groundwater exploitation in the puebla valley aquifer system, mexico. Hydrogeology Journal. 14, 1216–1230. doi:10.1007/s10040-006-0029-0.

Freeze, A., Cherry, J., 1979. Groundwater. Prentice Hall, Waterloo, Ontario.

Gan, L., Hu, L., Wang, Z., Zhang, N., Yang, G., Yu, S., 2025. Decoding the nexus of surface water and groundwater in northwestern china: Insights from long-term irrigation activities and numerical modeling. Journal of Hydrology. 654, 132825. doi:10.1016/j.jhydrol.2025.132825.

Gebru, H., Gebreyohannes, T., Hagos, E., Perilli, N., 2025. Hydrogeological assessment and steady-state groundwater flow modeling for groundwater management in the golina river sub-basin, northern ethiopia, using modflow 6. Water. 17, 949. doi:10.3390/w17070949.

Ghazi, B., Jeihouni, E., Kalantari, Z., 2021. Predicting groundwater level fluctuations under climate change scenarios for tasuj plain, iran. Arabian Journal of Geosciences. 14, 115. doi:10.1007/s12517-021-06508-6.

Giglou, A.N., Nazari, R.R., Jazaei, F., Karimi, M., 2023. Numerical analysis of surface hydrogeological water budget to estimate unconfined aquifers recharge. Journal of Environmental Management. 346, 118892. doi:10.1016/j.jenvman.2023.118892.

Guevara-Ochoa, C., Sierra, A.M., Vives, L., Barrios, M., 2024. Impact of rainfed agriculture on spatio-temporal patterns of water balance and the interaction between groundwater and surface water in sub-humid plains. Science of The Total Environment. 912, 169247. doi:10.1016/j.scitotenv.2023.169247.

Hermans, T., Goderniaux, P., Jougnot, D., Fleckenstein, J., Brunner, P., Nguyen, F., Linde, N., Huisman, J., Bour, O., Lopez-Alvis, J., Hoffmann, R., Palacios Pierluissi, A., Cooke, A.K., Pardo-Álvarez, A., Blazevic, L., Pouladi, B., Haruzi, P., Fernandez Visentini, A., Nogueira, G., Borgne, T., 2023. Advancing measurements and representations of subsurface heterogeneity and dynamic processes: towards 4d hydrogeology. Hydrology and Earth System Sciences. 27, 255–287. doi:10.5194/hess-27-255-2023.

Hernández-Cruz, A., Sandoval-Solís, S., Mendoza-Espinosa, L.G., 2022. An overview of modeling efforts of water resources in mexico: Challenges and opportunities. Environmental Science & Policy. 136, 510–519. doi:10.1016/j.envsci.2022.07.005.

Hernández-Espriú, A., Arango-Galván, C., Reyes-Pimentel, A., Martínez-Santos, P., Pita de la Paz, C., Macías-Medrano, S., Arias-Paz, A., Breña-Naranjo, J.A., 2017. Water supply source evaluation in unmanaged aquifer recharge zones: The mezquital valley (mexico) case study. Water. 9. doi:10.3390/w9010004.

Hill, M.C., Tiedeman, C.R., 2007. Effective Groundwater Model Calibration: With Analysis of Data, Sensitivities, Predictions, and Uncertainty. John Wiley & Sons.

Igwebuike, N., Ajayi, M., Okolie, C., Kanyerere, T., Halihan, T., 2025. Application of machine learning and deep learning for predicting groundwater levels in the west coast aquifer system, south africa. Earth Science Informatics. 18, 1–18. doi:10.1007/s12145-024-01623-w.

Jimenez, J.I., Tripathi, N.K., Pandey, A., Chao, K.C., Shrestha, S., 2025. Assessment of the spatiotemporal dynamics of river discharge and groundwater recharge to support sustainable water management for irrigated agriculture in the padsan river watershed. Earth Science Informatics. 18, 1–21. doi:10.1007/s12145-025-01707-1.

Kaur, N., Kaur, S., Tsolakis, N., et al., 2023. Managing groundwater demand through surface water and reuse strategies in an overexploited aquifer of indian punjab. Modeling Earth Systems and Environment. 9, 2009–2026. doi:10.1007/s40808-022-01602-4.

Kinoti, I., Leblanc, M., Lekula, M., Tweed, S., Kenabatho, P.K., Olioso, A., Lubczynski, M.W., 2024. Hydrogeological conceptual model of stampriet transboundary aquifer system in southern africa. Groundwater for Sustainable Development. 26, 101301. doi:10.1016/j.gsd.2024.101301.

Lévesque, Y., Chesnaux, R., Walter., J., 2023. Using geophysical data to assess groundwater levels and the accuracy of a regional numerical flow model. Hydrogeology Journal. 31, 351–370. doi:10.1007/s10040-023-02591-z.

Martinez, S., Escolero, O., Perevochtchikova, M., 2015. A comprehensive approach for the assessment of shared aquifers: the case of mexico city. Sustainable Water Resources Management. 1, 111–123. doi:10.1007/s40899-015-0010-y.

Mustafa, S., Bahar, A., Aziz, Z.A., Darwish, M., 2020. Solute transport modelling to manage groundwater pollution from surface water resources. Journal of Contaminant Hydrology. 233, 103662. doi:10.1016/j.jconhyd.2020.103662.

Márquez Molina, J.J., Lemeillet, A.F., Sainato, C.M., 2021. Hydrogeological conceptual model of an irrigated agricultural area, buenos aires province, argentina. Groundwater for Sustainable Development. 12, 100486. doi:10.1016/j.gsd.2020.100486.

Nejatian, N., Abbaspour, M., Javidan, P., Nia, M.Y., Shacheri, F., Azizi, H., Pazoki, M., Amir, M.J., Abbasi, S., 2024. Evaluation of the vulnerability and pathways of groundwater pollution in the zanjanrud river basin by an integrated modeling approach. Modeling Earth Systems and Environment. 10, 2295–2308. doi:10.1007/s40808-023-01897-x.

Omar, P.J., Gaur, S., Dwivedi, S.B., Dikshit, P.K.S., 2021. Development and Application of the Integrated GIS-MODFLOW Model. Springer Singapore, Singapore. pp. 305–314. doi:10.1007/978-981-15-6564-9_16.

Pleasants, M.S., Kelleners, T.J., Parsekian, A.D., Befus, K.M., Flerchinger, G.N., Seyfried, M.S., Carr, B.J., 2025. Hydrogeophysical inversion using a physics-based catchment model with hydrological and electromagnetic induction data. Journal of Hydrology. 647, 132376. doi:10.1016/j.jhydrol.2024.132376.

Poeter, E.P., Hill, M.C., 1997. Inverse models: A necessary next step in groundwater modeling. Groundwater. 35, 250–260.

Salcedo-Sánchez, E.R., Esteller, M.V., Garrido Hoyos, S.E., Martínez-Morales, M., 2013. Groundwater optimization model for sustainable management of the valley of puebla aquifer, mexico. Environmental Earth Sciences. 70, 337–351. doi:10.1007/s12665-012-2131-z.

Samani, S., 2025. Illuminating groundwater flow modeling uncertainty through spatial discretization and complexity exploration. Acta Geophysica. 73, 603–617. doi:10.1007/s11600-024-01346-y.

Shahbazi, A., Saeidi, A., Chesnaux, R., 2020. A review of existing methods used to evaluate the hydraulic conductivity of a fractured rock mass. Engineering Geology. 265, 105438. doi:10.1016/j.enggeo.2019.105438.

Tanachaichoksirikun, P., Seeboonruang, U., Fogg, G.E., 2020. Improving groundwater model in regional sedimentary basin using hydraulic gradients. KSCE Journal of Civil Engineering. 24, 1655–1669. doi:10.1007/s12205-020-1781-8.

Tiwari, S., Saviano, S., Polemio, M., 2024. Modelling approach integrating climate projections for coastal groundwater management. Science of The Total Environment. 949, 175216. doi:10.1016/j.scitotenv.2024.175216.

Vianney, J.M., Hoth, N., Moro, K., Wardani, D.N.W., Drebenstedt, C., 2025. Modeling of water inflow zones in a swedish open-pit mine with modelmuse and modflow. Sustainability. 17. doi:10.3390/su17062466.

Villegas, A., 2024. ¿quién consume más agua en puebla? URL: https://www.eluniversalpuebla.com.mx/estado/quien-consume-mas-agua-en-puebla/. el Universal Puebla, May 30.

Chapter 7

Discussion of results

The integrated results demonstrate that combining geophysical (TEM), hydrogeological (piezometric measurements, pumping tests) and hydrogeochemical methods (anions, cations, trace elements) provides robust characterization of the Valle de Puebla aquifer system. This multidisciplinary approach fulfills the core objective of analyzing the hydrological cycle in terms of both quality and quantity, revealing a dual aquifer functioning model:

1. Natural component: Governed by water-rock interactions in volcano-sedimentary sequences.
   - Flows from Sierra Nevada (associated with volcanic rocks, primarily andesites and basalts) show local, intermediate and regional contributions, with distinctive chemical signatures (Na and K enrichment).
   - Flows from La Malinche (linked to carbonate rocks like limestones) are restricted to intermediate and regional components, dominated by Ca, HCO_3 and SO_4.
2. Anthropogenic component: Significant alterations to water balance and quality.
   - Cone of depression in the southern valley, with potential water stress risk if current extraction rates continue.
   - NO_3 contamination ($>$11 mg/L) in agricultural areas and SO_4 in deep wells ($\sim$100 m), demonstrating vertical fluid migration through breached confinement of the sulfurous aquifer, attributable to overexploitation.

The geological medium characteristics and structural framework (summarized as horst-graben systems) condition the system dynamics:

- Geoelectrical units with resistivities of 56-301 $\Omega \cdot$ m: fractured aquifer in volcanic rocks, showing high transmissivity and rapid recharge response.
- Resistivities of 4-10 $\Omega \cdot$ m: sulfurous waters, manifesting in thermal springs in some Puebla areas.
- Resistivities $>$97 $\Omega \cdot$ m in deep zones: Potential for sustainable exploitation as a management alternative.

These findings validate the initial hypothesis: the water's chemical signature reflects natural water-rock interaction processes but is also modified by human activities (land use change, irrigation returns). A clear example is the spatial coincidence between agricultural-urban areas and elevated salinity levels.

The identification of critical zones, particularly the southern valley where the cone of depression coincides with converging flows from Sierra Nevada and La Malinche, reinforces the need to prioritize annual piezometric monitoring, regulate unregistered wells near fault areas, and protect recharge zones essential for maintaining water availability.

In summary, this research demonstrates that the Puebla Valley aquifer functions as a multiphase system, where geological heterogeneity defines its storage capacity and flow characteristics, while human pressures (intensive extraction and contamination) disrupt its natural equilibrium. The applied methodological integration not only answered the research question but also provides a replicable technical framework for managing aquifers in volcano-sedimentary contexts, where subsurface complexity demands adaptive approaches.

These results prove the system responds not only to geological controls but also to complex socio-environmental dynamics. The transformation of the hydrological cycle into a hydrosocial cycle, influenced by water-related decisions, uses, and conflicts, highlights the need for multidimensional management. The proposed methodological approach, combining hydrogeological characterization with anthropogenic pressure analysis, establishes foundations for more adaptive and sustainable water governance, particularly in volcanic-sedimentary regions with high water demand.

Conclusions

Hydrogeological units and conceptual model.

- Upper unconfined granular aquifer, formed by alluvial deposits, gravel, sand and clays. Approximately 150 m thick with good water quality suitable for agricultural, public and urban use. Static water levels are shallow, reaching up to 5 m in the northwest valley.

- Intermediate confined aquifer, separated from the upper aquifer by a low-permeability clay aquitard. Average thickness of 200 m with sulfurous waters. In western Puebla city, geological faults enable hydraulic mixing between aquifers due to confinement breach.

- Lower fractured aquifer, separated by an aquiclude of very low permeability limestones and marls. This aquifer lies on fractured limestones and is currently unexploited; no well records exist, so water quality and actual thickness remain unknown. The geological basement is inferred to consist of metamorphic schists from the Acatl'an Complex.

The hydrogeological characterization, combined with geophysical data (TEM), established a coherent conceptual model supporting system analysis and serving as basis for numerical simulation.

Water resource availability.

- Hydrogeological balances show that despite considerable recharge from Sierra Nevada and La Malinche, overexploitation in urban/agricultural areas has created imbalance.

- By 2021, static levels reached depths of 125 m in urban areas, consolidating an expanding cone of depression that confirms human impact on natural system balance.

- The depression cone in south-central Puebla expanded from 303.4 km^2 (2010) to 295.0 km^2 (2021), maintaining SW-NE orientation that highlights recharge zone importance.

Groundwater quality and hydrogeochemical processes.

- Salinization processes identified in south-central valley, linked to irrigation returns, agrochemicals and potential industrial discharges.

- Water-rock interaction with ion exchange, carbonate/sulfate dissolution, secondary mineral precipitation, and tectonic mixing have modified groundwater chemical signatures, confirming geological-anthropogenic interactions.

- Recharge zones (Sierra Nevada/La Malinche) show low mineralization indicating recent infiltration, while valley areas exhibit higher mineralization from longer residence times and volcanic interactions.

Aquifer vulnerability and validation.

- DRASTIC adaptation to volcano-sedimentary environment revealed highest vulnerability coincides with agricultural/industrial areas.

- WQI validation showed spatial coherence between high vulnerability and contaminants, reinforcing need for integrated hydrogeochemical/hydrogeological approaches.

Numerical model projections.

- Modeling shows that considering climate change and increased agricultural/urban withdrawals, static levels could drop over 50 m in some areas by 2050.

- The depression cone will maintain SW-NE orientation but expand NW-SE, increasing water availability risks.

- Recharge zones show no significant variations, underscoring their system resilience role.

Bibliography

Boelens, R., Hoogesteger, J., Swyngedouw, E., Vos, J., and Wester, P. (2016). Hydrosocial territories: a political ecology perspective. *Water International*, 41(1):1–14.

Brassington, R. (2017). *Field Evaluation of Aquifers*, chapter 3, pages 29–48. John Wiley & Sons, Ltd.

Hornberger, G. M., Wiberg, P. L., P, J., Raffensperger, and D'Odorico, P. (2014). *The Science of Hydrology*, pages 1–19. JHU Press.

Jacob, B. and Verruijt, A. (1987). *Modeling Three-Dimensional Flow*, pages 53–84. Springer Netherlands, Dordrecht.

Jiménez, G. (2005). *Exploración de modelo de flujo y transporte en el acuífero del valle de Puebla*. Doctoral dissertation, Universidad Nacional Autónoma de México, Instituto de Geofísica, Posgrado en Ciencias de la Tierra, Distrito Federal, México.

Linton, J. (2008). Is the hydrologic cycle sustainable? a historicalâ€“geographical critique of a modern concept. *Annals of the Association of American Geographers*, 98(3):630–649.

Linton, J. and Budds, J. (2014). The hydrosocial cycle: Defining and mobilizing a relational-dialectical approach to water. *Geoforum*, 57:170–180.

Loaiciga, H. A., Valdes, J. B., Vogel, R., Garvey, J., and Schwarz, H. (1996). Global warming and the hydrologic cycle. *Journal of Hydrology*, 174(1):83–127.

McFarlane, D. J., George, R. J., and Farrington, P. (1993). Changes in the hydrologic cycle. In *Reintegrating fragmented landscapes: towards sustainable production and nature conservation*, pages 146–186. Springer New York, New York, NY.

Morales, M. M., SÃ¡nchez, E. R. S., Hoyos, S. E. G., and Esteller, M. V. (2015). Simulación de diferentes alternativas de gestión de los recursos hídricos del acuífero de puebla-atoyac. *IngenierÃa*, 19(1):62–72.

Perrin, M.-E. (2023). *Hydro-Social Cycle*, pages 433–437. Springer International Publishing, Cham.

Silva Pérez, D. (2003). *Modelo evolutivo del acuífero del Valle de Puebla*. PhD thesis, Universidad Nacional Autónoma de México, Distrito Federal, México.

Smith, L. (2015). Hydrogeology. In *Reference Module in Earth Systems and Environmental Sciences*. Elsevier.

Swyngedouw, E. (2006). Technonatural revolutions â€“ the scalar politics of franco's hydro-social dream for spain, 1939-1975. *Transactions of the Institute of British Geographers New Series*, 32(1):9–28.

Villar-Navascués, R. A. and Arahuetes, A. (2020). *The Hydrosocial Cycle: Understanding Water as a Socionatural Production*, pages 1–11. Springer International Publishing, Cham.

Xu, X., Huang, G., Zhan, H., Qu, Z., and Huang, Q. (2012). Integration of SWAP and MODFLOW-2000 for modeling groundwater dynamics in shallow water table areas. *Journal of Hydrology*, 412-413:170–181. Hydrology Conference 2010.